Effects of Strong Interactions in Ultracold Rydberg Gases

Jovica Stanojevic, Ph.D.

University of Connecticut, 2007

In this thesis I present several theoretical methods to explore the excitation dynamics of ultracold Rydberg systems in various regimes. For some applications the details of interactions between Rydberg atoms have to be carefully examined, while for others, the many-body aspect of Rydberg excitation may be crucial. In both cases, the basic prerequisite is to know the interactions sufficiently well. I will review the basic concepts how to evaluate molecular potentials in various Hund's cases and approximations. Long-range Rydberg-Rydberg interactions between Rydberg atoms induce ℓ-mixing which in certain situations gives rise to molecular resonances. For these resonances, we calculate long-range potentials in Hund's case (c) by diagonalization of an interaction matrix. The excitation dynamics of the resonances is always modeled as pair excitation. At high principal quantum number n, the interactions between Rydberg atoms can blockade the excitation of many surrounding atoms in the range of few μm. The atoms within this range are strongly correlated so that many-body treatments are, in general, needed. To describe this blockading effect and other manifestations of the collective behavior of Rydberg excitation, such as the many-body Rabi oscillations, spatial correlations between atoms and the fluctuations of the number of excited atoms, I have used three different approaches. In the mean-field approach the interactions between different atoms is modeled by a distribution of mean-field shifts for which a distribution of probabilities is calculated. A good agreement between the theoretical model and experimental measurements is found. To study the correlations between atoms the many-body wavefunction is numerically computed. The possibility of observing the many-body Rabi oscillations of Rydberg excitation and other aspects of many-body dynamics is analyzed. Although strong interactions cannot be treated perturbatively other expansions may be feasible. I will show that the expansion in powers of the single atom Rabi frequency can be evaluated in the interaction and Heisenberg picture. The expansion is expected to behave well for arbitrary strong interactions.

Effects of Strong Interactions in Ultracold Rydberg Gases

Jovica Stanojevic

M.Sc. Theoretical Physics, University of Belgrade, Belgrade, Serbia, 2000

A Dissertation
Submitted in Partial Fullfilment of the
Requirements for the Degree of
Doctor of Philosophy
at the
University of Connecticut

2007

APPROVAL PAGE

Doctor of Philosophy Dissertation

Effects of Strong Interactions in Ultracold Rydberg Gases

Presented by

Jovica Stanojevic, M.Sc. Th.Phys.

Major Advisor

Robin Côté

Associate Advisor

Juha Javanainen

Associate Advisor

Phillip Gould

University of Connecticut

2007

ACKNOWLEDGEMENTS

I would like to thank all the people who have contributed to this thesis in one way or another. First of all, I would like to thank my remarkably understanding advisor Robin Côté for giving me the opportunity to work in this interesting field, for being always open and friendly, advising me about anything I asked, and for helping me in the pursuit of my academic career. I have learned a great deal on atomic and molecular physics from the leaders of the Rydberg project: Prof. Edward Eyler, Prof. Phillip Gould and Prof. Robin Côté. I want to thank Prof. Edward Eyler for giving me a chance to work on the experiment, for his devotion to teaching and for his generous support during my attempt to become an experimental physicist. I also want to thank Prof. Phillip Gould for the inspiring discussions and careful reading of my thesis. I have always like and appreciated his tendency, not only to point out possible weak points and problems, but also to offer well thought and concrete improvements and solutions. Big thanks to Prof. Juha Javanainen for reading the thesis and giving many helpful suggestions.

My special thanks to my old friends Zoran Pavlovic and Mihajlo Kornicer for their friendship and support in numerous occasions.

I would also like to thank the former and present members of the experimental group

for their help and nice company: Dr. Shahid Farooqi, Dr. Yangpeng Zhang, Sulabha Krishnan, Hyewon Kim-Pechkis, David Thong, Joe Pechkis, and Marco Ascoli. I am especially grateful to Sulabha Krishan for beeing an exceptional friend and for her unmatched generosity.

I had the privilege to know and work with nice and skillful members of my group: Dr. Philippe Pellegrini, Zoran Pavlovic, Elizabeth Taylor-Juarros, Ionel Simbotin and Marko Gacesa. I have enjoyed their company and greatly benefited from their extensive computer-related and programming-related knowledge.

My time here would not be the same without many excellent graduate student Li Fang, Uttam Shrestha, Tun Wang, Javier Peressutti, James Zickefoose, Igor Senderovich, Otim Odong, Kalum Palandage, Renuka Rajapakse,...

My thanks go to Prof. Matthias Weidemüller and his graduate student Kilian Singer for the joint effort on the long-range potentials between Rydberg atoms and the great job they did in writing the related numerical code.

Finally, I would like to thank to the great office staff of the Physics Department, Kim Giard, Dawn Rawlinson, Cecile Stanzione and Nicole Hryvniak for their rare kindness and patience with students.

TABLE OF CONTENTS

LIST OF FIGURES

LIST OF TABLES

Introduction

Rydberg atoms have long been studied for their unique properties, such as long radiative lifetimes, large cross sections or huge polarizabilities [1,2]. These exaggerated properties of highly-excited Rydberg atoms provide the motivation for this recent interest [3,4]. Long lifetimes and the possibility to interact strongly at large distances have made ultracold Rydberg atoms interesting systems for possible quantum information applications. Nutral atoms are good candidates because of their weak coupling to the environment [5–7]. The electron in a Rydberg state is very far from the nucleus and thus sensitive to external fields or the presence of neighboring Rydberg atoms. Due to the huge polarizabilities of Rydberg atoms, it is possible to induce relatively large electric dipole moments using small electric fields. The capability to turn on and off the interactions just by switching the external field is an important aspect of this approach to quantum computation. In this way decoherence effects due to the interactions between atoms or with the environment, can be significantly reduced. Strong interactions can be used to entangle neutral atoms and achieve fast quantum gates [8,9], as well as to blockade excitation by shifting many-atom excited states out of resonance. It has been proposed to use this blockading effect to realize scalable quantum gates [10]. The evidence of excitation blockade has been found in several experiments with a narrow laser bandwidth. In [11], a local blockade of Rydberg state excitation in a mesoscopic sample due to strong van der Waals (vdW) interactions has been observed using a pulse-amplified single-mode laser. Significant suppression of Rydberg excitation has also been observed using cw excitation [12]. This Rydberg excitation, strongly influenced by interactions, exhibits sub-Poissonian atom counting statistics [13,14]. The blockade effect due to dipole-dipole interactions in an ultracold sample of Cs atoms [15] has been reported. Also, an interesting antiblockade effect in two-step excitation processes was predicted [16,17].

At high principal quantum numbers, interaction forces between Rydberg atoms become extremely large. These forces have been shown to accelerate ultracold rubidium (Rb) Rydberg atoms from 10 cm/s to 10 m/s [18]. The classical treatment of these collisions [19] shows that 0.1-1% of the internal binding energy can be transferred into kinetic energy, which is for ultracold Rydberg atoms significantly larger than their initial kinetic energy. For larger interaction times and higher Rydberg atom densities, Rydberg gases spontaneously evolve into ultracold plasmas [20–23], while for moderate densities long-lived Rydberg states are formed due to ℓ-changing collisions between slow free electrons and initially excited (low-ℓ) Rydberg atoms [24]. A selection of initial colliding pairs of atoms has been done experimentally [25,26] by varying the detuning of the excitation laser. In this experiment the production of ions in collisional processes is consistent with the assumption of an attractive van der Waals potential and a theoretical estimate of its magnitude. Manifestations of long-range interactions have been also seen in ultracold collisions [27–29] and density-dependent line broadening of resonances in atomic beams [30].

In ultracold Rydberg systems, the thermal motion and Doppler shifts are greatly reduced so that the effects of interatomic interactions can be investigated and utilized in a more controllable manner. In many situations the motion of atoms can be completely ignored and the system considered as a "frozen Rydberg gas". In such a frozen Rydberg gas resonant excitation exchange has been reported [31,32] and described as a many-body diffusion process [32,33]. Resonant conditions can be achieve by tuning the energy levels of Rydberg atoms using external electrical fields [34,35]. In this process, pairs of excited states, not atoms, diffuse. An ss' pair of excited states is first created into a pair of closely-spaced Rydberg atoms and then subsequently transferred to another pair of Rydberg atoms via resonant $ss' - pp'$ processes and so on. Long lifetimes of highly excited Rydberg states also bring the possibility of trapping Rydberg atoms. High-angular momentum Rydberg atoms have been trapped in a superconducting magnetic ($B = 2.9$ T) trap [36].

There have been two proposals for weakly bound long-range molecules involving Rydberg atoms but they have not been detected yet. The term "long-range molecules" was coined a long time ago, referring to molecules in high vibrational states close to the dissociation limit, whose properties are determined by the long-range interactions [37–39]. The so called "trilobite" and "butterfly" states are molecular states formed by a pair of atoms, with one of the atoms in the ground state and the other one in a Rydberg state [40–44]. Weakly bound states of two Rydberg atoms, labeled macrodimers, have also been proposed [45]. Although such exotic molecules have not been detected yet, molecular resonances caused by Rydberg-Rydberg interactions have been observed [46]. Here the important effect is ℓ-mixing caused by interactions, so that otherwise forbidden transitions become allowed.

To make quantitative predictions and to interpret experimental data, one needs to obtain accurate expressions for the long-range molecular potentials. Also, different potential curves are accessible in different excitation schemes and processes so it is important to systematically study long-range interaction potentials between Rydberg atoms. The most often used method to evaluate long-range potentials is based on the perturbation expansion of (in general) degenerate level [47] and the bipolar expansion for the residual Coulomb interaction. The bipolar expansion in various cases of overlapping and non-overlapping electronic distributions is presented in [48]. Recently, these potentials have been systematically calculated for various asymptotes of many heteronuclear diatomic molecules [49]. The same type of calculations has been done for homonuclear molecules as well [50–52]. This approach has been extended to high Rydberg states in [45,52]. Accurate calculations that include retardation [53,54] and relativistic effects [55,56] have been performed. In most cases, the potential curves are evaluated ignoring fine structure. However, in many experiments, fine structure can be resolved. It can be included in the second order of perturbation theory as well

[54,57–59]. However, for the study of long-range molecular resonances perturbation theory is not applicable. Also, for Rb and cesium (Cs), atomic fine structure cannot be ignored in the calculation of molecular potentials. Including fine structure, I have obtained long-range molecular potentials, in Hund's case (c), by diagonalization of an interaction matrix.

This thesis

In this thesis, I present several theoretical methods to evaluate the excitation dynamics of ultracold Rydberg systems in various regimes. For some applications, the details of interactions between Rydberg atoms have to be carefully examined, while for others, the many-body aspect of Rydberg excitation may be crucial. In both cases, the basic prerequisite is to know the interactions sufficiently well. The theory of how to calculate molecular potentials in various Hund's cases and approximations is given in Chapter 1. Some technical notes related to this chapter are located in Appendix A.

In Chapter 2 we describe in detail several treatments of long-range molecular resonances. In single photon UV excitation of the $5s$ ground state, the resonances occur at energies corresponding to excited atom pairs $(n{-}1)d+ns$ and $(n{-}1)p_{3/2}+(n{+}1)p_{3/2}$ due to ℓ-mixing caused by long-range Rydberg-Rydberg interactions. For these resonances, we need to calculate long-range potentials in Hund's case (c) by diagonalization of an interaction matrix. The excitation dynamics is always modeled as pair excitation. Appendices B and C are related to this chapter. Appendix B contains all the matrices used to connect diatomic states in the space and molecule-fixed frames. In Appendix C, I show our results on $(n-1)p_{3/2} + (n+1)p_{3/2}$ resonances, which are closer than $(n-1)d + ns$ ones to the atomic np resonance.

In Chapter 3, we analyze the mean-field methods used to describe a local blockade of Rydberg state excitation in macroscopic samples due to strong vdW interactions [11,12]. The $5s$ ground state atoms were excited by one photon UV transitions to high $np_{3/2}$ Rydberg states. Rydberg excitation exhibited dramatic suppression compared to the non-interacting case. A mean-field type model was proposed [11] to explain these experimental results. In the model, different atoms interact differently depending on their locations. Different interaction energies were modeled by a distribution of mean-field shifts for which a distribution of excitation probabilities was calculated. A good agreement between the theoretical model and experimental measurements was found.

We investigate the collective aspects of Rydberg excitation in Chapter 4. Strong interactions between Rydberg atoms influence the excitation process and impose correlations between excited atoms. The manifestations of the collective behavior of Rydberg excitation are the many-body Rabi oscillations, spatial correlations between atoms, as well as the fluctuations in the number of excited atoms. We study these phenomena in detail by numerically solving the many-body Schrödinger equation. We explore the dynamics of such systems, especially the possibility of many-body Rabi oscillations of Rydberg excitation. It is plausible to investigate these oscillations in smaller systems because one would not normally expect to achieve the coherent manipulation of large groups of atoms. The many-body approach developed in [60] is quite suitable for this analysis and we use it here. We only modify some technical details on how to treat interactions in this approach.

Finally, In Chapter 5, I show how to evaluate the Ω-expansion of the most interesting physical quantities in the interaction and Heisenberg pictures. This Ω is the Rabi frequency for a single atom. The expansion is expected to be well-behaved for arbitrarily strong interactions. For homogeneous large samples, I give the explicit form of the expansion of excitation probabilities, up to Ω^4, for the most important cases of excitation pulses and interactions. The main results of my thesis are summarized in the conclusions.

Chapter 1

Molecular Potentials and Excitation Resonances

Very long lifetimes of Rydberg atoms allow studying utracold Rydberg gases under various experimental conditions. For long experimental times (several μs), the large internal energy of Rydgerg atoms can be released due to collisions and ultracold plasmas can be formed. For shorter times ($\lesssim$ 100 ns), the effects of interactions between Rydberg atoms can be explored. For such experimental times the motion of atoms is usually ignored completely and the system considered as a "frozen Rydberg gas". In order to analyze experimental results and make predictions, we need to learn more about molecular potentials. These potentials are described by some quantum numbers defined by the symmetry of diatomic molecules. In this chapter, I review the basic elements needed to calculate these molecular potentials.

1.1 Molecular symmetries

All geometric symmetry operations of homonuclear diatomic molecules form the point group $D_{\infty h}$ [61,62]. The symmetry elements that we usually consider are rotations about the internuclear axis, reflections through a plane containing the rotation axis and the inversion i of the spatial coordinates about the center point between both atom cores. Multiple applications of these symmetry operations generate the whole point group.

In quantum mechanics, we are rather interested in the representations $D(G)$ of the symmetry group G [63,64]. We consider how molecular states are transformed under symmetry operations $D(g)$, $g \in G$. Depending on their properties under these transformations, molecular states are divided into several sets. We commonly call them symmetries, but strictly speaking, these sets are related to different irreducible representations [64,65] of G. The labels and quantum numbers of irreducible representations are used for the classification of molecular states. States of different irreducible representations form orthogonal subspaces of the Hilbert space. The importance of symmetry in quantum mechanics relies on the reduction of the Hamiltonian in each of these subspaces. In other words, the Hamiltonian commutes with all the projectors onto subspaces of irreducible representations. These projectors and the Hamiltonian form a complete set of commuting observables. This would not be very useful if we did not know, in general, how to construct these projectors. Wigner has shown that they are linear combinations of $D(g)$ and entirely defined by $D(G)$ and G [66]. In our case $G = D_{\infty h}$ and we present two constructions of properly symmetrized states in Appendix A. The symmetry group is relatively simple so we do not need the help of the general theory by Wigner to find proper basis sets.

The projection of the total electronic angular momentum $M = m_1 + m_2$ onto the molecular axis is conserved as a consequence of the rotation symmetry. The exact definitions of M and m_i depend on the actual physical problem. If spin-dependent molecular interactions are negligible, the spin part of the diatomic wavefunction is separable and can be excluded from the analysis. In this case M and m_i are respectively the projections of $\hat{\boldsymbol{\ell}}_1 + \hat{\boldsymbol{\ell}}_2$ and $\hat{\boldsymbol{\ell}}_i$ onto the molecular axis, where $\hat{\boldsymbol{\ell}}_i$ is the orbital angular momentum of atom "i". This M is usually labeled as Λ. We also consider spin-dependent interactions, where M and m_i are respectively the projections of $\hat{\boldsymbol{j}}_1 + \hat{\boldsymbol{j}}_2$ and $\hat{\boldsymbol{j}}_i$. In this case $\hat{\boldsymbol{j}}_i$ is the total angular momentum of atom "i" and M is labeled as Ω. If $M \neq 0$, reflections through a plane containing the molecular axis, represented by the reflection operator σ_v, changes the sign of the projection of the angular momentum on the axis. For $M \neq 0$, the reflected molecular state has the same energy as the initial one. Consequently, the (anti)symmetrization $|M^{\pm}\rangle = \left((1 \pm \sigma_\nu)/\sqrt{2}\right)|M\rangle$ of the $M \neq 0$ states does not break the degeneracy between the states with the same absolute value of M. Only for Σ-states can the (anti)symmetrization $|\Sigma^{\pm}\rangle = \left((1 \pm \sigma_\nu)/\sqrt{2}\right)|\Sigma\rangle$ give nondegenerate states. Thus the symmetry property under reflections can be used to distinguish different molecular potentials. It turns out that the representation of σ_ν in the molecule-fixed coordinate system is not unique because the position of the symmetry axis of a linear molecule is determined only by two Euler angles [67]. The absence of off-axis nuclei impedes a unique definition of the way the third Euler angle is transformed under a space-fixed inversion, giving an additional phase factor in the representation of σ_ν. This factor is fixed by an additional convention (1.1.3) [67].

The inversion operation i inverts the single electronic state relative to the respective atom core and then translates the state to the other atom core so that the first electron is located near the second atom core and vice versa. As $i^2 = 1$ the eigenvalues p of i must be either $+1$ or -1. Molecular states which do not change the sign of the spatial wave function under this symmetry operation are called gerade (g) states and those that change the sign are called ungerade (u) states.

The choice of a convenient basis of molecular states is very important. This choice is not completely determined by symmetry alone, although all good quantum numbers from the symmetry have to be built in the basis. As mentioned, it also depends on the actual physical problem, i.e. type of interactions. The Rydberg-Rydberg interaction is essentially the residual Coulomb interaction, so it is spin-independent, and cannot mix states with different Λ, total spin S, or eigenvalues of i and σ_ν. It can be diagonalized in the basis $\left|{}^{2S+1}\Lambda_{g/u}\right\rangle \left|S, M_S\right\rangle$. We consider two molecular basis sets in Hund's cases (a) and (c). In Appendix A, we show that the symmetrized spatial part of the electronic wave function of the homonuclear atom pair, with no overlap of atomic wavefunctions, has the following asymptotic form in Hund's case (a)

$$\begin{aligned}&\left|{}^{n_1\ell_1 m_1}_{n_2\ell_2 m_2}, \Lambda; \sigma; p\right\rangle \sim \\ &\qquad \left|n_1\ell_1 m_1; \mathbf{R}_1\right\rangle \left|n_2\ell_2 m_2; \mathbf{R}_2\right\rangle + \sigma p(-1)^{\ell_1+\ell_2} \left|n_2\ell_2 m_2; \mathbf{R}_1\right\rangle \left|n_1\ell_1 m_1; \mathbf{R}_2\right\rangle\end{aligned} \tag{1.1.1}$$

where $\sigma = (-1)^S$, n_1 and n_2 are the principal quantum numbers, and ℓ_1 and ℓ_2 the angular momentum quantum numbers. The separate projections of the angular momentum of each atom onto the molecular axis satisfy the constraint $\Lambda = m_1 + m_2$. In our notation, the ket $|n_i\ell_i m_i; \mathbf{R}_k\rangle\,|n_j\ell_j m_j; \mathbf{R}_{k'}\rangle$ means that the first electron is in state $n = n_i$, $\ell = \ell_i$ and $m = m_i$ while the second electron is in state $n = n_j$, $\ell = \ell_j$ and $m = m_j$. $\mathbf{R}_k$ and $\mathbf{R}_{k'}$ are the positions of the two nuclei k and k', where $k, k' = 1, 2$.

The previous symmetrization is appropriate if fine structure can be ignored, which is not always possible. Because the spin-orbit interaction H_{fs} depends on spin, it mixes states with different Λ. It is diagonal in the basis of properly symmetrized $|\ell_1\, j_1, m_1\rangle\,|\ell_2\, j_2, m_2\rangle$ states. This basis is more appropriate to describe molecular asymptotes (at $R \to \infty$), and it facilitates the calculation of lineshapes in the next section. The projection of the total angular momentum onto the molecular axis $\Omega = m_1 + m_2$ is conserved. This is Hund's case (c). Assuming that there is no overlap of the electronic wave functions belonging to different atoms, the properly symmetrized asymptotic states for $\Omega \neq 0$ have the form [68]

$$\begin{aligned}&|n\ell_j, m_j; n'\ell'_{j'}, \Omega - m_j; \Omega_{g/u}\rangle \sim \\ &\qquad |n,\ell,j,m_j\rangle|n',\ell',j',\Omega - m_j\rangle - p(-1)^{(\ell+\ell')}|n',\ell',j',\Omega - m_j\rangle|n,\ell,j,m_j\rangle.\end{aligned} \tag{1.1.2}$$

This expression is also derived in Appendix A.

If $\Omega = 0$, we distinguish between symmetric and antisymmetric states under σ_ν via $\left|0^{\pm}_{g/u}\right\rangle = \left((1 \pm \sigma_\nu)/\sqrt{2}\right)|0_{g/u}\rangle$; the action of the σ_ν operator is consistent with the following rules [67]

$$\sigma_\nu \left|\Lambda\right\rangle = (-1)^\Lambda \left|-\Lambda\right\rangle \ , \tag{1.1.3}$$

$$\sigma_\nu \left|S, M_S\right\rangle = (-1)^{S-M_S} \left|S, -M_S\right\rangle \ . \tag{1.1.4}$$

The action of the σ_ν on states (1.1.1) is also given by the first rule (1.1.3). It is obviously not applicable if $\Lambda = 0$. The correct result of σ_ν on such states follows from its action on atomic states $\sigma_\nu \left|\ell, m\right\rangle = (-1)^m \left|\ell, -m\right\rangle$.

We have asumed in this analysis that there is no background electric field. If a background electric field is included, then the group symmetry of the electronic Hamiltonian is not $D_{\infty h}$. Consequently, the quantum numbers based on this symmetry are not good anymore and we cannot reduce the interaction matrix in the basis of states of a given symmetry. In general, one has to include all possible basis states and used them to diagonalize the interaction matrix [69,?].

1.2 Long-range interactions

The residual Coulomb interaction between two charge distributions for large separations R is conveniently expressed by the bipolar expansion in powers of $1/R$ [47,48]

$$V(\mathbf{r}_1, \mathbf{r}_2) = \sum_{\ell, L=1}^{\infty} \frac{V_{\ell L}(\mathbf{r}_1, \mathbf{r}_2)}{R^{\ell+L+1}} \tag{1.2.1}$$

with $\mathbf{r}_1$ and $\mathbf{r}_2$ the relative position of each electron with respect to its atom core, and

$$V_{\ell L}(\mathbf{r}_1, \mathbf{r}_2) = \frac{(-1)^L 4\pi}{\sqrt{\hat{\ell}\hat{L}}} \sum_m \sqrt{\binom{\ell+L}{\ell+m}\binom{\ell+L}{L+m}} r_1^\ell r_2^L Y_{\ell m}(\hat{r}_1) Y_{L-m}(\hat{r}_2) \tag{1.2.2}$$

where $\hat{\ell} = 2\ell + 1$, $\hat{L} = 2L + 1$, $\binom{n}{k} = n!/[k!(n-k)!]$ is the binomial coefficient and $Y_{\ell m}(\hat{r})$ is the spherical harmonic. In order for equations (1.2.1) and (1.2.2) to be valid the electron wave functions of the two atoms must not overlap so that exchange and charge overlap interactions can be neglected. This is the case if R is larger than the Le Roy radius R_{LR} [71]:

$$R_{LR} = 2\left[\langle n_1\ell_1|\, r^2\, |n_1\ell_1\rangle^{1/2} + \langle n_2\ell_2|\, r^2\, |n_2\ell_2\rangle^{1/2}\right], \tag{1.2.3}$$

with $\langle n_1\ell_1|\, r^2\, |n_1\ell_1\rangle$ being the expectation value of r^2 for the radial wave function belonging to the valence electron of an alkali atom. The most important contributions to Eq. (1.2.1) are from dipole ($\sim 1/R^3$) and quadrupole ($\sim 1/R^5$) interactions.

1.2.1 Interaction potentials: Hund's case (a)

At large internuclear separations R, the interaction between two atoms can be expanded as a sum of powers of $1/R$ [47]. For two atoms in the same np state, and neglecting fine structure effects, it takes the following form [45,51]

$$V_{pp}(R) = -\frac{C_5}{R^5} - \frac{C_6}{R^6} - \frac{C_8}{R^8} - \cdots . \tag{1.2.4}$$

where the C's are the dispersion coefficients. In [45,52], these coefficients were computed. The C_5, C_6, and C_8 coefficients scale as n^8, n^{11}, and n^{15}, respectively. The exact values of these coefficients depend on the molecular symmetry: for the $np+np$ asymptote, a total of 12 molecular states exist, grouped in 6 pairs, each pair having the same dispersion coefficients. For Rb atoms, the C_6 van der Waals coefficient of one pair of ${}^1\Sigma_g^+ -{}^3\Sigma_u^+$ states is almost two order of magnitude larger than for any other C_6 of $np+np$ molecular potentials (for $n=70$, $C_6 \simeq 2\times 10^{22}$ a.u.). The reason is that this is the only pair strongly coupled with nearby $(n+1)s+ns$ states. Because Rydberg-Rydberg interactions do not mix states with different Λ, S, and eigenvalues of i and σ_ν, only configurations of the same symmetry (described by the same quantum numbers) can be coupled. By examining all possible symmetry configurations, we find that ${}^1\Sigma_g^+ - {}^3\Sigma_u^+$ is the only common symmetry of asymptotic $(n+1)s+ns$ and $np+np$ states. Therefore, the coupling between $(n+1)s+ns$ and $np+np$ states exists for this symmetry only. Besides the strong coupling, the proximity of $(n+1)s+ns$ and $np+np$ states greatly enhances the C_6 coefficient of the ${}^1\Sigma_g^+ - {}^3\Sigma_u^+$ pair, according to Eqs. (A.3.9-A.3.10).

These potential curves may intersect potential curves correlated to nearby asymptotes, leading to avoided crossing and/or mixing between states with the same symmetry. In general, the np+np potential curves can couple to curves correlated to n_1s+n_2s, n_1s+n_2d, or n_1d+n_2d through dipole interactions. The C_6 coefficients depend on the couplings by dipole interactions. Quadrupole interactions are mostly relevant for the couplings within np+np states. This coupling determines the C_5 term in the previous expansion (1.2.4). Although higher order multipoles could couple other states, the strength of such couplings decreases rapidly.

At large R, the leading terms of the curves for n_1s+n_2s, which are denoted as $V_{ss'}$, are

$$V_{ss'}(R) = -\frac{C_6}{R^6} - \frac{C_8}{R^8}\,, \tag{1.2.5}$$

while those for $n_1s + n_2d$ or $n_1p + n_2p$, labeled V_{sd} and $V_{pp'}$ respectively, have the same form as Eq. (1.2.4), namely

$$V_{sd/pp'}(R) = -\frac{C_5}{R^5} - \frac{C_6}{R^6} - \frac{C_8}{R^8}\,. \tag{1.2.6}$$

Finally, the leading terms for $n_1d + n_2d$, labeled $V_{dd'}$, are

$$V_{dd'}(R) = -\frac{C_5}{R^5} - \frac{C_6}{R^6} - \frac{C_7}{R^7}\,. \tag{1.2.7}$$

Naturally, the C_n coefficients are different for the various asymptotes, and depend on the particular molecular symmetries considered (see [52] and Appendix A for details). For some applications, the details of the interactions are not crucial, and one can safely ignore effects such as fine structure coupling, ℓ-mixing, etc. For example, in the study of inhibition of Rydberg excitations due to long-range interactions [11], the interaction between atoms in $np_{3/2}$ states was described by the C_6-coefficient, assuming that all np states had the energy of the $np_{3/2}$ fine structure component. This approximation greatly simplified the description of the excitation dynamics. In addition, the internuclear separations R between atoms were significantly greater in [11] than those considered here, so that curve crossing/mixing was not an issue. To describe strong ℓ-coupling relevant for the molecular resonances, a much more accurate description of the interactions is needed. We have to diagonalize the interaction matrix to find molecular potentials and to see how states with different ℓ are coupled together.

The dispersion coefficients are obtained using perturbation theory. The technical details are explained in A.3. We give a list of the unperturbed molecular states in Table A.1 for the *ns-ns*, *np-np* and *nd-nd* asymptotes. In Tables A.2-A.6 we list the C_6, C_8, and C_{10} coefficients for the *ns-ns* asymptotes, the C_5, C_6, and C_8 coefficients for the *np-np* asymptotes and the C_5, C_6, and C_7 coefficients for the *nd-nd* asymptotes of all alkali atoms. The major dependence on n of C_5, C_6, C_7, C_8 and C_{10} is n^8, n^{11}, n^{12}, n^{15}, n^{22}, respectively. The residual dependence on n is fitted to a polynomial of the form $a + bn + cn^2$. In a few cases, for some symmetries and some values of n, two adjacent diatomic asymptotes are very close to each other and the second-order correction (A.3.9) gives large values. For these cases perturbation theory fails. We have added a resonance term of the form $c_1/(n - n_0)$ to the polynomial in order to simplify the representation of the data by the fitted polynomial when faraway from the resonance. Atomic fine structure, which is especially important for Rb and Cs, was ignored in these calculations. Depending on whether one takes the center-of-gravity for the energy levels entering the second-order perturbation expressions or the energy of one of the fine-structure components, for Rb the results deviate for some C_6 by a factor of 3-5. The reason for these large uncertainties is explained in the following section.

1.2.2 Potentials and symmetries: Hund's case (c)

The potentials in the previous section are obtained in the second order of perturbation theory, and thus share its limitations. In addition, the effects of spin and ℓ-mixing were ignored. To describe the resonances observed in a cold dense gas of rubidium Rydberg atoms, we cannot use them directly, since the interaction energies of pairs of Rydberg atoms contributing to these resonances are many times greater than the energies for which perturbation theory is applicable. Also, formally, the C-dispersion coefficients are well defined only if fine structure can be ignored, which is appropriate only if the energy separation between adjacent $n\ell + n'\ell'$ asymptotic levels is much greater then the relevant fine-structure splitting. This is not true for Rydberg states of rubidium. For example, the asymptotic ($R \to \infty$) spacing between the $70s_{1/2}+71s_{1/2}$ and $70p_{3/2}+70p_{3/2}$ levels is 213 MHz, and the fine-structure splitting of the $70p_{1/2}+70p_{1/2}$ and $70p_{3/2}+70p_{3/2}$ diatomic levels is 569 MHz. Depending on the energy separation, states belonging to different fine structure levels of $70p_j$+$70p_{j'}$ are coupled differently to the $\left|70s_{1/2}71s_{1/2}\right\rangle$ states. It turns out that the coupling between $|np_j np_{j'}\rangle$ and $\left|ns_{1/2}(n+1)s_{1/2}\right\rangle$ states is very important for the strongly attractive np+np potentials. This happens because the np states lie almost exactly halfway between the adjacent ns and $(n+1)s$ states, and because of the large dipole moments between ns and np, as well as $(n+1)s$ and np states. In our discussion, we focus on such strong potentials because they will mix with other potential curves as soon as they get close enough, resulting in avoided crossings and strong ℓ-mixing (especially the mixing of p-character which allows states with otherwise forbidden transitions to be coupled to the $5s$ ground state). An additional reason to include fine structure in our theoretical treatment is that the experiment [46] has shown that the resonances are related to certain fine-structure components.

We include long-range Rydberg-Rydberg interactions $V_{\mathrm{Ryd}}(R)$ and the atomic spin-orbit interaction H_{fs} (which gives rise to atomic fine structure). We then diagonalize the interaction matrix for a given R

$$U(R) = V_{\mathrm{Ryd}}(R) + H_{\mathrm{fs}} \,. \tag{1.2.8}$$

The eigenproblem of the interaction matrix is greatly simplified by molecular symmetry, which gives some good quantum numbers and a prescription for constructing a symmetry-adapted basis. As explained in section 1.1, for homonuclear diatomic molecules, the quantum numbers corresponding to the $D_{\infty h}$ point group are associated with rotations about the internuclear axis, reflections through a plane containing the rotation axis, and the inversion i of the spatial coordinates about the center point between both atom cores. The appropriate basis is given by Eq. (1.1.2). We choose to represent $U(R)$ in this basis since it is more appropriate to describe molecular asymptotes (at $R \to \infty$), and it facilitates the calculation of lineshapes (see next section). Note that only a few molecular states with similar quantum numbers n_1 and n_2 need to be considered, because coupling (i.e. the multipole matrix element $\langle n_1 j_1 || r^{\alpha} || n_2 j_2 \rangle$) vanishes very fast as $|n_1 - n_2|$ increases.

The resonances we want to describe require strong ℓ-mixing; the strong mixing of p

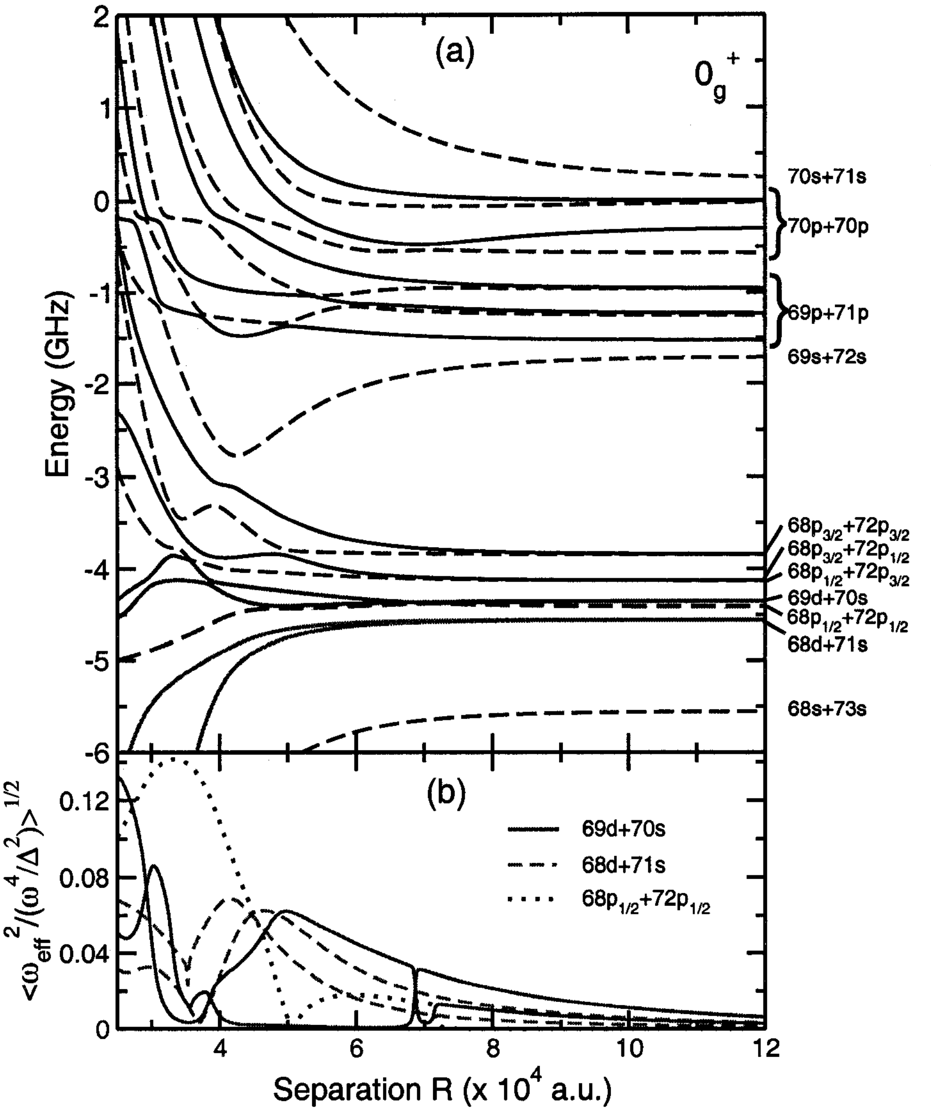

Fig. 1.1: (a) Potentials curves for the 0_g^+ symmetry. We present all the potential curves between $70s$+$71s$ and $68s$+$73s$. Molecular states, besides those that coincide with the asymptotic $70p + 70p$ states, may become accessible due to ℓ-mixing induced by interactions. The resonance is dominantly produced by the $69d + 70s$ states, altough, significant contributions are due to the $68d$+ $71s$ and $68p_{1/2} + 72p_{1/2}$ states. There are two $69d$+ $70s$ and $68d$+ $71s$ states of this symmetry and only one from the $68p_{1/2} + 72p_{1/2}$ asymptote. (b) Average radial dependencies of the two-photon Rabi frequency. The excitation probability of an atom pair depends on its separation R since the fraction of p-character of any molecular state is a function of R. The radial dependence is shown for all states of the three asymptotes contributing to the resonance.

character corresponds to crossings with the strongly attractive np+np potentials. As explained before, strong np+np potentials correspond to the ${}^1\Sigma_g^+ - {}^3\Sigma_u^+$ symmetries in Hund's case (a). After adding spin, there are three possible symmetries in Hund's case (c), 0_g^+, 0_u^- and 1_u, and only these states lead to strongly attractive potentials. Although molecular symmetries give a necessary condition for strong mixing, one has to diagonalize the interaction matrix (1.2.8) for each symmetry individually to find which states of these molecular configurations actually give strong mixing.

We consider dipolar and quadrupolar interactions only. The interactions obtained from Eq. (1.2.2) for $\ell = L = 1$ (dipole terms) and $\ell = L = 2$ (quadrupole terms) have the following form

$$V_L(R) \;=\; -\frac{(-1)^\ell 4\pi/\hat{L}}{R^{2L+1}} \sum_m B_{2\ell}^{L+m} r_1^L r_2^L Y_L^m(\hat{r}_1) Y_L^{-m}(\hat{r}_2), \tag{1.2.9}$$

where $L=1$ ($L=2$) for dipolar (quadrupolar) interactions and B_n^m is the binomial coefficient.

Defining $|a\rangle|b\rangle \equiv |n_a, \ell_a, j_a, m_a\rangle|n_b, \ell_b, j_b, \Omega - m_a\rangle$, one can show that the matrix elements of $V_\ell(R)$ are

$$\begin{aligned}\langle 1,2|V_L|3,4\rangle &= (-1)^{j_1+j_2+j_3+j_4+L-1-\Omega}\sqrt{\hat{\ell}_1\hat{\ell}_2\hat{\ell}_3\hat{\ell}_4\hat{j}_1\hat{j}_2\hat{j}_3\hat{j}_4}\;\frac{\mathcal{R}_{13}\mathcal{R}_{24}}{R^{2L+1}} \\ &\times \begin{pmatrix} \ell_1 & L & \ell_3 \\ 0 & 0 & 0 \end{pmatrix} \begin{pmatrix} \ell_2 & L & \ell_4 \\ 0 & 0 & 0 \end{pmatrix} \begin{Bmatrix} j_1 & L & j_3 \\ \ell_3 & \frac{1}{2} & \ell_1 \end{Bmatrix} \begin{Bmatrix} j_2 & L & j_4 \\ \ell_4 & \frac{1}{2} & \ell_2 \end{Bmatrix} \\ &\times \sum_{m=-L}^{L} B_{2L}^{L+m} \begin{pmatrix} j_1 & L & j_3 \\ -m_1 & m & m_3 \end{pmatrix} \begin{pmatrix} j_2 & L & j_4 \\ -\Omega + m_1 & -m & \Omega - m_3 \end{pmatrix},\end{aligned} \tag{1.2.10}$$

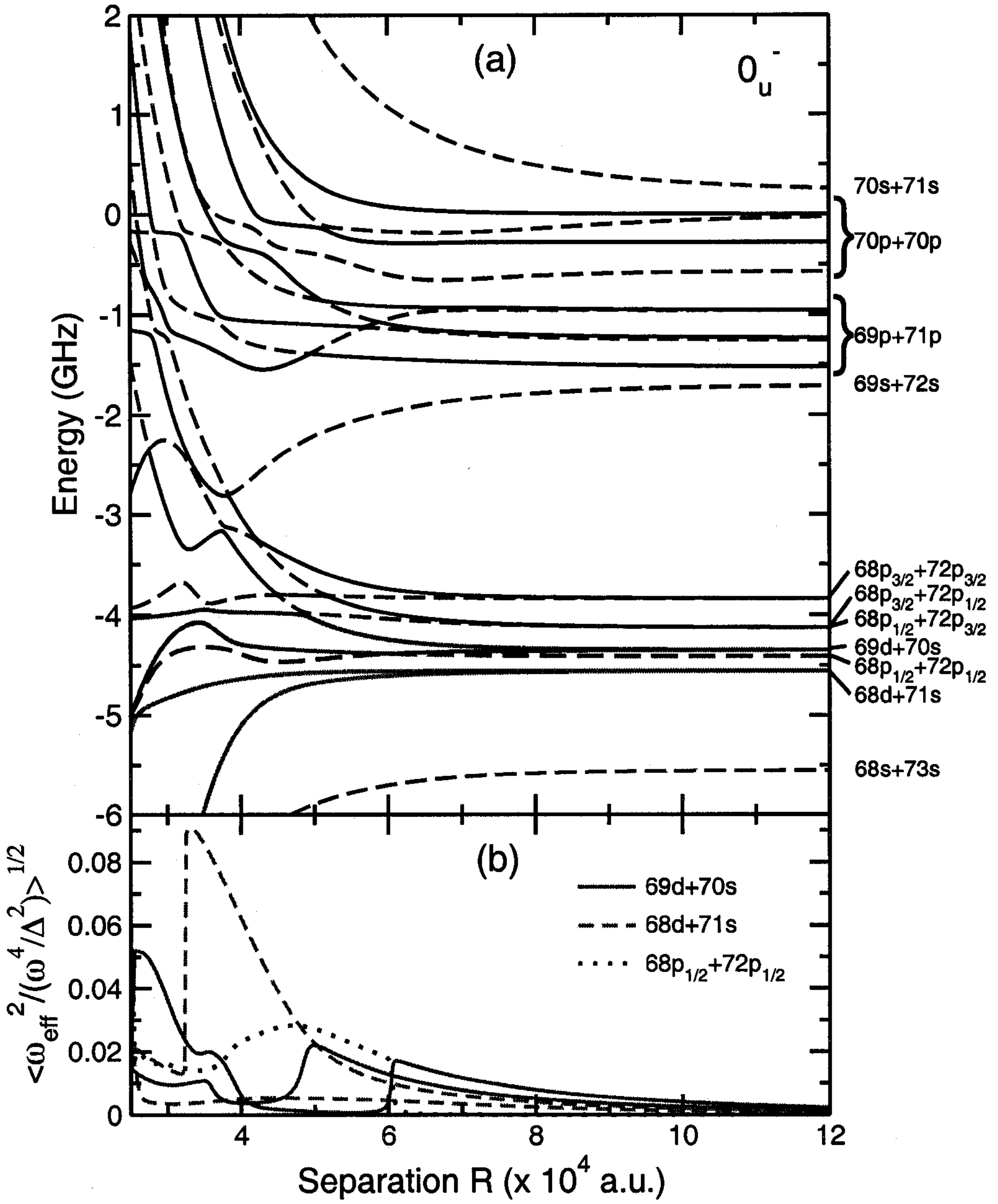

Fig. 1.2: Same as Fig. 1.1 but for the 0_u^- symmetry

where $\hat{\ell}_i = 2\ell_i + 1$, $\hat{j}_i = 2j_i + 1$, and $\mathcal{R}_{ij}$ is the radial part of the matrix element $\langle i|r^L|j\rangle$.

The asymptotic basis used to represent $U(R)$ consists of all $np+np$, $(n-1)d+ns$ and $(n-2)d+(n+1)s$ asymptotic states, as well as all the states in between with a significant coupling to these asymptotes. These include the $(n-1)p+(n+1)p$, $(n-1)s+(n+2)s$ and $(n-2)p+(n+2)p$ asymptotes. These states are our primary interest, but to describe them correctly at short internuclear distances one should also include other nearby states strongly coupled to them. Included nearby asymptotes are $ns+(n+1)s$, $(n-2)s+(n+3)s$, $(n-3)d+(n+2)s$, $nd+(n-1)s$, $(n-3)f+np$ and $(n-2)f+(n-1)p$. While the dipole-dipole interaction couples states belonging to different $n\ell + n'\ell'$ asymptotes, the quadrupole interaction is mainly relevant for states within the same $n\ell + n'\ell'$ asymptote. The only exceptions are the off-diagonal quadrupole matrix elements between $(n-1)d+ns$ and $(n-2)d+(n+1)s$ asymptotes. As mentioned before, the coupling depends on $|n_1 - n_2|$, or to be precise, $|n_1^* - n_2^*|$, where the quantum defect δ_ℓ is included in the effective principal quantum number n_i^* as follows: $n_i^* = n_i - \delta_\ell$. Since the difference in effective principal quantum numbers of states $(n-1)d$ and $(n+1)s$, as well as $(n-2)d$ and ns states, is only 0.22 for Rb (for high Rydberg states $\delta_{\ell=0} \approx 3.13$ and $\delta_{\ell=2} \approx 1.35$ [74]), the off-diagonal quadrupole matrix element is several times larger than the diagonal ones. These asymptotes are very close in energy (separated by only 200 MHz for $n=70$) so that at $R \sim 30000$ a_0 and $n=70$, quadrupole off-diagonal coupling is comparable with the asymptotic

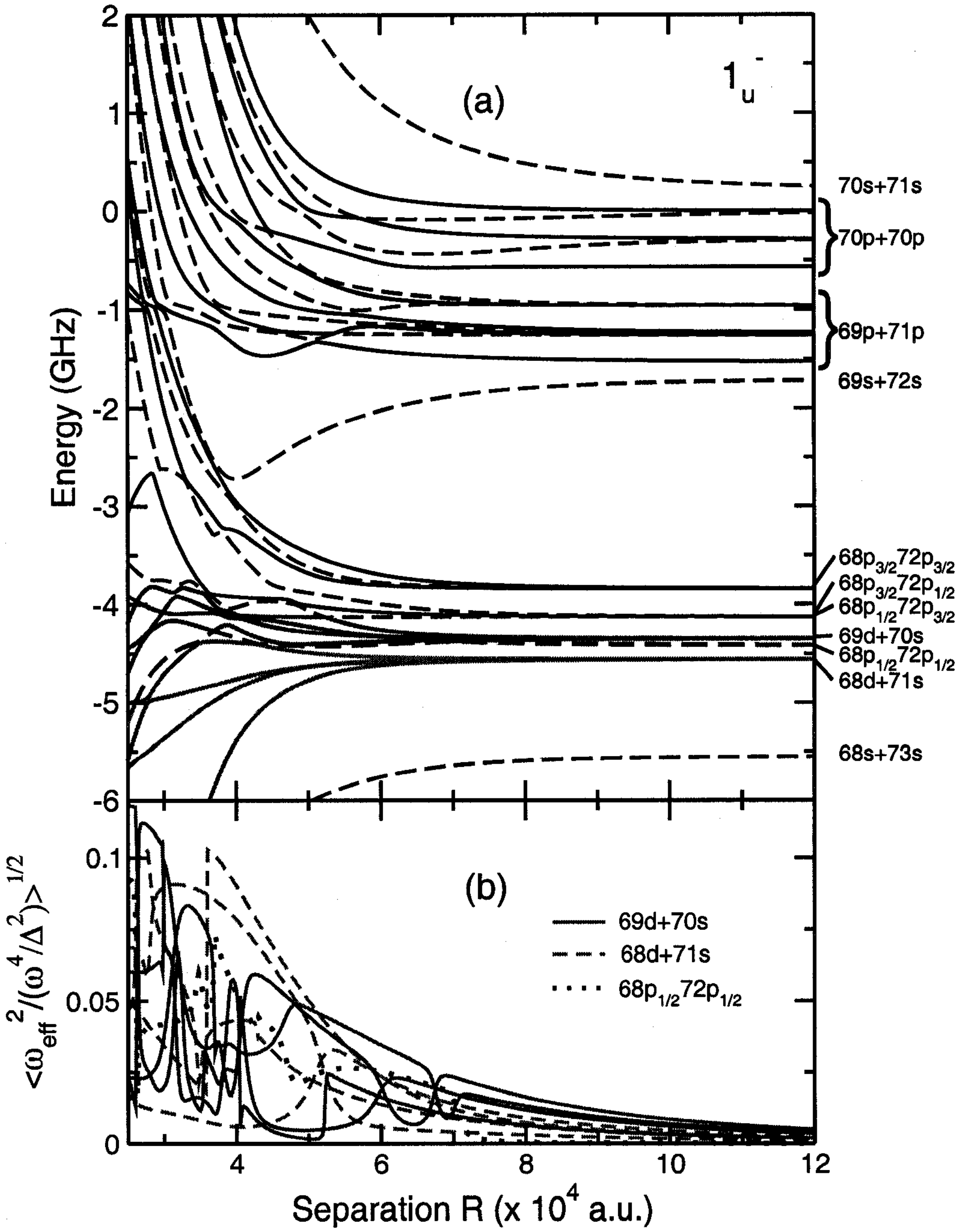

Fig. 1.3: Same as Fig. 1.1 but for the 1_u symmetry, except that each $nd + n's$ asymptote has four states of this symmetry.

energy spacing and these states become well mixed. This off-diagonal quadrupole coupling is relevant for the shape of $(n-1)d+ns$ and $(n-2)d+(n+1)s$ resonances.

1.3 Molecular resonances

In this section we primarily study the $(n-1)d+ns$ resonances reported in [46]. They occur at the average energy of excited atom pairs $(n-1)d$ and ns, and do not correspond to any single-atom transitions. The theoretical treatment of $(n-1)p_{3/2}+(n+1)p_{3/2}$ resonances is presented in [68] and the main results are collected in Appendix C. The contribution of diatomic potentials which coincide with the asymptotic $(n-1)d+ns$ levels is dominant, although, there is a significant contribution of $(n-2)d+(n+1)s$ and $(n-2)p_{1/2}+(n+2)p_{1/2}$ potentials, with approximately the same asymptotic energies. In one-photon transitions from the $5s$ ground state, dipole transitions to nd and ns states are not allowed. However, at high principal quantum numbers, long-range Rydberg-Rydberg interactions cause ℓ-mixing so that other molecular states, besides $np+np$, become accessible. Although the physics of this resonance and the $(n-1)p+(n+1)p$ one is very similar, the treatment of $(n-1)d+ns$ resonances is technically much more demanding. There are many more asymptotic states between $np+np$ and $(n-1)d+ns$ asymptotes and they all have to be included in order to describe the ℓ-mixing correctly. To make the potentials accurate at short distances, many nearby asymptotes have to be also included in the asymptotic basis. In addition, the laser intensity used to excite them was almost two order of magnitude greater than that used for $(n-1)p+(n+1)p$ resonances so there could be more power-dependent terms to consider, besides the two-photon Rabi frequency. We have used several different approaches to evaluate the results of the Rydberg excitation of atom pairs and they all give consistent results.

1.3.1 Excitation of a pair of interacting Rydberg atoms

We treat the $(n-1)d+ns$ molecular resonances as two-body phenomena, which is supported by the fact that their energies coincide with the average value of only two atomic energies [46]. The resonances are far red-detuned, so normally there should not be many excited atoms and presumably pair-wise excitation is the dominant mechanism. The general problem to be solved is the same as in [68] for $(n-1)p+(n+1)p$ resonances. However, the analysis of $(n-1)d+ns$ resonances is technically much more demanding and some approximations we have applied before may not be satisfactory here. To check it, we have used several different ways to evaluate the contributions to the number of excited atoms from various molecular states. We discuss them in the results section.

We consider a two-body Hamiltonian that includes long-range interactions and a linearly polarized optical field. For simplicity, we include only one molecular state $|\varphi_\lambda\rangle$ and the corresponding molecular potential $\epsilon_\lambda(R)$. The Hamiltonian is (in the rotating frame and in the rotating-wave approximation)

$$\begin{aligned} H &= \sum_{i=1}^{2}\left[\Delta\sigma_{ee}^{i}+\Delta'\sigma_{e'e'}^{i}\right]+\sum_{i=1}^{2}\left[\frac{\omega}{2}\sigma_{eg}^{i}+\frac{\omega'}{2}\sigma_{e'g}^{i}+\text{h.c.}\right] \\ &+\left[\Delta_{\lambda}+\epsilon_{\lambda}(R)\right]|\varphi_{\lambda}\rangle\langle\varphi_{\lambda}|\,, \end{aligned} \tag{1.3.1}$$

where ω, ω', and Δ, Δ' are single-photon Rabi frequencies and detunings relative to the $np_{3/2}$ and $np_{1/2}$ fine-structure components, respectively. Here Δ_{λ} is the two-photon detuning from the asymptotic $\epsilon_{\lambda}(R \to \infty)$ molecular level. The operators σ_{eg}^{i} and σ_{ee}^{i} are defined as follows: $\sigma_{eg}^{i}=\sum_{m}|e_i,m\rangle\langle g_i,m|$ and $\sigma_{ee}^{i}=\sum_{m}|e_i,m\rangle\langle e_i,m|$. To calculate ω and ω' we use the experimental values for the oscillator strength $f_{3/2}$ [73] and the ratio [72] $\omega/\omega' = \sqrt{f_{3/2}/f_{1/2}} \approx 2.3$, which reflects the non-statistical character of the oscillator strengths $f_{3/2}$ and $f_{1/2}$.

The excitation process is essentially a three-level scheme, although the number of states involved in the process is greater than three. We assume that a pair of ultracold Rb atoms is initially in the $5s+5s$ ground states. There are four possible ground states $|5s,m_j\rangle|5s,m_j'\rangle$, corresponding to different projections of spin $m_j = \pm 1/2$. Ultimately, the total probability is averaged over all possible initial states. In the first excitation step, one of the atoms is excited to a given np_j state. There are two intermediate states if the ground-state atoms have the same projections m_j, otherwise there are four of them. These intermediate states are further excited in the second step. The final state in this excitation scheme can be a single molecular state $|\varphi_{\lambda}(R)\rangle$ or a superposition of states. We consider both cases but in the equations a single molecular state is assumed. Including more states in the equations is very straightforward and there is no need to do it explicitly. Eventually, to get the final excitation probability per atom for a given optical frequency, the contributions from all molecular potentials and all atom pairs that include a given atom are collected.

To get pair excitation probabilities we are solving the time-dependent Schrödinger equation for the ground diatomic state, all intermediate states and a given doubly-excited molecular state $|\varphi_\lambda\rangle$. Here we present in detail the treatment if two m_j of the diatomic ground state are different and give the final result when they are the same (this case is considered in detail in [68] and Appendix C). Utilizing the fact that symmetric and antisymmetric states have independent time evolutions, the first step is to construct symmetric and antisymmetric combinations

$$|ij\rangle = \frac{1}{\sqrt{2}} \left\{ |i,m\rangle \, |j,-m\rangle + q \, |i,-m\rangle \, |j,m\rangle \right\}, \tag{1.3.2}$$

where $q = 1(-1)$ for symmetric(antisymmetric) states and $m = 1/2$ for linear laser polarization. In this way the diatomic ground state $|gg\rangle$, four intermediate states $|ge\rangle$, $|eg\rangle$, $|ge'\rangle$, $|e'g\rangle$, and four doubly-excited states $|ee\rangle$, $|ee'\rangle$, $|e'e\rangle$, $|e'e'\rangle$ are defined. Here e and e' refer to $np_{3/2}$ and $np_{1/2}$ states, respectively. If there were no interactions, diatomic states $|ee\rangle$, $|ee'\rangle$, $|e'e\rangle$, $|e'e'\rangle$ would be the states directly accessible in two-photon excitation. Any molecular state $|\varphi_\lambda\rangle$ is accessible if it has some components of these diatomic states. Due to ℓ-mixing induced by interactions, many $|\varphi_\lambda(R)\rangle$ gain a significant np fraction at some finite internuclear separation R.

The wave function is modeled as follows

$$|\psi\rangle = c_0 \, |gg\rangle + c_{11} \, |ge\rangle + c_{12} \, |eg\rangle + +c'_{11} \, |ge'\rangle + c'_{12} \, |e'g\rangle + c_2 \, |\varphi_\lambda\rangle \, . \tag{1.3.3}$$

Solving the time-dependent Schrödinger equation $i\partial\psi/\partial t = H\psi$ ($\hbar = 1$) leads to the coupled system for the excitation amplitudes $c(t)$,

$$
\begin{aligned}
i\frac{dc_0}{dt} &= \frac{\omega^*}{2}(c_{11}+c_{12})+\frac{\omega'^*}{2}(c'_{11}+c'_{12}), && (1.3.4)\\
i\frac{dc_{11}}{dt} &= \Delta c_{11}+\frac{\omega}{2}c_0+\frac{\omega^*}{2}\langle ee|\varphi_\lambda\rangle c_2+\frac{\omega'^*}{2}\langle e'e|\varphi_\lambda\rangle c_2, && (1.3.5)\\
i\frac{dc_{12}}{dt} &= \Delta c_{12}+\frac{\omega}{2}c_0+\frac{\omega^*}{2}\langle ee|\varphi_\lambda\rangle c_2+\frac{\omega'^*}{2}\langle ee'|\varphi_\lambda\rangle c_2, && (1.3.6)\\
i\frac{dc'_{11}}{dt} &= \Delta c'_{11}+\frac{\omega'}{2}c_0+\frac{\omega^*}{2}\langle ee'|\varphi_\lambda\rangle c_2+\frac{\omega'^*}{2}\langle e'e'|\varphi_\lambda\rangle c_2, && (1.3.7)\\
i\frac{dc'_{12}}{dt} &= \Delta c_{12}+\frac{\omega}{2}c_0+\frac{\omega^*}{2}\langle ee|\varphi_\lambda\rangle c_2+\frac{\omega'^*}{2}\langle ee'|\varphi_\lambda\rangle c_2, && (1.3.8)\\
i\frac{dc_2}{dt} &= (\Delta_\lambda+\epsilon_\lambda(R))c_2+\left(\frac{\omega}{2}\langle\varphi_\lambda|ee\rangle+\frac{\omega'}{2}\langle\varphi_\lambda|e'e\rangle\right)c_{11}+\left(\frac{\omega}{2}\langle\varphi_\lambda|ee\rangle+\frac{\omega'}{2}\langle\varphi_\lambda|ee'\right)c_{12}\\
&\quad+\left(\frac{\omega}{2}\langle\varphi_\lambda|ee'\rangle+\frac{\omega'}{2}\langle\varphi_\lambda|e'e'\rangle\right)c'_{11}+\left(\frac{\omega}{2}\langle\varphi_\lambda|ee\rangle+\frac{\omega'}{2}\langle\varphi_\lambda|ee'\rangle\right)c'_{12}. && (1.3.9)
\end{aligned}
$$

The analogous system of equations for $m_j = m'_j = 1/2$ was considered in detail [68] and is shown in Appendix C for the analysis of $(n-1)p + (n+1)p$ resonances. The projections onto the molecular state are defined as: $a_{ee}(\lambda) = \langle ee|\varphi_\lambda\rangle$, $a_{ee'}(\lambda) = \langle ee'|\varphi_\lambda\rangle$, $a_{e'e}(\lambda) = \langle e'e|\varphi_\lambda\rangle$, and $a_{e'e'}(\lambda) = \langle e'e'|\varphi_\lambda\rangle$. We assume that all of the a_{ij} coefficients are real.

One can obtain a tractable system after the elimination of the excitation amplitudes of all intermediate states. This is justified by the fact that the dominant frequencies governing their time evolutions are Δ and Δ' which are much larger than the relevant Rabi frequencies. On a molecular resonance, Δ and Δ' are about $2\pi \cdot 2.2$ GHz, while the peak values of ω and ω' are about 2.3 GHz and 1 GHz, respectively (for the actual experimental parameters). Laser intensities used in this experiment were almost two order of magnitude higher than the ones used for the $(n-1)p+(n+1)p$ resonances so that we have to check for the effects of higher laser fields. We adiabatically eliminate c_{11}, c_{12}, c'_{11} and c'_{12}, as in [68], but this time keeping power-dependent terms. The result is equivalent to the Bloch equations of a two-level system

$$\begin{aligned} i\frac{dc_0}{dt} &= -\omega_g(t)c_0 - \frac{\omega^*_{\text{eff}}}{2}c_2 &\quad (1.3.10)\\ i\frac{dc_2}{dt} &= \left[\Delta_\lambda + \epsilon_\lambda(R) - \omega_e(t)\right]c_2 - \frac{\omega_{\text{eff}}}{2}c_0, &\quad (1.3.11)\end{aligned}$$

where the effective two-photon Rabi frequency is

$$\omega_{\text{eff}} = \frac{\omega^2}{\Delta}a_{ee}(\lambda) + \frac{\omega\,\omega'}{2}\frac{\Delta+\Delta'}{\Delta\,\Delta'}\left(a_{ee'}(\lambda) + a_{e'e}(\lambda)\right) + \frac{\omega'^2}{\Delta'}a_{e'e'}(\lambda), \qquad (1.3.12)$$

and the power-dependent terms ω_g and ω_e are

$$\begin{aligned} \omega_g &= \frac{|\omega|^2}{2\Delta} + \frac{|\omega'|^2}{2\Delta'}, &\quad (1.3.13)\\ \omega_e &= \frac{|\omega a_{ee} + \omega' a_{e'e}|^2}{4\Delta} + \frac{|\omega a_{ee} + \omega' a_{ee'}|^2}{4\Delta} + \\ &\quad \frac{|\omega'(t)a_{e'e'} + \omega(t)a_{ee'}|^2}{4\Delta'} + \frac{|\omega' a_{e'e'} + \omega a_{e'e}|^2}{4\Delta'}. &\quad (1.3.14)\end{aligned}$$

These $\omega_g(t)$ and $\omega_e(t)$ can be interpreted as power dependent shifts of the diatomic ground and doubly-excited states, respectively. Also, ω_g is much greater than ω_e because it does not depend on a_{ij}, which measure the p-character of the doubly-excite state. For the experimental parameters, the peak value of $\omega_g(t)$ on a molecular resonance is about 280 MHz, which is comparable with the laser bandwidth.

In the vicinity of the molecular resonance, the second term on the right-hand side of Eq. (1.3.10) is much smaller than the first one, and thus can be ignored. After neglecting that term, Eq. (1.3.10) can be solved

$$c_0(t) = \exp\left[i \int_{t_0}^{t} \omega_g(t')\, dt'\right]. \tag{1.3.15}$$

This c_0 can be used to find c_2 after the phase transformation $c_2 \equiv \exp[-i(\Delta_\lambda + \epsilon_\lambda(R))t - \int_{t_0}^{t} \omega_e(t')\, dt']\bar{c}_2$ is performed. The excitation amplitude $\bar{c}_2$ is

$$\bar{c}_2 = i \int_{t_0}^{t} dt_1 \frac{\omega_{\text{eff}}(t_1)}{2} e^{i(\Delta_\lambda+\epsilon_\lambda(R))t_1+\int_{t_0}^{t_1}(\omega_g(t_2)-\omega_e(t_2))dt_2}. \tag{1.3.16}$$

We assume that excitation laser pulses have a Gaussian time profile. It has been shown that the excess bandwidth in this experimental setup is mainly due to a linear frequency chirp. Because of the constant ratio ω/ω', both ω and ω' have the same time dependence $\omega, \omega' \sim \exp(-(1+i\gamma)t^2/\sigma^2$, where σ measures the pulse duration and γ is a chirp parameter related to the laser bandwith Γ and duration σ as follows

$$\gamma = \sqrt{\frac{\pi^2\Gamma^2\sigma^2 - 2\ln 2}{2\ln 2}}. \tag{1.3.17}$$

The probability to excite $|\varphi_\lambda(R)\rangle$ from the initial state $|5s, m_{1/2}\rangle|5s, m_{1/2}\rangle$ is $P_1(\lambda) = |\bar{c}_2(t \to \infty)|^2$. According to Eqs. (1.3.13-1.3.14), ω_g and ω_e do not depend on the chirp. If ω_g and ω_e in Eq. (1.3.16) can be ignored, a simple formula can be derived [68].

$$|\bar{c}_2|^2 = \frac{\beta^2(\lambda)\pi}{2} \frac{I^2}{I_{\text{sat}}^2} \frac{\pi \ln^2 2}{\tau^3 \Gamma} 2^{-[\Delta_\lambda+\epsilon_\lambda(R)]^2/2\pi^2\Gamma^2}, \tag{1.3.18}$$

where I_{sat} is the saturation intensity for ideal unchirped light and isolated $np_{3/2}$ atoms and τ is a Gaussian pulse duration (FWHM). The approximation applied to get this formula is equivalent to neglecting the ω_e-term in Eq. (1.3.11) and both terms in the right-hand side of Eq. (1.3.10) (i.e. using $c_0 = 1$). In Eq. (1.3.18), $\beta(\lambda)$ is a time-independent part of ω_{eff} defined via $\omega_{\text{eff}}(t) = \beta(\lambda)\omega^2(t)$.

If all a-coefficients are equal to zero, according to Eq. (1.3.12), the effective two-photon Rabi frequency is also zero. These coefficients measure different p-characters in $|\varphi_\lambda(R)\rangle$. To evaluate them, we have to express the double-excited states $|ee'\rangle$, $|ee\rangle$, and $|e'e'\rangle$ (defined in the space-fixed frame) in the molecule-fixed reference frame, where all $|\varphi_\lambda(R)\rangle$ are naturally defined [68]. Apparently, all angular dependence related to different orientations of the molecular axis is contained in these a-coefficients, and the observable quantities have to be averaged over all spatial orientations of the internuclear axis.

For the case $m_j = m_j' = \pm 1/2$, the ground and doubly-excited states are respectively $|gg\rangle = |g,m\rangle|g,m\rangle$ and $|ee\rangle = |e,m\rangle|e,m\rangle$. Intermediate states $|ge\rangle$, $|ge'\rangle$ and doubly-excited state $|ee'\rangle$ have the form $|ij\rangle = \frac{1}{\sqrt{2}}\{|i,m\rangle|j,m\rangle + |j,m\rangle|i,m\rangle\}$. The coefficients a_{ij} are defined as before. After the elimination of excitation amplitudes of all intermediate states, one gets again the system (1.3.10-1.3.11) with different $\omega_{\text{eff}}(t)$ and $\omega_e(t)$

$$\omega_{\text{eff}} = \frac{\omega^2}{\Delta}a_{ee}(\lambda) + \frac{\omega\,\omega'}{\sqrt{2}}\frac{\Delta+\Delta'}{\Delta\,\Delta'}a_{ee'}(\lambda) + \frac{\omega'^2}{\Delta'}a_{e'e'}(\lambda), \tag{1.3.19}$$

$$\omega_e = \frac{|\omega a_{ee} + \omega' a_{ee'}/\sqrt{2}|^2}{2\Delta} + \frac{|\omega' a_{e'e'} + \omega a_{ee'}/\sqrt{2}|^2}{2\Delta'}. \tag{1.3.20}$$

The solutions for these initial states are also given by Eq. (1.3.16), or for low laser intensity by Eq. (1.3.18). These excitation probabilities must also be averaged over all spatial orientations of the internuclear axis. In (1.3.18) this is applied to $\beta(\lambda)$

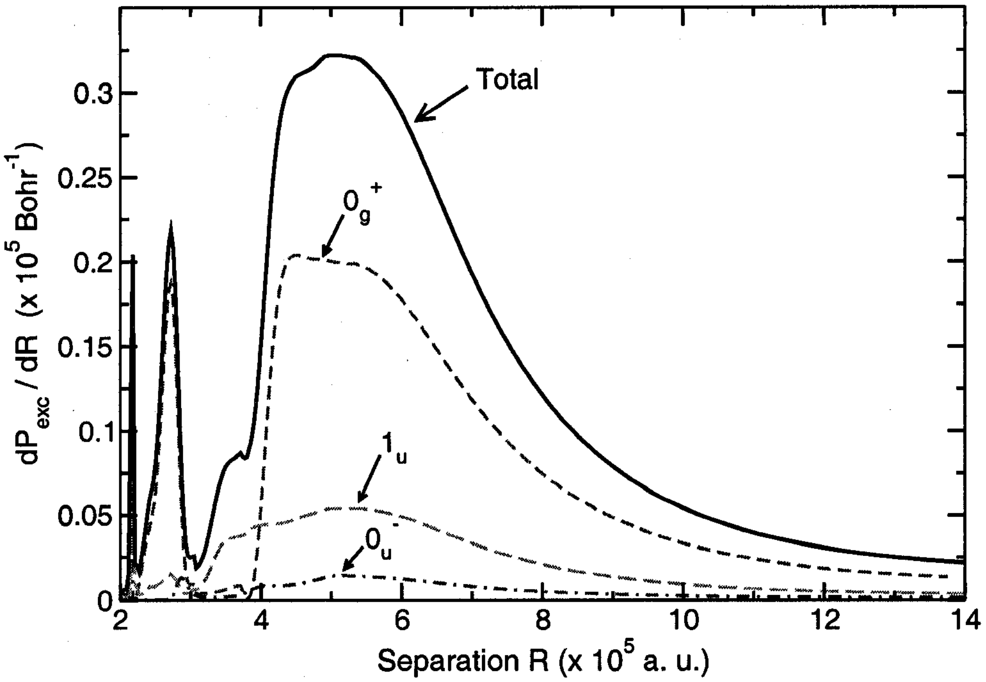

Fig. 1.4: Pair excitation probability as a function of separation R. We show contributions from all states associated with the three most relevant asymptotes. The total dependence includes twice the contribution of 1_u since this state is two-fold degenerate. According to Eq. (1.3.21), $dP_{\rm exc}/dR = 4\pi\rho R^2 P_2(R)$,where $P_2(R)$ is the excitation probability of an atom pair. Note that the weighted factor R^2 is included in the shown dependence. This figure shows that pairs at shorter distances are difficult to excite, even though ℓ- mixing and their $\langle\omega^2_{\rm eff}\rangle$ is much greater there (Figs. 1.1-1.3) because they are very detuned from the resonance. The main contribution comes from pairs at separations $R \geq 40000\ a_0$.

only.

For an unpolarized sample of ultracold atoms, all initial states are equally probable, so that excitation probabilities have to be averaged over all initial diatomic states and then all contributions to a given $|\varphi_\lambda(R)\rangle$ are summed up. This is done for many $|\varphi_\lambda\rangle$ to include the possibility of exciting different molecular potentials. The result is the averaged excitation $P_2(R)$ of an atom pair. The excitation probability per atom is the sum of all excitation probabilities of atom pairs that include a given atom,

$$P_{\text{exc}} = 4\pi \int_0^\infty dR\, R^2 \rho\, P_2(R), \tag{1.3.21}$$

where ρ is the sample density.

Molecular potentials can be very close to each other for some R, as shown in Figs. 1-3. For such R atom pairs are excited into superpositions of molecular states. Altough the extension of the system (1.3.4-1.3.9) to include more molecular states $|\varphi_\lambda\rangle$ is simple, the technical difficulties of solving it are not negligible. Not only do we have four parameters to vary (R, I, laser frequency and the orientation of the molecular axis), but we also have many molecular potentials and several symmetry cases. Also, for a given optical frequency, different molecular states are excited at different distances R. This is especially true at short R for which the potentials vary significantly. Instead of doing this, we choose a different approach to account for possible superpositions of molecular states. This approach is in many ways as complete as the full numerical calculation that includes the full set of doubly-excited states and at the same time is no more difficult than the calculation of molecular potentials itself. As Eq. (1.3.18) suggests, only a few parameters related to the excitation laser, such as the bandwidth and pulse duration, are important. The details of the laser pulse cannot be of fundamental importance, so we can substitute for the actual chirped Gaussian pulse a square pulse with the parameters chosen to give probabilities consistent with (1.3.18). We have to match the pulse area and the width (actually FWHM) of the Fourier spectrum corresponding to the two-photon Rabi frequency ω_{eff}. Therefore, Γ

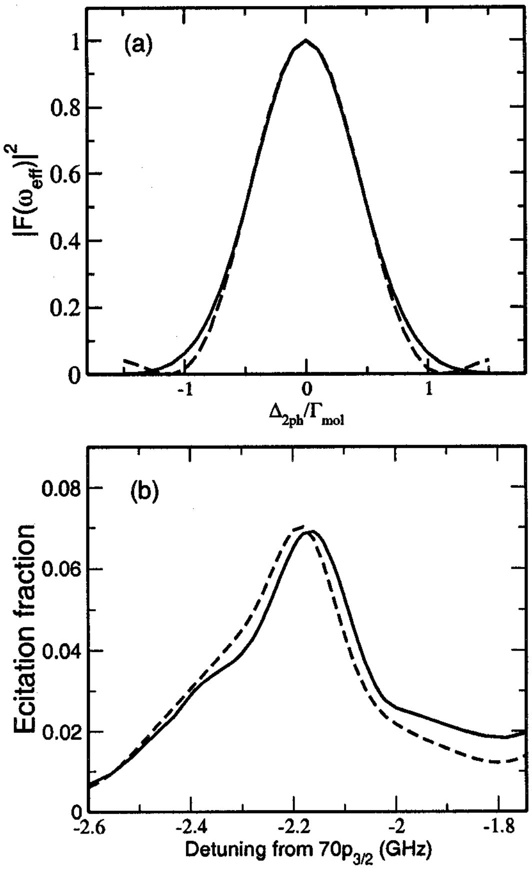

Fig. 1.5: (a) Fourier transforms of $\omega_{2\text{ph}}(t)$ of a chirped Gaussian pulse (dashed line) and its counterpart square pulse (solid line). The pulse areas and $\Gamma_{2\text{ph}}$ (FWHM) of $\omega_{2\text{ph}}(t)$ for both pulses are matched to minimize the difference in the excitation probabilities. The tail of the square pulse vanishes much slower so it is truncated at $\Delta_{2\text{ph}}/\Gamma_{2\text{ph}} = 1.6$, where $\Delta_{2\text{ph}}$ is two-photon detuning. The remaining small difference between the pulses is expected to diminish further after summing over all atom pairs in (1.3.29). (b) Comparison between calculated molecular signals using Eq. (1.3.18) (dashed line) and Eq. (1.3.24) (solid line). The latter one is based on the exact solution for a square pulse assuming that, in general, superpositions of molecular states are excited. The differences are somewhat larger just above the molecular resonance, where there are many very close molecular potentials, as shown in Figs. 1.1-1.3. The assumed laser bandwidth in this plot is 200 MHz.

and τ are not our direct concern, but rather Γ_{2ph} and T_{2ph}, which characterize $\omega_{\text{eff}}(t)$. For a Gaussian pulse $\Gamma_{\text{2ph}} = \sqrt{2}\Gamma$. This Γ_{2ph} would also be the FWHM of a square pulse if its duration were chosen to be $T_{\text{sq}} = 2.783/\pi\Gamma_{\text{2ph}}$. The single-photon Rabi frequency ω_{sq} of the square pulse is chosen to provide equal pulse areas of $\omega_{\text{eff}}(t)$ of the actual pulse and its substitute. A great adventage of this approach is that now we can easily write and calculate the exact excitation probabilities of all molecular states. The total Hamiltonian H_{tot} of the system consists of the long-range interaction part $U(R)$, given by Eq. (1.2.8) and the optical field ($\hbar = 1$).

$$H_{\text{tot}}(R) = U(R) + \sum_{i=1}^{2} \left[\Delta\sigma^i_{ee} + \Delta'\sigma^i_{e'e'}\right] + \sum_{i=1}^{2} \left[\frac{\omega_{\text{sq}}}{2}\sigma^i_{eg} + \frac{\omega'_{\text{sq}}}{2}\sigma^i_{e'g} + \text{h.c.}\right]. \qquad (1.3.22)$$

To represent H_{tot} we use the basis of $U(R)$ completed by the intermediate states and the ground diatomic states. The matrix elements of H_{tot}, corresponding to these added basis states, are essentially given by Eqs. (1.3.4-1.3.9). The only modification is to replace $|\varphi_\lambda\rangle$ by a superposition of different $|\varphi_\lambda\rangle$. The matrix of H_{tot} is only slightly bigger than the matrix of $U(R)$, so solving the eigenproblem of H_{tot} does not impose additional difficulties. If $\varepsilon_i(R)$ are the eigenvalues related to the eigenvectors $|\phi_i(R)\rangle$ of $H_{\text{tot}}(R)$, then the solution of the time-dependent Schrödinger equation $i\partial\,|\psi\rangle\,/\partial t = H_{\text{tot}}\,|\psi\rangle$ is

$$|\psi(t;R)\rangle = \sum_i \langle\phi_i(R)|gg\rangle\, e^{-i\varepsilon_i(R)t}\,|\phi_i(R)\rangle\,. \qquad (1.3.23)$$

Unlike Eqs. (1.3.16,1.3.18), the last formula does not give unphysical probabilities for large laser power. In the actual calculation we use a modification of Eq. (1.3.23) to account for the difference in excitation probabilities for large detunings. Excitation probabilities for a square pulse do not vanish sufficiently fast. This happens because the tails of the Fourier spectra of these two types of pulses are very different at large detunings. This is illustrated in Fig. 1.5(a). We overcome this by truncating the contributions from large detunings

$$|\psi_e(t;R)\rangle = \sum_i \Theta(|\varepsilon_i(R) - 2\Delta| - \eta\Gamma_{\mathrm{mol}})\, \langle\phi_i(R)|gg\rangle\, e^{-i\varepsilon_i(R)t}\, |\phi_i(R)\rangle\,, \qquad (1.3.24)$$

where Θ is the Heaviside function and η is the cut-off parameter (our choice $\eta = 1.6$ is justified by Fig. 1.5(a)). We note that the radial dependence, shown in Fig. 1.4, is obtained using the last equation. One can find the same dependence using the simpler formula (1.3.16). Both ways give essentially the same radial dependence. In the last formula all $\varepsilon_i(R)$ are expressed with respect to the energy of asymptotic $np_{3/2}+np_{3/2}$ states.

1.3.2 n-scaling

Now we estimate the major contribution to the n-scaling of the $(n{-}1)d+ns$ resonance signal. For this purpose we use a rather simplified description of these states and the resonances. First we ignore fine structure. As Fig. 1.4 suggests, the major contribution to the molecular signal does not come from the region of strong ℓ-mixing, but rather from the long-range region with considerably weaker mixing. In this estimate we completely neglect the contribution of strong ℓ-mixing at short R to the molecular

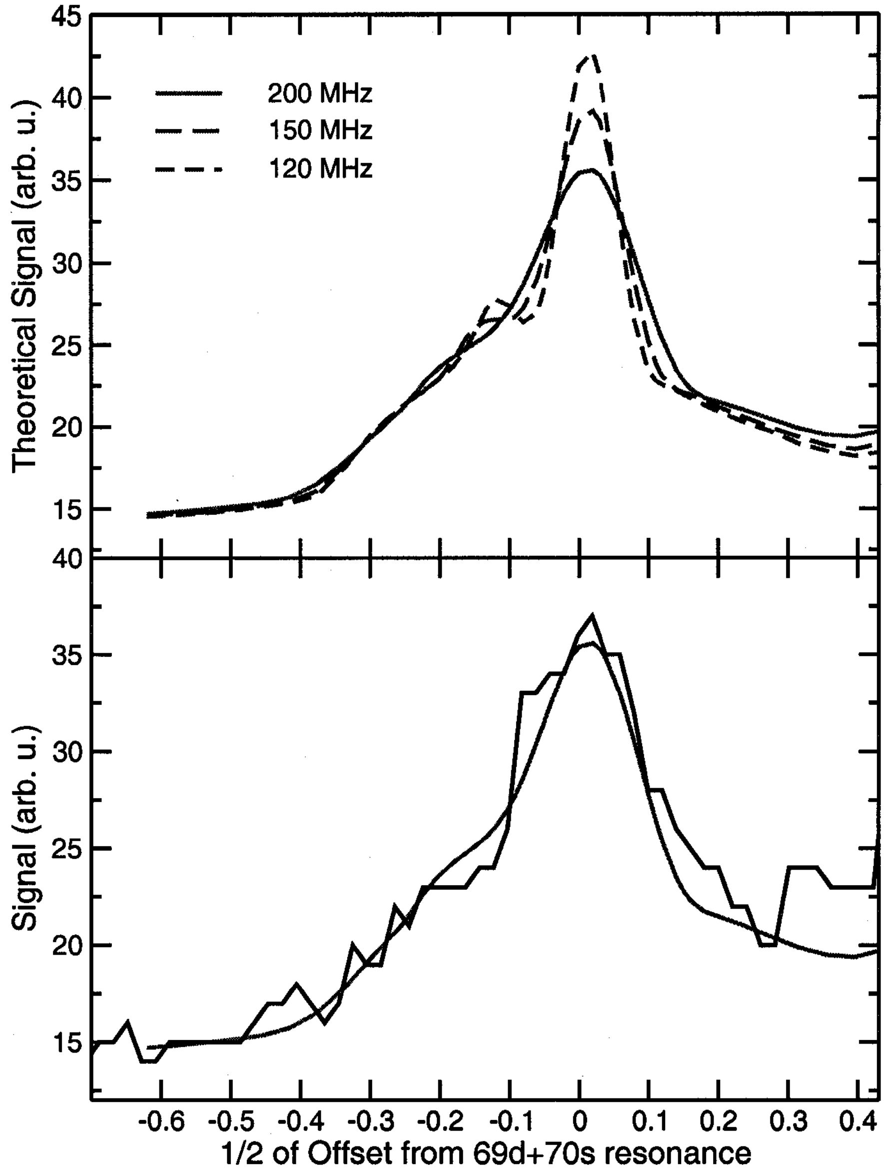

Fig. 1.6: (a) Calculated molecular signal for different laser bandwidths of the excitation laser, as indicated in the plot. The linewidth of the resonance is dominantly determined by the details of long-range interactions and it is significantly larger than the laser bandwidth. (b) Comparison of the theoretical signals shown in Fig. 1.5(b) and experimental one. This is the best fit of the experimental data, altough the actual bandwidth was likely smaller than the one we used for the comparison.

signal. The wave function of $(n-1)d+ns$ states can be expanded as follows

$$|(n-1)d\,ns;R\rangle = |(n-1)d\,ns^{(0)}\rangle + \alpha_{pp}(R)|np\,np^{(0)}\rangle + |\varphi_{res};R\rangle\ , \tag{1.3.25}$$

where $|\varphi_{res};R\rangle$ is the residue of the expansion and $|ndn's^{(0)}\rangle$, $|npnp^{(0)}\rangle$ are asymptotic states $|(n-1)dns;R\rightarrow\infty\rangle$ and $|npnp;R\rightarrow\infty\rangle$. In general, there are more than one $|np\,np^{(0)}\rangle$ state in the last expansion but the scaling law, in this approximation, does not depend of their number so keeping only one term is sufficient for our purpose. We want to find the function $\alpha_{pp}(R)$ because the two-photon Rabi frequency is directly proportional to it. The Hamiltonian is still given by Eq. (1.2.8). In the first approximation $\alpha_{pp}(R)$ is

$$\alpha_{pp}(R) = \frac{\langle np\,np^{(0)}|V_{Ryd}(R)|nd\,n's^{(0)}\rangle}{Eds_0 - Epp_0}, \tag{1.3.26}$$

where $Eds_0 - Epp_0$ is the asymptotic energy spacing of diatomic $(n-1)d+ns$ and $np+np$ levels. The last formula is valid in the region of weak ℓ-mixing for $(n–1)d+ns$ states. We conclude that

$$\alpha_{pp}(R) \sim n^7/R^3, \tag{1.3.27}$$

since only the dipole-dipole part of $V_{Ryd}(R)$ couples those asymptotic states, and $Eds_0 - Epp_0 \sim n^{-3}$.

We proceed using the results of the previous sections, but ignoring many details which are not of great importance for n-scaling. The n-scaling is well defined only if there is no saturation of excitation so that the two-photon absorption probability P_2 per pair is

$$P_2 \sim |\omega_{\text{eff}}|^2 \,. \qquad (1.3.28)$$

We have $\omega_{\text{eff}} \sim \omega^2 \alpha_{pp}(R)/\Delta$, where ω is the single-atom Rabi frequency defined in the previous sections and $\Delta \approx (Eds_0 - Epp_0)/2$ is the detuning from the atomic np resonance. Note that ω^2/Δ is in the first approximation n-independent because the single photon Rabi frequency ω scales as the dipole matrix element $n^{-3/2}$ and $\Delta \sim n^{-3}$.

To get the excitation probability P_{exc} we use Eq. (1.3.28)

$$P_{\text{exc}} \sim \frac{\omega^4}{\Delta^2} \int_{R_0}^{\infty} dR\, R^2 |\alpha_{pp}(R)|^2 \sim n^{14}/R_0^3. \qquad (1.3.29)$$

The lower limit R_0 is set as follows. We assume that the laser frequency corresponds to the two-photon resonance, whose position coincides, to a very good approximation, with the asymptotic energy of the $(n-1)d + ns$ state. A pair of atoms will be out of two-photon resonance if its interaction energy $U_{ds}(R_0)$ is greater than $\Gamma_{2ph} \sim \Gamma$, therefore $|U_{ds}(R_0)| \sim \Gamma$. Because the laser bandwidth is considerably narrow (close to the Fourier transform limit), $U_{ds}(R_0)$ is not very large, and assuming weak ℓ-mixing, we can use second order perturbation theory to find an estimate for it. Eventhough the $(n-2)p + (n+2)p$ states are very close to $(n-1)d + ns$ states, they are very weakly coupled to them so they basically have no influence on this estimate. Ignoring the fine structure of $(n-1)d + ns$ states, $|U_{ds}(R_0)|$ should be equal to $|C_6|/R_0^6$, where C_6 is the C coefficient for the $(n-1)d + ns$ state. The estimate for the lower limit R_0

is $R_0^{-3} \sim \sqrt{\Gamma/|C_6|}$. Since $C_6 \sim n^{11}$, we finally find

$$P_{\text{exc}} \sim n^{8.5}. \tag{1.3.30}$$

1.3.3 Results and discussion

Numerical evaluation of excitation probabilities

We have used four different ways to evaluate excitation probabilities. One has to verify that the approximations are applicable for all conditions under which they are used. These conditions are different for different asymptotes. One can try to use the method [68] (based on Eq. (1.3.18)) to get the lineshape of $(n-1)d + ns$ resonances. However, it is assumed in this method that the effective two-photon Rabi frequency is sufficiently small and the molecular potentials are well separated. Therefore, for any pair of atoms at a certain separation R, only one doubly-excited molecular state is involved in the excitation (not necessarily the same one for all R). However, the two-photon Rabi frequency is almost an order of magnitude higher in this case so it is not obvious that some power-dependent terms can always be ignored. Such terms are included in Eq. (1.3.16). We find that, for most potentials, the formulae (1.3.16)-(1.3.18) give overall very similar lineshapes, with the position of the resonance slightly shifted, but the shape and amplitude are well preserved. It turns out that the approximate Eqs. (1.3.18) and (1.3.16), for the experimental parameters, cannot be used for all laser frequencies and all asymptotes. By varying the laser frequency, we actually vary the region of internuclear separations R for which

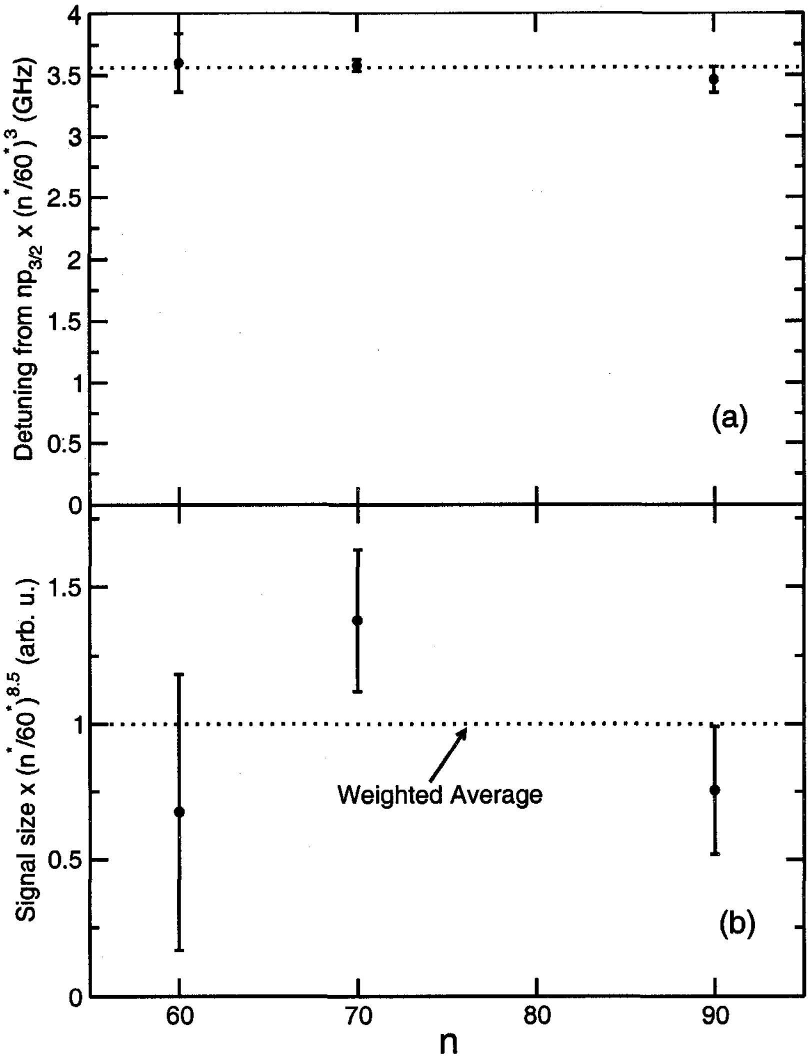

Fig. 1.7: (a) Scaling of the position of molecular $(n{-}1)d{+}ns$ resonances with respect to the atomic $np_{3/2}$ resonance. The position follows the characteristic n^{-3} scaling. (b) Scaling of the molecular signal. Here we test the expected $n^{8.5}$ scaling (1.3.30). This comparison is more difficult to make because many experimental conditions influence the signal. This plot shows a reasonable agreement with the $n^{8.5}$ scaling.

atom pairs are on resonance. The two-photon Rabi frequency ω_{eff} is R-dependent and, if the ℓ-mixing is too large, the approximations may not be be valid. To check if such parameters significantly affect the final probabilities, we have numerically solved the system (1.3.4)-(1.3.9).

It is solved for many different internuclear separations, spatial orientations of the molecular axis, laser intensities and laser frequencies. This calculation is repeated for the states $|\varphi_\lambda\rangle$ which have dominant contributions to the resonance lineshape. They coincide with the asymptotic $69d+70s$, $68d+71s$ and $68p_{1/2}+72p_{1/2}$ states. In these numerical calculations, only one molecular state $|\varphi_\lambda\rangle$ was considered as a final doubly-excited state of an atom pair. As explained previously, at some R, one should consider superpositions of molecular states $|\varphi_\lambda\rangle$. This is taken into account in Eqs. (1.3.23) and (1.3.24). Even though we do not consider the actual pulse shape in this case, the parameters of the substituted pulse are chosen to minimize any quantitative difference between the pulses. Since we use exact solutions of (1.3.22), this approach should give a rather fair description of the resonance phenomenon.

It turns out that all these different methods lead to the same physical results, although, for some particular parameters, they may be significantly different. Most of the differences vanish after summing over all potential curves and all atom pairs. The remaining variations are mainly due to the slight difference in the resonance positions and lineshapes obtained using different methods. The real physical parameters, such as the linewidth, signal size, n-scaling or even the resonance position, are practically unchanged, as shown in Fig. 1.5. Here we present the result based on Eqs. (1.3.23)-(1.3.24), the most complete method we use, and the results from the simplest method based on Eq. (1.3.18). This gives an estimate of the variations between these methods. Our calculation shows that the probabilities of the 0_u^- asymptotes are about one order of magnitude less then the contribution of the other two symmetries so that for 0_u^- symmetry we only use Eq. (1.3.16). Interestingly, for $(n-1)p+(n+1)p$ resonances, the contribution of the 0_g^+ symmetry was insignificant.

Comparison with theoretical lineshapes

In Figs. 1.1(a)-1.3(a), we show three sets of molecular potentials corresponding to the three symmetries considered. At short distances these potentials have very complicated shapes due to multiple avoided crossings. At these avoided crossings the ℓ-mixing is the strongest. The $np+np$ components of various nearby potentials are the most important for the molecular resonance. The relevant physical quantity which depends on the fraction of $np+np$ states is the two-photon Rabi frequency ω_{eff}, defined by Eq. (1.3.12). Asymptotes $(n-1)d+ns$, $(n-2)d+(n+1)s$ and $(n-2)p_{1/2}+(n+2)p_{1/2}$ give the essential contributions to the resonance. In parts (b) of Figs. 1.1-1.3 we present the magnitude of the radial dependence ω_{eff} for the three asymptotes and all their states. For each of these states, the radial dependence is obtained after averaging ω_{eff}^2 over different orientations of the molecular axis and initial states. Even though ω_{eff} for atom pairs at short distances is larger due to stronger ℓ-mixing, such pairs are difficult to excite because they are very detuned from the molecular resonance. The actual pair excitation probability as a function of R, on exact molecular resonance, is shown in Fig. 1.4. The weighting factor R^2

is included in the presented dependence. There is a significant contribution to the molecular signal from the pairs at larger distances, which was not quite expected.

We illustrate different methods used to calculate the resonance lineshape in Fig. 1.5(b). We present the simplest method, given by Eq. (1.3.18), and the method based on the exact solution for square pulses (1.3.23-1.3.24). Only the latter method allows superpositions of molecular states to be excited. This possibility is relevant if potentials are very close to each other. These two methods give overall very similar lineshapes, and the difference is only in the details. The relative difference between them is somewhat larger just above the resonance, where there are many potentials very close to each other. For the position of the molecular resonance, this method gives -2.18 GHz from the atomic $70p_{3/2}$ resonance, which is in agreement with the experimental position of 2.21(3) GHz. It appears that the position of the resonance obtained using the simplest method is closer to the experimental value. However, this is likely just a coincidence because, in that calculation Δ and Δ' were replaced by their average value, so that fine details of the atomic level positions were not included.

We have tested the n-scaling of the molecular resonance, both numerically and experimentally. As mentioned, this scaling law makes sense only if, for a given laser intensity, the two-photon transition is not saturated for all values of n for which the scaling law is used. The calculated ratio (using Eq. (1.3.18)) of the signals for all $n = 70$ and $n = 60$ is 3.915, while $(70^*/60^*)^{8.5} = 3.920$. Also the same ratio for $n = 90$ and $n = 70$ is 9.274, while $(90^*/70^*)^{8.5} = 9.115$. The experimental dependence for the n-scaling of the molecular signal is shown in Fig. 1.7(b). The agreement is fairly good and the deviation could be explained by variations of experimental parameters between these three experimental scans. The n-scaling of the resonance position is in an excellent agreement with the expected scaling law, as shown in Fig. 1.7(a).

In Fig. 1.6(a) we present calculated lineshapes for several laser bandwidths, as indicated in the graph. The linewidth of the resonance is significantly larger than the laser bandwidth and it is primarily determined by the details of the molecular potentials and ℓ-mixing. The convoluted lineshapes for a laser bandwidth of 200 MHz is shown in Fig. 1.6(b). We get the best agreement for this bandwidth. The actual laser bandwidth was probably smaller than this one. For the actual experimental conditions, this theory cannot be used to fit the portion of the red tail of the spectrum closer to the atomic resonance because the excitation fractions are much larger. The presence of excited atoms could modify the pair excitation probability so that Eq. (1.3.21) is not applicable. Also, the simple pair excitation model cannot be used to explain the excitation process at larger excitation fractions. At such fractions, ℓ-mixing could be more efficient because close molecular potentials could additionally mix due to the interactions with nearby excited atoms. This could explain why the experimental red tail, for the experimental conditions, is just a simple monotonous function even though there are many potential curves and avoided-crossings between $np + np$ and $(n-1)d + ns$ asymptotic levels.

We compare experimental and theoretical signal sizes assuming a typical 5×10^{10}

cm^{-3} density. The laser intensity is typically in the range of 400-500 MW cm^{-2}. Experimental signals are about 300 ions per shot. The details of the experimental setup are given in [46]. From the scaling factor introduced in order to compare the theoretical and experimental lineshapes, we find that the calculated number of atoms is about 6-7 times higher than the experimental value. This is probably acceptable considering the number of factors which influence this estimate. Besides uncertainties in the experimental parameters, this scaling factor may also suggest that there was some excitation blockade [11,12].

1.4 Conclusion

We have presented long-range molecular potentials of 0_g^+, 0_u^- and 1_u symmetries. These potentials are important in describing the effects of interactions in single-photon excitation to high *np* Rydberg states. We have illustrated the ℓ-mixing induced by interactions over a broad range of internuclear distances. Several methods to evaluate the spectrum of the excitation of interacting Rydberg pairs of atoms were presented and they all gave similar results. The analysis showed that molecular resonances at the average atomic *nd* and *ns* energies are expected to occur. The calculated properties of the resonance, such as position, linewidth, *n*-scaling and signal size are reasonably close to the experimental observation, but a complete understanding of the spectral features of Rydberg excitation requires improved theoretical models.

Chapter 2

Local Blockade of Rydberg Excitation and Mean-Field Models

In mean-field models, all correlations between particles are ignored. After neglecting correlations, one gets a system of coupled equations for single-atom density matrices. Even in this approximation different atoms evolve differently because the interactions with surrounding atoms vary from one atom to another. Therefore interactions can often be a dephasing mechanism, even in the absence of other processes, such as spontaneous decay. In certain situations, interactions can force atoms to evolve in phase with each other. This possibility will be discussed in the chapter on collective oscillations. If the system is uniform on a large scale, one could ignore all differences between atoms and essentially work with a single density matrix. In this simpler class of mean-field models, interactions are described by some non-linear terms. First we will derive how such basic systems can be modeled consistently, then we will introduce a more complicated model which has been successful in explaining some overall properties of systems with strong interactions.

2.1 Simple mean-field models and nonlinear interactions

In various models, the interaction term in the Schrödinger equation is replaced by the nonlinear term $\lambda|\psi|^2$. The interactions between atoms in Bose-Einstein condensates is usually modeled by this nonlinear term giving rise to the Gross-Pitaevsky equation. It comes from replacing the actual potential by a delta-function contact potential. This is justified if the spatial extent of the atomic wavefunction, is much larger then the range of the interaction potential. In such cases, the details of the potentials are not important and using the delta-function potential is a good approximation. This physical assumption is not valid for the systems we investigate. Even though the standard approach is not directly applicable in our case, it may still be tempting to think that the interaction energy an atom feels should be proportional to the density of interacting atoms. Thinking along this line would lead to the interaction term $\lambda|\psi|^2$ again. However, following another line of logic presented in the next section, one could introduce different nonlinear terms to describe interactions. The goal of this section is to explore which mean-field nonlinear interactions are consistent with a general theory. For this purpose we compare some constants of motion of the appropriate many-body Hamiltonian and the mean-field counterpart. Because the atoms are ultracold, we ignore the effects of thermal motion during Rydberg excitation in this analysis. We start with the following many-body Hamiltonian of two-level atoms and

Rydberg-Rydberg interactions

$$H = \Delta \sum_{i=1}^{N} \hat{\sigma}_{ee}^{i} + \frac{\Omega}{2} \sum_{i=1}^{N} \left(\hat{\sigma}_{eg}^{i} + \hat{\sigma}_{ge}^{i} \right) + \sum_{i=1, j>i}^{N} \kappa_{ij} \hat{\sigma}_{ee}^{i} \hat{\sigma}_{ee}^{j} \,, \tag{2.1.1}$$

where Δ is the frequency detuning from the Rydberg level and the strength of Rydberg-Rydberg interactions is given by κ_{ij}. The nontrivial part of the σ-operators is defined as $\hat{\sigma}_{\alpha\beta}^{i} = |\alpha_i\rangle \langle\beta_i|$. The second term in the Hamiltonian is the dipole operator representing the interaction with the laser field. In our system, two atoms interact only if they are both in Rydberg states. We set $\Delta = 0$, since it does not affect this analysis. In this discussion, we assume that Ω describes a square pulse so that this H does not vary during the excitation process. Therefore, the expectation value $\langle H \rangle$ of the Hamiltonian does not vary during the excitation process as well. Assuming that all the atoms are initially in the ground state, the initial expectation value of $\langle H \rangle$ is zero and thus it has to be zero at all times

$$\frac{\Omega}{2} \sum_{i=1}^{N} \left(\langle \hat{\sigma}_{eg}^{i} \rangle + \langle \hat{\sigma}_{ge}^{i} \rangle \right) + \sum_{i=1, j>i}^{N} \kappa_{ij} \langle \hat{\sigma}_{ee}^{i} \hat{\sigma}_{ee}^{j} \rangle = 0. \tag{2.1.2}$$

This expression can be rewritten as follows

$$\sum_{i=1}^{N} \left(\frac{\Omega}{2} \left(\langle \hat{\sigma}_{eg}^{i} \rangle + \langle \hat{\sigma}_{ge}^{i} \rangle \right) + \frac{1}{2} \varepsilon_i \right) = 0, \tag{2.1.3}$$

where the interaction energy that atom "i" feels is

$$\varepsilon_i = \sum_{j \neq i}^{N} \kappa_{ij} \langle \hat{\sigma}_{ee}^{i} \hat{\sigma}_{ee}^{j} \rangle. \tag{2.1.4}$$

In the following step, we make the approximation often made in mean-field theories; assuming that the system (i.e. density of atoms) is uniform on a large scale, we ignore all the differences between atoms so that, after dropping the index "i", Eq. (2.1.3) becomes

$$\frac{\Omega}{2}\left(\langle\hat{\sigma}_{eg}\rangle+\langle\hat{\sigma}_{ge}\rangle\right)+\frac{1}{2}\varepsilon=0. \tag{2.1.5}$$

We do not consider spontaneous decay because the lifetime of Rydberg atoms is much longer than the processes we study. After making all these approximations, an atom can be described by two excitation amplitudes c_g and c_e of the ground and Rydberg state, respectively. Using these amplitudes, the first term in the previous equation can be expressed as follows

$$T\equiv\frac{\Omega}{2}\left(\langle\hat{\sigma}_{eg}\rangle+\langle\hat{\sigma}_{ge}\rangle\right)=\frac{\Omega}{2}\left(c_g^*c_e+c_gc_e^*\right). \tag{2.1.6}$$

Consequently, in order to be consistent with general theory, simple mean-field models have to satisfy the following relation

$$\frac{\Omega}{2}\left(c_g^*c_e+c_gc_e^*\right)+\frac{1}{2}\varepsilon=0, \tag{2.1.7}$$

or more compactly

$$T+\frac{\varepsilon}{2}=0. \tag{2.1.8}$$

Now we analyze constants of motion of the simple mean-field equations. In this model the effect of interactions is given by the energy shift of the excited level. The question is how to model this mean-field shift by the nonlinear term $\lambda|c_e|^s$ consistently with the condition (2.1.7). The mean-field equations are

$$\begin{aligned} i\frac{dc_g}{dt} &= \frac{\Omega}{2}c_e, & (2.1.9)\\ i\frac{dc_e}{dt} &= \frac{\Omega}{2}c_g+\lambda|c_e|^sc_e. & (2.1.10)\end{aligned}$$

One constant of these equations is, of course, the normalization $|c_g|^2+|c_e|^2$. To obtain another one, we first define a new quantity ϵ as $\epsilon = \lambda |c_e|^{s+2}$. It is easy to verify using Eqs. (2.1.9)-(2.1.10) that the following ratio is a constant

$$\frac{\delta T}{\delta\epsilon} = \frac{dT/dt}{d\epsilon/dt} = \frac{d\left(\frac{\Omega}{2}(c_g^* c_e + c_g c_e^*)\right)/dt}{d\left(\lambda |c_e|^{s+2}\right)/dt} = \frac{-2}{s+2}. \tag{2.1.11}$$

Since initially both T and ϵ are zero, we find

$$T + \frac{2}{s+2}\epsilon = 0. \tag{2.1.12}$$

Comparing (2.1.12) and (2.1.8) we conclude that a simple mean-field theory is consistent with general theory only if $s = 2$. This is a direct consequence of having only pair-wise interactions in the many-body Hamiltonian. Consistent with this comparison, we can interpret ϵ as the interaction energy per atom and the mean field shift $\lambda |c_e|^s$ as the interaction energy per excited atom. Considering all atoms to be equivalent is an important ingredient of this derivation.

The last equation can be used to find a simple relation between the suppression of excitation and λ. We define the suppression as a ratio of the largest possible amplitudes for $\lambda = 0$ and some nonzero λ. For $\lambda = 0$ the largest possible amplitude is 1, since the solution of Eqs. (2.1.9)-(2.1.10) is the simple Rabi flopping. For any given λ, the largest amplitude c_{e0} is determined from $d|c_e|^2/dt = 0$, which gives the result $c_{g0}c_{e0}^* - c_{g0}^* c_{e0} = 0$. This means that $c_{g0}c_{e0}^*$ is real so that $c_{g0}c_{e0}^* = \pm |c_{g0}||c_{e0}|$. According to Eq. (2.1.12), the plus sign is for negative λ and vice versa. The largest excitation fraction P_0 can be obtained from the constant of motion (2.1.12), after substituting $c_{g0}c_{e0}^* = \pm|c_{g0}||c_{e0}|$ and using the normalization condition. It satisfies the following simple equation

$$\Omega^2(1 - P_0) = |\lambda|^2 P_0^3. \tag{2.1.13}$$

This equation can be solved for $|\lambda|$ so that one can easily find out which λ is needed to achieve a certain saturation probability P_0. The suppression factor is just $1/P_0$. This general analysis cannot tell what λ is. In principle, it could be obtained by additional modeling. It has to depend on the density of atoms ρ because for $\rho \to 0$ there should be no interactions.

2.2 Modeling local blockade of Rydberg excitation

In [11], a local blockade of Rydberg state excitation in a macroscopic sample due to strong van der Walls interactions has been observed. The $5s$ ground state atoms were excited by one-photon UV transitions to high $np_{3/2}$ Rydberg states. Rydberg excitation exhibited dramatic suppression compared to the non-interacting case. The observed suppression was a function of the sample density and laser intensity. At high principal quantum number n, the interaction between Rydberg atoms is quite strong and it can blockade the excitation of many surrounding atoms in the range of a few μm. In the experiment [11], the ultracold sample of ^{85}Rb atoms had typically 10^7 atoms, with a peak density of up to 10^{11} cm^{-3}. The bandwidth of the excitation laser was about 100 MHz, which was approximately twice the Fourier transform limit due to frequency chirping.

We have proposed to describe this blockading with a mean-field model which also includes the many-body interaction through nonlinear terms of excitation amplitudes. The novelty is that we have a distribution of probabilities and the overall probability will be the average over this distribution. The distribution can be obtained by solving a system of nonlinear differential equations. A simple explanation of how one can come up with a distribution of probabilities might go as follows. Let's assume we have some density of excited Rydberg atoms in an ultracold gas. The excitation of a given ground-state atom will be suppressed because its excited level will be shifted due to its interaction with surrounding Rydberg atoms. However, not all atoms will be equally shifted because the shift depends on the separation from other excited atoms. So we have a distribution of shifts and thus a distribution of probabilities. Clearly, there is a consistency condition to be satisfied. The shifts depend ultimately on the density of excited atoms. On the other hand, the average of the distribution of probabilities has to be equal at all times to the assumed density of Rydberg atoms. So the density of excited atoms we calculate from the distribution of probabilities has to be equal to the density of Rydberg atoms used to get the distribution of mean-field shifts. Because of this condition, different components of the probability distribution do not evolve independently, and thus they all have to be calculated simultaneously. First we have to decide how to treat interactions because there are many $np + np$ potentials. If we consider an $np_{3/2}$ Rydberg atom located at $\mathbf{r}_i$, labelled $|p_i\rangle$, the first-order shift due to its interaction $\hat{V}_{\text{int}}$ with $|p_k\rangle$ is

$$\epsilon_{ik} = \langle p_i p_k | \, \hat{V}_{\text{int}}(\mathbf{r}_i - \mathbf{r}_k) \, | p_i p_k \rangle \,. \tag{2.2.1}$$

Interestingly, this form of interactions has also been used in [75]. to study Rydberg interaction in various situations At large separations, this shift is dominated by the vdW interaction corresponding to a pair of molecular states ${}^1\Sigma_g^+$ and ${}^3\Sigma_u^+$ [45,51,52]. The orbital part $|\Sigma\rangle$ is the same for these states and the only difference between them is the spin part. Since the interaction between Rydberg atoms is spin independent, these two states are degenerate. For n=70, $C_6 \approx 2 \times 10^{22}$ a.u. for both states. The other $np + np$ potentials are almost two order of magnitude weaker. Ignoring the weak potentials, the following form for $\hat{V}_{\text{int}}$ is more convenient

$$\hat{V}_{\text{int}}(\mathbf{r}_i - \mathbf{r}_k) = \frac{-C_6}{|\mathbf{r} - \mathbf{r}'|^6} |\Sigma\rangle\langle\Sigma| \otimes I^S, \tag{2.2.2}$$

where I^S is the identity operator in the spin factor space of both atoms. The asymptotic ($R \rightarrow \infty$) form of $|\Sigma\rangle$ is [51,52]

$$\begin{aligned} |\Sigma\rangle =& \sqrt{\frac{2}{3}} |np\, m{=}0\rangle |np\, m{=}0\rangle + \\ & \sqrt{\frac{1}{6}} \Big(|np\, m{=}1\rangle |np\, m{=}{-1}\rangle + |np\, m{=}{-1}\rangle |np\, m{=}1\rangle \Big), \end{aligned} \tag{2.2.3}$$

where $|np\, m\rangle$ are atomic orbital wavefunctions with the molecular axis as the quantization axis. Note that $|\Sigma\rangle$ is given in the molecule-fixed frame while $|p_i p_k\rangle$ is defined in the space-fixed one.

The details of the model depend on how we construct the distribution of mean-field shifts. This construction could be refined, in principle, but we propose a simple one.

For simplicity, we consider a spherical domain of radius R_d and volume $V_d = 4\pi R_d^3/3$ which contains several atoms, but by definition, only a single Rydberg atom $|p_i\rangle$. This means that the domain radius $R_d(t)$ is constructed so that at all times, a domain contains on average a single excited atom. The domain radius is initially very large because the density of excited atoms is very small, and it decreases to reach its final value at the end of the laser pulse. This excited atom in the domain does not necessarily have to be in the center, but could be anywhere within the domain. All other excited atoms, by construction outside the domain, contribute to the total shift of this Rydberg level

$$\varepsilon_i = \sum_{k \neq i} \varepsilon_{ki}. \tag{2.2.4}$$

The shift of $|p_i\rangle$, and therefore its probability of excitation, depends upon its location within the domain. The atoms near the center are the least shifted, thus most likely to be excited. For each value of the shift of the excited state, the excitation probability is calculated by solving the Bloch equations for the ground-state c_g and excited-state c_e amplitudes. The key point is to include the energy level shift ε due to interactions with nearby Rydberg atoms.

The domain radius R_d is determined from the condition

$$\rho \int_{V_d} d^3\mathbf{r} |c_e(\mathbf{r}, t)|^2 = 1, \tag{2.2.5}$$

where ρ, the local density of atoms, is assumed uniform within the domain. The amplitude $c_e(\mathbf{r}, t)$ of an atom located at $\mathbf{r}$ depends on its shift $\varepsilon(\mathbf{r}, t)$. In our mean-field model, we calculate this shift by replacing the discrete sum by an integral over the excited atoms outside the domain ($V' = V - V_d$) and considering their density $\rho_e(t)$ to be locally uniform in V':m

$$\varepsilon(\mathbf{r},t) = 2\pi\rho_e(t) \int_{V'} d^3r' \frac{-C_6}{|\mathbf{r}-\mathbf{r}'|^6} |\langle p_r p_{r'} \mid \Sigma\rangle|^2. \tag{2.2.6}$$

The radius R_d and density ρ_e are related self-consistently via $\rho_e V_d = 1$. The shift of an atom located at $\mathbf{r} = \mathbf{y}\, R_d$ can be rewritten as

$$\varepsilon(\mathbf{y},t) = -2\pi\tilde{C}_6\, g(\mathbf{y})/R_d^6(t), \tag{2.2.7}$$

where the effective vdW coefficient, $\tilde{C}_6$, and the spatial variation of the shift, $g(\mathbf{y})$ (with $g(0) = 1$), are obtained by numerical integration of Eq. 2.2.6. Substituting

$$R_d^{-3} = \rho \int_{|\mathbf{y}|\leq 1} d^3y |c_e(\mathbf{y},t)|^2 \tag{2.2.8}$$

into the expression for $\varepsilon(\mathbf{y},t)$ leads to non-linear Bloch-like equations for the time-dependent amplitudes $c_g(\mathbf{y},t)$ and $c_e(\mathbf{y},t)$,

$$i\frac{dc_g(t,\mathbf{y})}{dt} = \frac{\Omega}{2} e^{i\beta t^2} c_e(t,\mathbf{y}), \tag{2.2.9a}$$

$$i\frac{dc_e(t,\mathbf{y})}{dt} = -2\pi\rho^2\tilde{C}_6 g(\mathbf{y}) \left| \int_{|\mathbf{y}|\leq 1} d^3\mathbf{y}' |c_e(t,\mathbf{y}')|^2 \right|^2 c_e(t,\mathbf{y}) + \frac{\Omega}{2} e^{-i\beta t^2} c_g(t,\mathbf{y}). \tag{2.2.9b}$$

Here β characterizes the chirp of the laser pulse and $\Omega(t)$ is the Rabi frequency. The scaled position $\mathbf{y}$ is a continuous parameter. Therefore, the system (2.2.9) contains an infinite number of coupled equations. Fortunately, it can be approximated very well with a finite system. Using the adapted zeroth-order wavefunction (2.2.3) for $|\Sigma\rangle$ and averaging over projections m_j of the excited states $|n\, p_{j=3/2}\, m_j\rangle$ for atoms outside

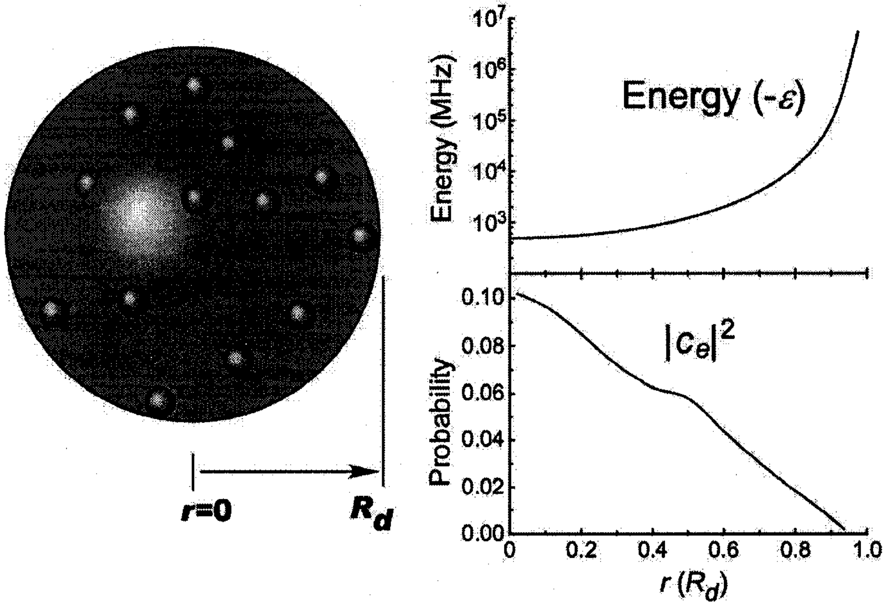

Fig. 2.1: Our theoretical model divides the region into domains of radius R_d. Within a given domain, any one of the numerous ground-state atoms may be excited into a Rydberg state. Because of strong Rydberg-Rydberg vdW interactions, the mean-field energy shift ε depends on the particular location, as does the excitation probability $|c_e|^2$. Atoms near the domain center are less shifted and their excitation is more probable than those near the periphery. The graphs correspond to n=80 atoms at $\rho = 6.5 \times 10^{10}$ cm^{-3} and scaled irradiance $I = 0.187$ MW/cm^2.

the domain and integrating over all possible angles of molecular axes, we find $\tilde{C}_6 = 7/60\ C_6$. We point out that this value is essentially model-dependent, although it has agreed well with the experimental data. By solving numerically Eqs. (2.2.9), we find the local density of excited atoms $\rho_e(\rho, \Omega_0)$ after the Gaussian laser pulse of peak Rabi frequency Ω_0 has ended. To compare with the experimental measurements, this function is averaged over the density and laser intensity profiles in the trapped sample to provide the overall fraction of atoms which is excited. Uncertainties in both ρ and $\tilde{C}_6$ are taken into account by using a scaling factor defined via $\rho_\alpha \tilde{C}_{6,\alpha}^{1/2} = \alpha\rho\tilde{C}_6^{1/2}$. The best agreement between the model and the data was found for α=0.96, i.e. almost no scaling was necessary. This α was used throughout the analysis. With this scaling factor, the agreement between the model and the data is quite good.

Let's review the the basic ideas of the model in a bit different, but complementary way. In the simplest approximation, for the interaction between Rydberg atoms given by the power law $\epsilon_{ik} \sim 1/R^s$, the average level shift ϵ is mainly determined by the average distance R_0 between two excited atoms $\epsilon \sim R_0^s$. This R_0 can be related to the excitation probability $|c_e|^2$ because $|c_e|^2 \sim 1/\rho R_0^3$, where ρ is the density of atoms. Combining these expressions we find for the average level shift to be $\epsilon \sim |c_e|^{2s/3}$. For the van der Walls interaction $s = 6$, thus $\epsilon \sim |c_e|^4$. One cannot use a single mean-field shift of this form, according to the conclusion of the previous section, so working with a distribution of mean-field shifts of this form is in some sense necessary. A good estimate of R_0 is difficult to make because, in $\epsilon \sim 1/R_0^6$, relatively small errors in the estimate of R_0 may cause large deviations in the estimate of ϵ. An additional difficulty is that R_0 varies in time as the population of excited atoms builds up, so the estimate of R_0 has to be good at all times. The model also deals with the fact that assuming the density of excited atoms ρ_e to be uniform, causes the integral $\int_0^\infty \rho_e C_6/R^6$ to be divergent. Always taking a region with only one excited atom could be understood as a physical way to regularize this integral because the interactions are pair-wise and apparently the contribution to the interaction energy from this region is minimal. This approximation works even better for strong interactions because multiple excitations

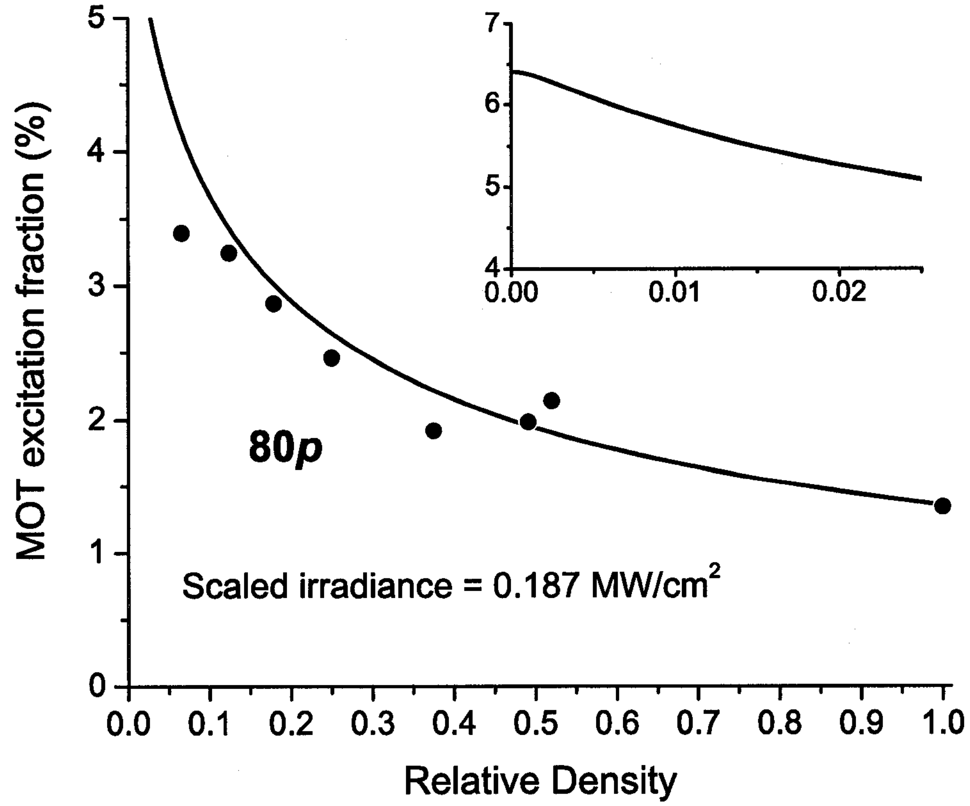

Fig. 2.2: Density dependence of the n=80 Rydberg signal. The solid curve shows the mean-field theoretical prediction

are additionally suppressed by interactions (if they do not change sign). Actually, this mean-field model does take into account the possibility that even atoms at very short distances can be excited (i.e. one just inside and one just outside the domain). These situation corresponds to $|\mathbf{y}| = \mathbf{1}$, for which the shift becomes divergent, as shown in Fig. 2.1. The model is essentially constructed by assuming that there are already many excited atoms and we want to excite some more. This picture is obviously not right at very low ρ_e because in this case only two-body effects are relevant. Even though the model has the noninteractiing limit built in, it slightly overestimates the suppression at low ρ_e [60]. However, for larger ρ_e the suppressions obtained by the model are very close to the results of full many-body calculations [60]. This is quite surprising for a mean-field model.

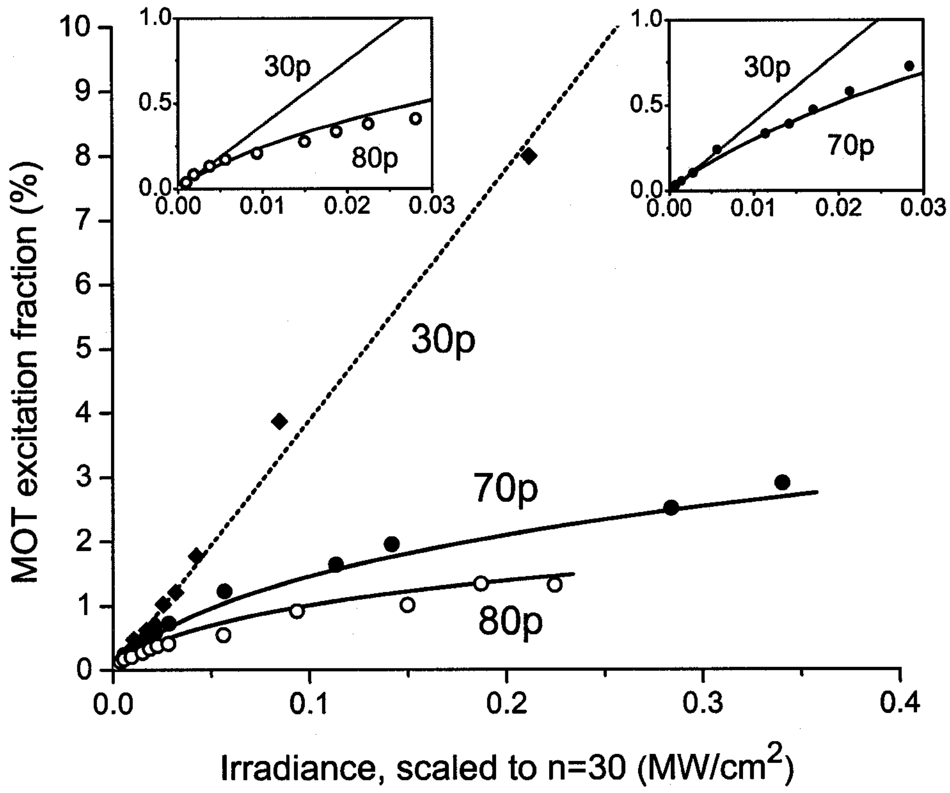

Fig. 2.3: Comparison of Rydberg excitation for the unblockaded (isolated atom) 30*p* state and the blockaded 70*p* and 80*p* states at a peak density of 6.5×10^{10} cm^{-3}. Irradiances are scaled by $(n^*/30^*)^3$ to account for the n dependence of the electric dipole transition probability. Insets show the region near the origin with an expanded scale. The dashed line for n=30 is a least-squares fit to the data, while the solid curves for n=70 and n=80 are theoretical predictions.

The measured excitation fraction for n=80 as a function of atomic density is shown in Fig. 2.2 along with the prediction of the model. Just as for the irradiance dependence in Fig. 2.3, the data and the model agree quite well. Note that in the absence of a blockade in Fig 2.2, one would expect a constant excitation fraction (here 6.4%) instead of the rapid decrease observed.

The salient feature of Fig. 2.3 is the dramatic suppression of Rydberg excitation for n=70 and 80 relative to the isolated atom (n=30) excitation curve. As expected, the suppression is larger for n=80 due to its stronger vdW interaction, reaching a factor of 6.4 at the highest intensities shown. The signal plotted is the fraction of the entire MOT sample that is excited. For each n, the irradiance values are scaled to n=30 by the factor $(30^*/n^*)^3$ in order to account for the decrease in transition strength with increasing n. Here $n^*=n-\delta$, and $\delta = 2.6415$ is the quantum defect for $p_{3/2}$ states [74]. For n=80, the maximum observed overall excitation fraction was 6.4 times smaller than for isolated atom excitation, and the theory indicates the suppression reaches a factor of 19 in the center of the MOT. Note that the n=30 saturation intensity for isolated atoms, defined as that required for an unchirped π-pulse in the center of the beam, is 0.36 MW/cm^2. With this irradiance scaling, the various n's would fall on a universal isolated atom excitation curve if the Rydberg levels were unshifted by atomic interactions. This is seen to be the case for the very lowest intensities, at which the Rydberg atoms are sufficiently sparse that interactions between them are negligible. Using longer pulses, one can also measure the time dependence of the excitation fraction [79].

2.3 Conclusion

I derived the form of nonlinear interactions in a simple mean-field model from the required balance between the neregy of the optical field and the interaction energy of excited atoms. I proposed a more advanced model to describe a local blockade of Rydberg excitation observed in a macroscopic sample due to van der Walls interactions. In this model, interaction energies were modeled by a distribution of mean field shifts for which a distribution of excitation probabilities was calculated. The dependence of the suppression of excitation on laser irradiance, atomic density, and principal quantum numbers were in a good agreement with theoretical predictions based on this model.

Chapter 3

Collective Behavior of Rydberg Excitation

We investigate the collective aspects of Rydberg excitation in ultracold mesoscopic systems. At high principal quantum number n, the interactions between Rydberg atoms are quite strong and they inhibit the excitation of many surrounding atoms within a range of few μm. The atoms within this range are strongly correlated so that a many-body treatment is, in general, needed. In [60] the many-body wave function was calculated by numerically solving the Schrödinger equation. This type of analysis can be important for quantum information applications [77] because precise control at the quantum level is essential in these applications. Strong interactions can affect the coherent manipulation of a large group of atoms so it is necessary to use a many-body treatment to evaluate the fidelity of quantum information protocols.

We consider the time evolution of the system to be unitary and, therefore, it can be reversed. The time evolution of Rydberg excitation has been experimentally reversed by applying an 'optical rotary echo' technique [78]. Note that this assumption was not true for the two-photon scheme used in the experiment [12] because, in the first step, the excitation of the $5p$ state was saturated and the excitation time was much longer than the lifetime of the $5p$ state.

We consider mesoscopic samples of $\sim$10 μm diameter containing up to 100 ground-state atoms which are excited by single photon transitions to high np Rydberg states. We study in detail the dynamics of such systems, especially the possibility of many-body Rabi oscillations of Rydberg excitation. It is plausible to investigate these oscillations in smaller systems because one would not normally expect to achieve the coherent manipulation of large groups of atoms. The many-body approach developed in [60] is quite suitable for this analysis and we use it here. We only modify some technical details on how to treat interactions in this approach.

3.1 Many-body effects in ultracold Rydberg systems and collective oscillations

Although models may be very useful in explaining some important overall properties of large strongly-interacting Rydberg systems, it is essential to include many-body correlations in the study of many-body effects. In ultracold Rydberg systems, the thermal motion of the atoms is greatly reduced so that in many situations it can be completely ignored.

The idea of these collective oscillations can be explained as follows. If the interactions between atoms are strong enough, all many-body states with two or more excited atoms will be greatly shifted by these interactions and thus far-off resonance. Such systems are effectively two-level systems because there are only two (collective) states that are populated: the ground state $|G\rangle = |g_1 g_2 \ldots g_N\rangle$, where all atoms are in the atomic ground state $|g_i\rangle$, and only one excited state $|E\rangle = 1/\sqrt{N}\sum_i |g_1 \ldots e_i \ldots g_N\rangle$ where any, but only one, atom can be excited. On atomic resonance such two-level systems are exactly solvable [76] and the solution, in terms of excitation probability P_{exc}, is

$$P_{\text{exc}}(t) = \frac{1}{N}\sin^2\left(\sqrt{N}\Omega F(t)\right), \tag{3.1.1}$$

where $\Omega F(t)$ is the pulse area and N is the number of atoms in the sample. Clearly, the collective oscillations are much faster then the isolated-atom Rabi frequency Ω. The question is whether these fast oscillations can exist in systems which are big enough that there can be several excited atoms, or alternatively with the interactions not strong enough to fully blockade the system.

Because the atoms are ultracold, we ignore the effects of thermal motion during Rydberg excitation in this analysis. We consider the following many-body Hamiltonian of two-level atoms and Rydberg-Rydberg interactions ($\hbar = 1$)

$$H = \Delta\sum_{i=1}^{N}\hat{\sigma}_{ee}^{i} + \frac{\Omega}{2}\sum_{i=1}^{N}\left(f(t)\hat{\sigma}_{eg}^{i} + f^{*}(t)\hat{\sigma}_{ge}^{i}\right) + \sum_{i=1,j>i}^{N}\kappa_{ij}\hat{\sigma}_{ee}^{i}\hat{\sigma}_{ee}^{j}, \tag{3.1.2}$$

where Δ is the frequency detuning and the interactions between Rydberg atoms are given by κ_{ij}. This Hamiltonian was practically introduced in the previous chapter. The second term in the Hamiltonian is the dipole operator representing the interaction with the optical field. The function $f(t)$ is the time evolution (envelope) of the laser pulse. The non-trivial parts of the σ-operators are defined as $\hat{\sigma}_{\alpha\beta}^{i} = |\alpha_i\rangle\langle\beta_i|$, where α, β reffer either to the ground state g or the excited state e.

We can always eliminate the detuning from the previous Hamiltonian by the unitary transformation $\exp\left(it\,\Delta\Sigma_{i=1}^{N}\hat{\sigma}_{ee}^{i}\right) H \exp\left(-it\,\Delta\Sigma_{i=1}^{N}\hat{\sigma}_{ee}^{i}\right)$. In the remaining part of the Hamiltonian, the only effect of this transformation is to replace $f(t)$ by $f(t)\exp(it\Delta)$. This transformation can simplify the use of other approximations applied to solve (3.1.2). We assume that it is always performed and there is no need to consider this term explicitly. In fact, we set $\Delta = 0$ in our simulation.

Since the dimensionality of the problem is 2^N, which is a huge number for numerical calculations with $N \approx 100$, it is necessary to make some approximations. The idea of local blockade is utilized here (more explanations can be found in [60]). We can group atoms in such a way that the probability to have two or more excited atoms within a group is practically zero. Such groups of atoms are often called superatoms. Each superatom "i" is a two-level system described by two collective states $|G_i\rangle$ and $|E_i\rangle$. In the next step, the actual many-body Hamiltonian is represented/approximated in terms of these superatoms. For convenience we define new operators $\sigma_{EG}^{i} = |E_i\rangle\langle G_i|$ and $\sigma_{EE}^{i} = |E_i\rangle\langle E_i|$. In terms of the new operators, the interaction with the laser field can be expressed as follows

$$\sum_{i=1}^{N}\frac{\Omega}{2}\left(f(t)\hat{\sigma}_{eg}^{i} + f^{*}(t)\hat{\sigma}_{ge}^{i}\right) \to \sum_{j=1}^{N_{\mathbf{sa}}}\frac{\Omega\sqrt{N_i}}{2}\left(f(t)\hat{\sigma}_{EG}^{j} + f^{*}(t)\hat{\sigma}_{GE}^{j}\right) \tag{3.1.3}$$

because

$$\langle E_i|\sum_{j=1}^{N}\left(f(t)\hat{\sigma}_{eg}^{j} + f^{*}(t)\hat{\sigma}_{ge}^{j}\right)|G_i\rangle = \frac{\sqrt{N_i}\Omega}{2}f(t),$$

where $N_{\mathbf{sa}}$ is the number of superatoms and N_j is the number of atoms in a superatom. The Rydberg interaction V_{Ryd} between superatoms "i" and "j" in their excited states is

$$k_{ij} = \langle E_i E_j | \, V_{Ryd} \, | E_i E_j \rangle = \frac{1}{N_i N_j} \sum_{p \leq N_i} \sum_{q \leq N_j} \kappa_{pq}. \tag{3.1.4}$$

In these sums, atoms "p" and "q" belong to different superatoms. The last formula gives the prescription for how to introduce the interaction between superatoms. It seems that the interaction between two superatoms in [60] was modeled using the distance between their centers of mass. Equation (3.1.4) suggests that the superatom interaction is rather defined by $\langle \kappa_{pq} \rangle$ instead of $\kappa(\langle r_{pq} \rangle)$. Using $\kappa(\langle r_{pq} \rangle)$ tends to underestimate the influence of interactions. The difference between these two ways can be significant if $\kappa(r)$ depends strongly on r, which is the case here. However, the effect of such differences in interaction energies on the results of simulations is hard to judge because the largest κ_{pq} do not contribute to the interactions between superatoms (explained later in the text) and because of the strong suppression of Rydberg excitation. This k_{ij}, as the relevant parameter to describe the interactions between superatoms, should be preferably used in the process of the superatom formation as well. These are the only modifications we make to the method [60]. Another useful simplification comes from the suppression of Rydberg excitation. Namely, the number of excited atoms is limited due to the blockade effect and there is no need to consider many-body states with high numbers of excited atoms. To illustrate the size of the problem after these steps, we note that for systems with twenty-three superatoms and at most seven of them excited, there are about four hundred thousand excitation amplitudes to solve.

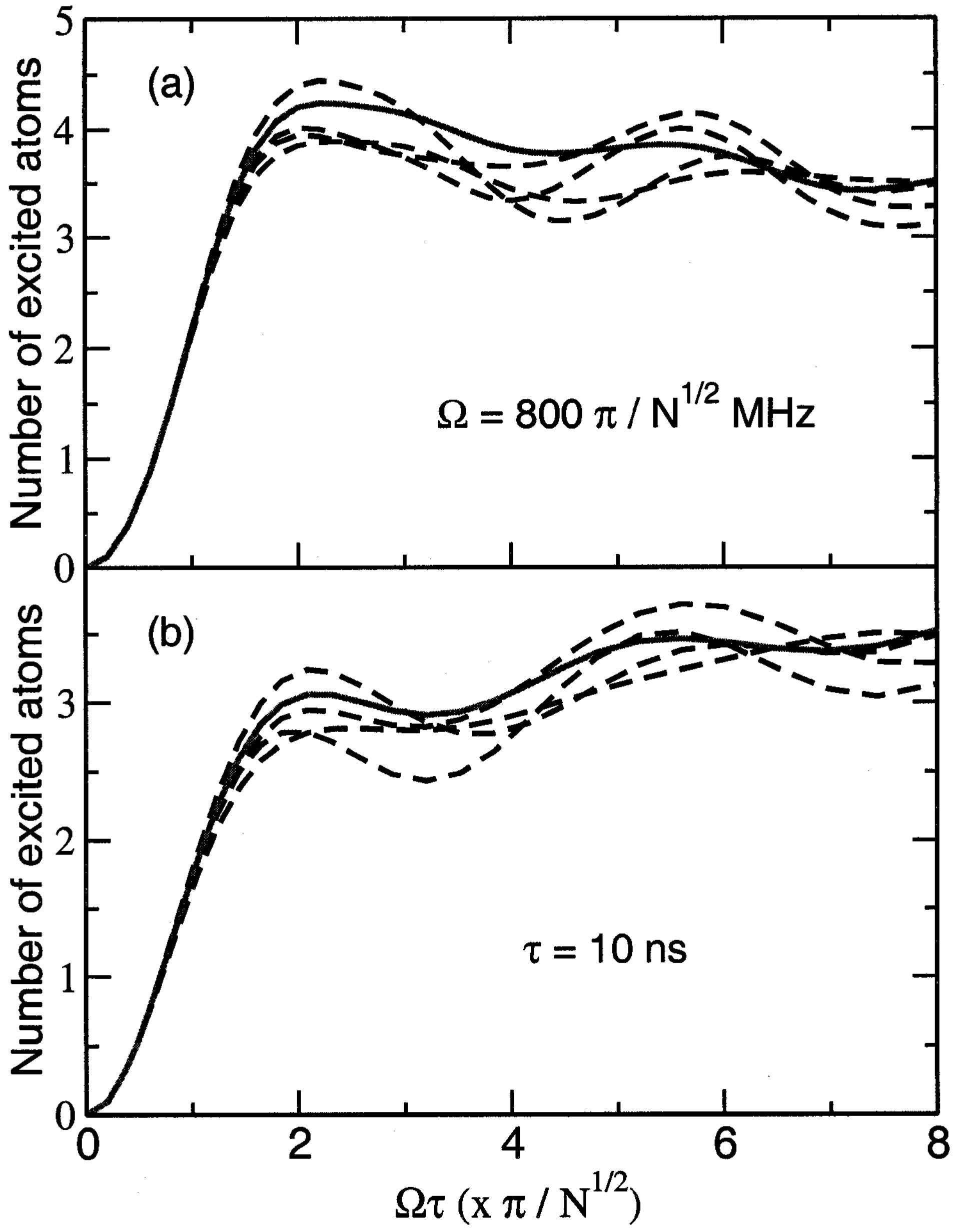

Fig. 3.1: The number of excited 70 $p_{3/2}$ atoms as a function of the pulse area for square laser pulses ($N = 70$ and $\rho = 10^{11}$ cm^{-3}). In (a) the pulse duration was varied and in (b) the single-atom Rabi frequency. In both graphs the dashed lines represent some particular random distributions of atoms, while the solid lines are the average dependencies over 100 random arrangements of atoms.

To form superatoms we use the same recursion described in [60], except that the largest k_{ij} is our guidance in deciding which (super)atoms to group together. We use the following recursion. We initially set the number of superatoms to be equal to the number of atoms. After that, we start the recursion. In the first step, we calculate the interactions between superatoms using Eq. (3.1.4). In the second step, we check if the number of superatoms is equal to the desired number (chosen in advance) of superatoms. If it is, the recursion is over, otherwise, we execute the third step. In this step, we group superatoms corresponding to the largest $|k_{ij}|$. Therefore, the number of superatoms is reduced by one and thus we need to recalculate all k_{ij}. This means that the recursion cycle is initiated again.

3.2 Results and discussion

We consider mesoscopic samples of $\sim$10 μm diameter containing up to 100 ground-state atoms. It is assumed that $5s$ ground state rubidium atoms are excited by one-photon transitions to $70p_{3/2}$ Rydberg states. The positions of atoms within a sample are randomly generated before the time evolution of the system takes place. We typically consider samples of 70 atoms and density of 10^{11} cm^{-3}. The only exception is the analysis of density fluctuations, shown in Fig 3.3, where the number of atoms varies according to a Poissonian distribution. The effect of changing the density is similar to changing the interaction strength, and so we can vary only one of them. We vary the scaled interaction strength which is obtained as follows. From the Schrödinger equation $i\partial\psi/\partial t = H\psi$, after the scaling $t \to t/\tau$, $\Omega \to \Omega\tau$ and $k_{ij} \to k_{ij}\tau$, we conclude that the final excitation probability P_{exc} is a function of the pulse area and the product $k_{ij}\tau \sim k_{ij}/\Gamma$, i.e. $P_{\text{exc}} = P_{\text{exc}}(\Omega\tau, k_{ij}\tau)$. Here τ is the pulse duration (for a Gaussian it is the FWHM) and Γ is the bandwidth. In our simulations, the range of possible pulse areas ($\sim \Omega\tau$) is the same for all types of laser pulses. Because the single-atom Rabi frequency Ω is scaled by $\sqrt{N_i}$, in the regime where the correlations between atoms are significant, the many-body characteristics of Rydberg excitation should be present at relatively small Ω.

The effect of interactions can be amplified, not only by increasing k_{ij}, but also τ. Increasing τ also means reducing the bandwidth (for ideal pulses). When, for some τ, the interactions between nearest neighbors become comparable with the bandwidth, the influence of interactions on the excitation dynamics should become noticeable. In our simulations the interactions between atoms are given by $k_{ij} = \tilde{C}_6/R_{ij}^6$. This type of interactions is also supported by the experiment [25], in which the production of ions in collision processes is consistent with the assumption of an attractive van der Waals potential and a theoretical estimate of its magnitude. In the model presented in [11], we calculated the effective vdW coefficient $\tilde{C}_6$ to be $7C_6/60$, where C_6 is the dispersion coefficient of the strongest np+np potential [52]. As explained previously, this $\tilde{C}_6$ is model-dependent. However, using this value we had a good agreement with the experimental data and thus we use it in this calculation as well.

In Fig. 3.1, the time and omega dependencies of the excitation probability are shown for square laser pulses in panels (a) and (b), respectively. These two dependencies are presented as functions of the pulse area. In both graphs the dashed curves correspond to particular random distributions of atoms within the sample. The solid curves are the average over the results obtained from one hundred random arrangement of atoms. If we use fifty different placements instead of one hundred, the difference in the average excitation probability is only about 1 %. The evaluation of the omega dependence is much more demanding because for each value of Ω we have to calculate the corresponding time dependence first. Although excitation probabilities for particular random distributions of atoms clearly exhibit many-body oscillations, when averaged over many distributions, these oscillations are significantly suppressed. Collective oscillations presented in Fig. 3.3 are more pronounced because a much greater scaled interaction strength is used.

In Fig. 3.2 the average time and omega dependencies of the excitation probability for square and Gaussian pulses are presented. Here we show how different pulse shapes affect Rydberg excitation. It is known that for resonant single-atom excitation, the excitation probabilities depend only on the pulse area. However, from $P_{\text{exc}} = P_{\text{exc}}(\Omega\tau, k_{ij}\tau)$, we see that varying the pulse area by changing τ or Ω leads, in general, to different results. Only in the limit of a full blockade, according to Eq. (3.1.1), does P_{exc} again become a function of the pulse area only. The average time dependencies, for both types of pulses, slowly decrease after reaching saturation (the first maximum). This slow decrease can be explained by the reduction of the bandwidth Γ for longer

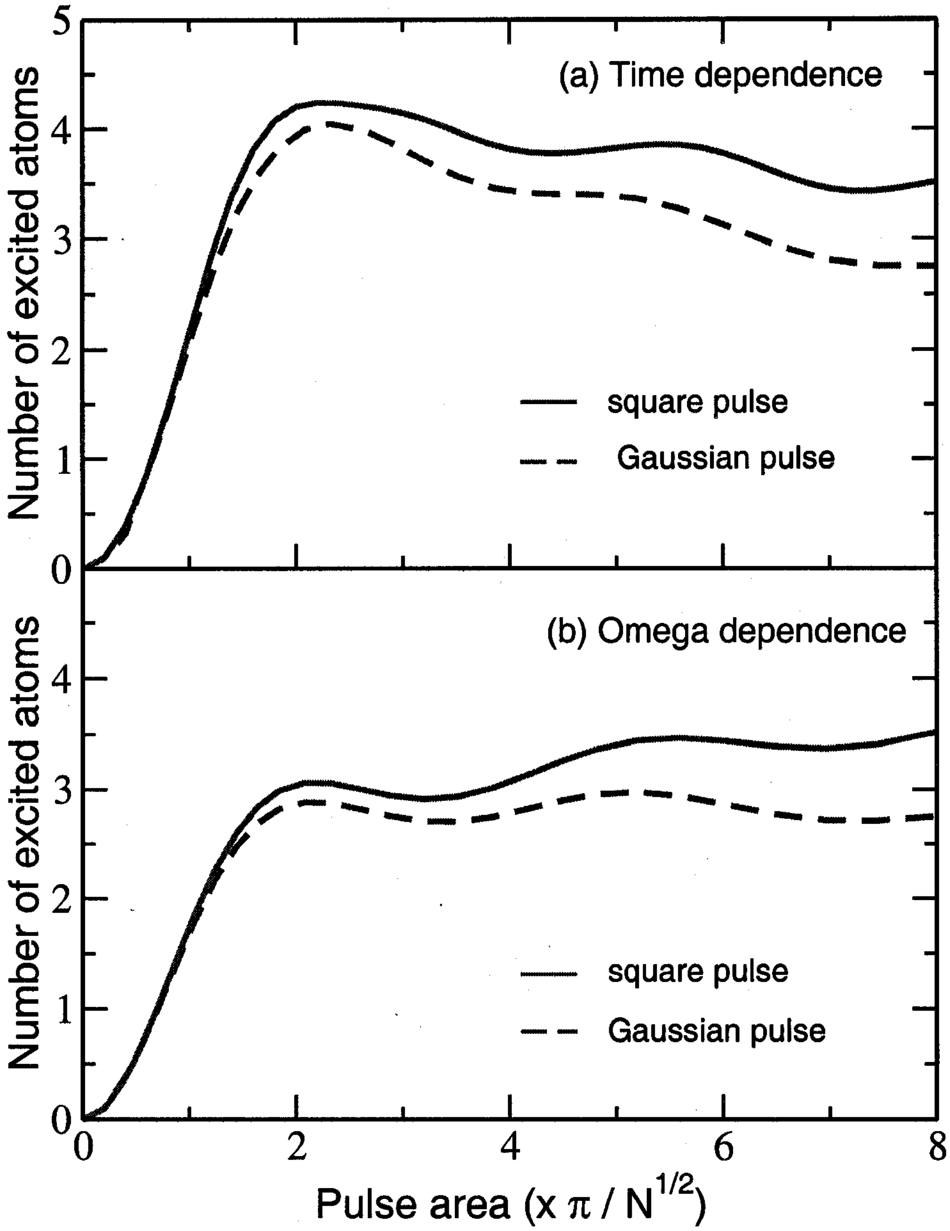

Fig. 3.2: The average dependencies of the number of excited 70 $p_{3/2}$ atoms versus the pulse area for different types of laser pulses ($N = 70$ and $\rho = 10^{11}$ cm^{-3}). In the absence of interactions all these dependencies should be the same. In (a) the pulse duration was varied and in (b) the single-atom Rabi frequency. Both solid lines correspond to square pulses and dashed lines to Gaussian ones. This plot demonstrates that the excitation blockade is a bit more efficient for Gaussian pulses.

pulse durations, i.e. the blockading due to interactions becomes more effective. The slow increase with omega, after reaching saturation, is expected to happen due to higher laser power. This figure shows that the excitation probabilities for Gaussian pulses are systematically lower than those for square pulses. This is also expected because of the following somewhat oversimplified argument. From the point of view of mean-field theory, the effect of interactions is a level shift, which can be expressed as some effective detuning of the excited level. Ignoring the time dependence of such level shifts, and in the first approximation, the probabilities are given by the Fourier transform of the pulse envelope. However, the Fourier transform of a Gaussian is also a Gaussian so that the Fourier components of a Gaussian vanish much faster for large detunings than the corresponding Fourier components of a square pulse (which fall off as $\sim 1/\Delta$).

In the previous figures we have assumed the interactions between $70p_{3/2}$ Rydberg atoms and, for square pulses, pulse durations of 10 ns at most. However, the product $k_{ij}\tau$ can still be significantly increased, either by going to higher principal quantum numbers n (increasing k_{ij} due to the n^{11} scaling of C_6) or using longer pulses. In practice both ways should probably be used because for high n the diatomic energy levels become very close to each other and the interactions at short internuclear distances have complicated forms due to avoided crossings between potential curves. However, increasing τ also means decreasing Γ so that the excitation of atoms at shorter internuclear separations can be ignored and thus the van der Waals form of interaction can still be appropriate. Actually, the approximations in the superatom approach are justifiable if such excitation can be ignored. In fact, the largest κ_{pq} have no influence on superatom interactions k_{ij} because for such κ_{pq}, ideally, both atoms p and q should belong to the same superatom. The simulation shown in Fig. 3.3 is obtained for the product $k_{ij}\tau$ 15 times larger than the value used in Figs. 3.1-3.2. This would roughly correspond to the interactions between $n = 90$ Rydberg atoms with the same bandwidth Γ. Both curves are obtained after averaging over many random spatial distributions of atoms. The oscillations are obviously more pronounced here than in Fig. 3.1-3.2. To see how robust these oscillations are against density fluctuations, we varied the number of atoms in the sample according to a Poissonian statistics. The dashed curves is obtained after this additional averaging over density fluctuations.

In the first approximation, we can find an approximate parametrization of collective oscillations as follows. From the fact that the initial excitation probabilities do not depend on interactions, and the assumption that as soon as the interactions start to dominate the process they quickly saturate the excitations, one readily derives the following approximate formula

$$P_{\text{exc}}^{(1\text{max})} = \frac{N_{\text{exc}}^{(1\text{max})}}{N} = \frac{F^{(1\text{max})2}}{4}, \tag{3.2.1}$$

where $P_{\text{exc}}^{(1\text{max})}$ and $N_{\text{exc}}^{(1\text{max})}$ are respectively the excitation probability and the number of excited atoms at the first maximum of P_{exc}, and $F^{(1\text{max})}$ is the corresponding pulse area. The last formula is just the excitation probability for isolated (noninteracting)

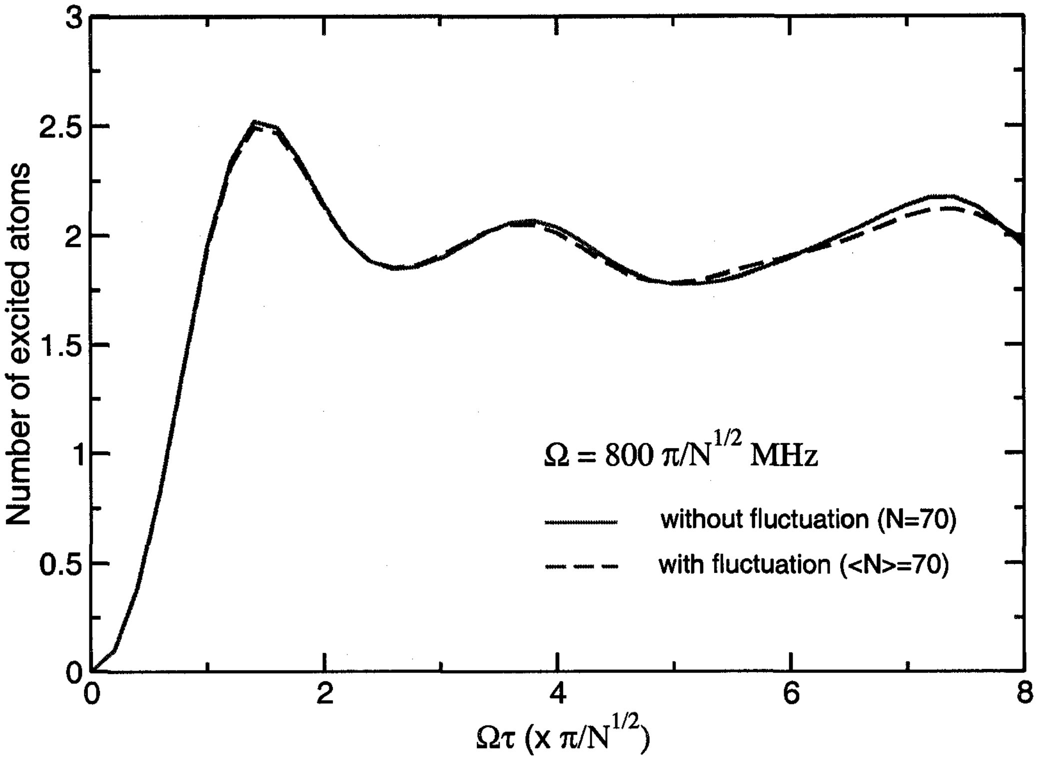

Fig. 3.3: The time dependence of the number of excited atoms for the scaled interaction strengths k_{ij} 15 times larger than those used in the other simulations (Figs. 3.1 and 3.2). To check the robustness of the many-body oscillations against density fluctuations, the number of atoms in the sample is varied according to a Poissonian distribution. The solid curve is the dependence for $N = 70$ and the dashed curve is the average dependence over density fluctuations with $\langle N \rangle = 70$.

atoms if the pulse area is small. We can use it because, initially, there are no excited atoms and so there are no effects of interactions. In the next chapter we give a formal proof (4.2.22) for this claim. The effects of interactions for small pulse areas F are proportional to F^4. Depending on the strength of interactions, this saturation can be achieved much faster than the one in single-atom processes. In terms of frequency, the collective phenomena are faster than their counterparts in single-atom processes.

Assuming that the phase ϕ_{coll} of collective oscillations can be simply characterized by some collective frequency Ω_{coll} (i.e. $\phi_{\text{coll}} \sim \Omega_{\text{coll}}\tau$), where $\Omega_{\text{coll}} = \alpha\Omega$, the scaling parameter α can be obtained from the saturation condition

$$\alpha F^{(1\text{max})} \approx \pi. \tag{3.2.2}$$

Combining the last two equations one gets

$$\alpha \approx \sqrt{\frac{\pi}{4}}\sqrt{\frac{N_{\text{exc}}^{(1\text{max})}}{N}}. \tag{3.2.3}$$

To illustrate excitations in large samples with a significant excitation blockade, a domain (or "bubble") picture is often used. Each domain represents a region in which there exists exactly one Rydberg atom. Denoting the number of atoms in a domain by N_D, then $N_D = N_{\text{exc}}^{(1\text{max})}/N$, $\alpha = \sqrt{\pi/4}\sqrt{N_D}$ and

$$\Omega_{\text{coll}} \approx \sqrt{\frac{\pi}{4}}\sqrt{N_D}\Omega. \tag{3.2.4}$$

The factor $\sqrt{\frac{\pi}{4}} = 0.886... \approx 1$ can (and probably should) be approximated by one (because for $N_D = N$, according to Eq. (3.1.1), $\Omega_{\text{coll}} = \sqrt{N}\Omega$). We conclude that it seems that $\sqrt{N_D}$ is the scaling factor of collective oscillations. We can verify this estimate by comparing with the numerical calculations shown in Fig. 3.2 and Fig. 3.3. Also, if the phase of collective oscillations can be really described by a simple parameter Ω_{coll} (or $\sqrt{N_D}$), then the ratio of the pulse areas corresponding to the second and the first maximum of P_{exc} should be three. The figures clearly show that the actual many-body behavior is much more complicated, so we just want to verify how much it deviates from the simple picture. For convenience, we define two

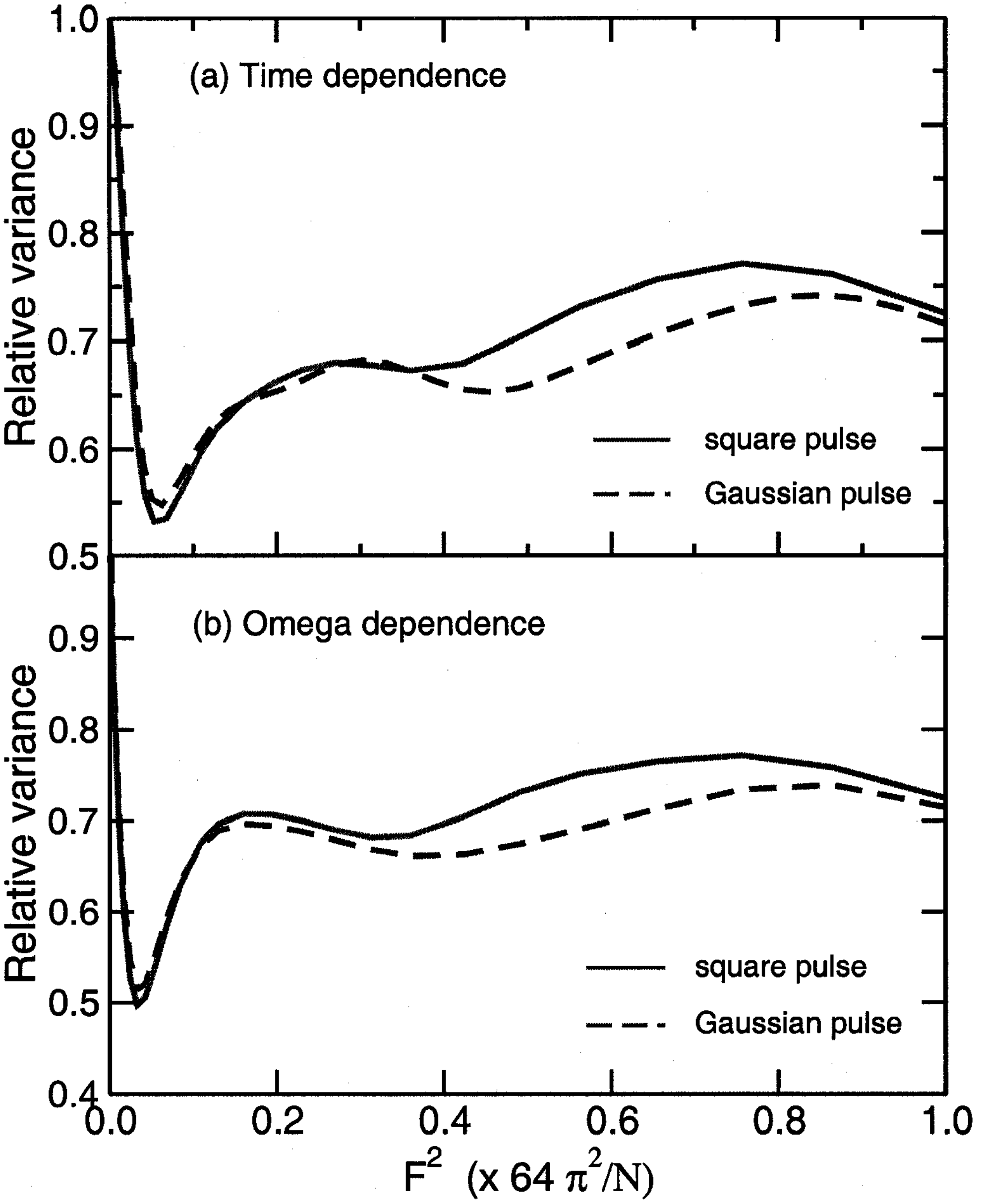

Fig. 3.4: The relative variance $\Delta n_{\text{exc}}/\Delta n'_{\text{exc}}$ of the number of excited Rydberg atoms versus the square of the pulse area for the same parameters used in Figs. 3.1-3.2. The actual variance Δn_{exc} is expressed using the calculated variance $\Delta n'_{\text{exc}}$, obtained from P, assuming no correlation between excited atoms. In (a) pulse duration was varied and in (b) the single-atom Rabi frequency. Both solid lines correspond to square pulses and dashed lines to Gaussian ones.

parameters $\gamma = \alpha/\sqrt{N_D}$ and $\beta = F^{(2\max)}/F^{(1\max)}$. Interestingly, for all square pulse results presented in Figs. 3.2 and 3.3, we find $\beta = 2.5$, while for the Gaussian pulses in Fig. 3.2, $\beta = 2.3$. The parameter γ varies more. For a square laser pulse in panels (a) and (b) in Fig. 3.2, γ is respectively 0.95, 0.84 and 1.07. For the Gaussian ones in plots (a) and (b) in Fig. 3.2, γ is 0.87 and 0.77.

Besides the many-body Rabi oscillations, there are other manifestations of correlations between interacting excited atoms. One can study the fluctuations of the number of excited atoms. Without these correlations, the probability to have a certain number of excited atoms is determined by the average excitation probability P and the total number of atoms N. The probability $P(n_{\text{exc}})$ to get any number $n_{\text{exc}} \leq N$ of excited atoms is given by the Bernoulli formula

$$P(n_{\text{exc}}) = \begin{pmatrix} N \\ \\ n_{\text{exc}} \end{pmatrix} P^{n_{\text{exc}}}(1-P)^{N-n_{\text{exc}}}. \qquad (3.2.5)$$

For a given excitation probability P, one can calculate the expected variance $\Delta n'_{\text{exc}}$ assuming no correlations, and then compare it with the actual Δn_{exc}. We take the relative size of these variances as the measure of these fluctuations. This procedure can be done experimentally as well. In Fig. 3.4, we show the ratio $\Delta n_{\text{exc}}/\Delta n'_{\text{exc}}$ as a function of the pulse area. This ratio is smaller than one because there are some restrictions on which combinations of excited atoms can be likely excited in the presence of interactions. On the other hand, in the absence of correlations, all combinations of excited atoms are equally probable. This figure also shows that after reaching the minimum, the ratio $\Delta n_{\text{exc}}/\Delta n'_{\text{exc}}$ increases again due to decoherence.

The experimental results [13] on counting statistics of somewhat larger samples than we consider here do show the sub-Poissonian character of Rydberg excitation.

We have also calculated the spatial correlation function between the central atom and other atoms in mesoscopic samples. For larger samples, this function was calculated in [60]. They also found some interesting correlations if there is some frequency chirp of the laser pulse. In the presence of chirp, there is a region of internuclear separations R for which the correlation function is greater than one. In the absence of chirp this region does not exist. We do not include any chirp in our simulations because it is known that it destroys even the single-atom Rabi flopping. A delicate point for calculating the correlation function is that what we really calculate is the correlations beetwen superatoms and these superatoms are quite extended objects. Their linear size is about one third of the sample radius. Averaging over many random arrangements of atoms improves the determination of the correlation functions, but we do not insist on having many points for this function (Fig. 3.5). In the supperatom approach, the correlation function $c(p,q)$ between any atom p belonging to superatom i and any atom q belonging to superatom j is the same for all p and q and equal to the correlation function $C(i,j)$ between superatoms i and j. In addition, $c(p,q)=0$ for atoms p and q belonging to the same superatom. This suggests that the correlation function $c(p,q)$ implicitly contains, in some sense, spatial averaging over the spatial extension of a superatom. Since, on average, excitation probabilities $P(i)$ depend on

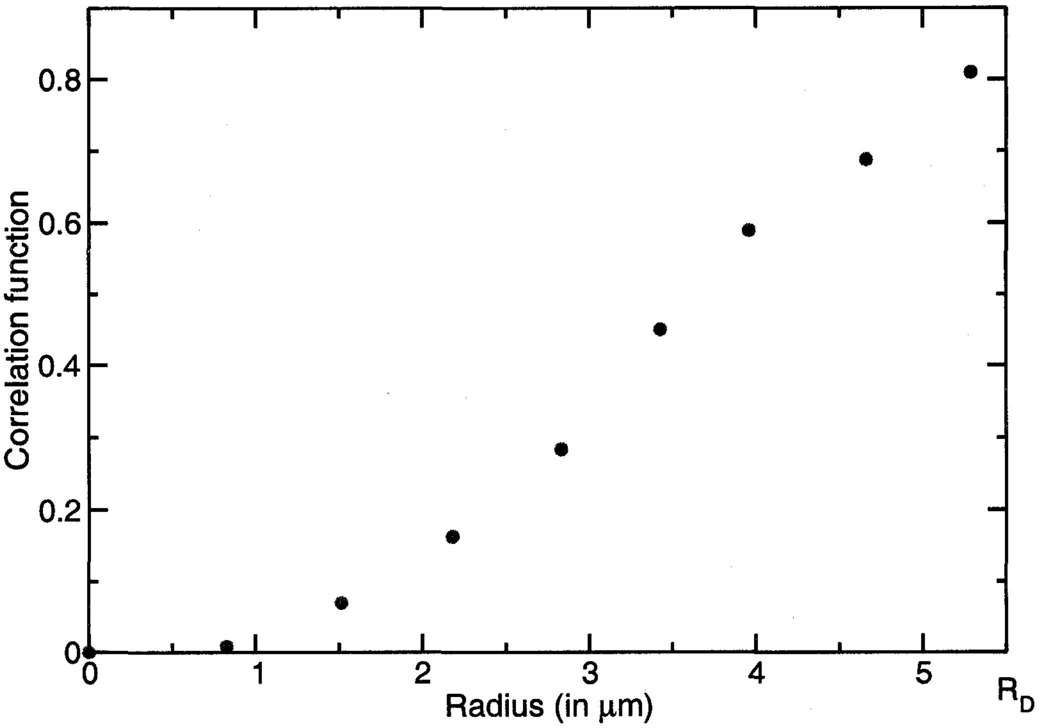

Fig. 3.5: The correlation function between a central atom and other atoms versus the distance between them for the same parameters used in Figs. 3.1-3.2. This function is obtained by averaging over one hundred different random placements of 70 atoms. This means that 6900 atom pairs are used to get this dependence.

the atom's location, the correlation function has to be

$$c(p,q) = \frac{P(p,q)}{P(p)P(q)}, \tag{3.2.6}$$

where $P(p,q)$ is the probability to excite simultaneously atoms p and q. In our case one of atoms p and q is always a central atom. The correlation function averaged over one hundred random positions of atoms is presented in Fig. 3.5. This figure shows that there are almost no correlations (i.e. $c(p,q) \approx 1$) between the central atom and the atoms near the sample surface.

Chapter 4

Many-Body Dynamics of Rydberg Excitation Using the Ω-Expansion

We have analyzed so far different approximate methods to compute the excitation dynamics of "frozen gases". In this chapter, we show how to obtain the Ω-expansion, where Ω is the single atom Rabi frequency, of the most interesting physical quantities relevant to Rydberg excitation in the interaction and Heisenberg pictures. First, we expand the wavefunction in the interaction picture. For a square pulse, we give a closed formula for any term in the expansion in any order. We will find an analogous expansion in the Heisenberg picture. In this picture we expand the σ-operators and give recurrence relations to calculate any order of the expansion.

4.1 Ω-Expansion in the interaction picture

We consider again a system of N ultracold two-level atoms for which the upper level is a Rydberg state. We use the same Hamiltonian we have introduced for the so called "frozen" gases. We assume strong interactions between Rydberg atoms and expect many-body effects to occur.

We start again with the many-body Hamiltonian of interacting two-level atoms

$$H = \Delta \sum_{i=1}^{N} \hat{\sigma}_{ee}^{i} + \frac{\Omega}{2} \sum_{i=1}^{N} \left(f(t) \hat{\sigma}_{eg}^{i} + f^{*}(t) \hat{\sigma}_{ge}^{i} \right) + \sum_{i=1, j>i}^{N} \kappa_{ij} \hat{\sigma}_{ee}^{i} \hat{\sigma}_{ee}^{j} , \tag{4.1.1}$$

Solving this Hamiltonian is trivial in two limits, when all $\kappa_{ij} \rightarrow \infty$ and when all $\kappa_{ij} \rightarrow 0$. An arbitrary big ensemble of atoms in the limit of infinitely strong interactions becomes fully blockaded. This means that there cannot be more than one excited atom in the sample. Any many-body state with the number of excited atoms greater than one would be infinitely shifted due to interactions and practically inaccessible for any many-photon transitions. Such systems are effectively two-level systems, with the collective ground state $|G\rangle = |g_1 g_2 \ldots g_N\rangle$ and the collective excited state $|E\rangle = 1/\sqrt{N} \sum_i |g_1 \ldots e_i \ldots g_N\rangle$. Consequently, the equivalent Hamiltonian H' in the limit $\kappa_{ij} \rightarrow \infty$ is

$$H' = \Delta |E\rangle \langle E| + \frac{\sqrt{N}\Omega}{2} \left(f(t) |E\rangle \langle G| + f^{*}(t) |G\rangle \langle E| \right) . \tag{4.1.2}$$

This is formally the Hamiltonian for isolated atoms, only the Rabi flopping is scaled as $\sqrt{N}$. If the detuning Δ is zero and $f(t)$ real, the solution is [76]

$$P_{\text{exc}}(t) = |C_E(t)|^2 = \frac{1}{N} \sin^2 \left(\sqrt{N} \Omega F(t)/2 \right) , \tag{4.1.3}$$

where C_E is the excitation amplitude of the collective excited state and the pulse area is $\Omega F(t) = \Omega \int_{t_0}^{t} f(t')dt'$, where t_0 is the initial time of laser excitation. The last formula (4.1.3) has been discussed in the context of collective oscillations. Also, approximate methods can be checked against this limit.

We can solve the equations of motion by expanding ψ or σ-operators in powers of Ω. It is remarkable that, in principle, all terms in the expansion can be calculated exactly. In this sense, the Hamiltonian (4.1.1) is exactly solvable. Actually, we can find the Ω-expansion of any relevant quantity we want. In this section we calculate the wavefunction of the system and its expansion in the interaction picture. It follows from Eq. (4.1.3) that the expansion is well defined and convergent in the limit $\kappa_{ij}\rightarrow\infty$. Clearly, it is also fine for isolated atoms (the limit $\kappa_{ij}\rightarrow 0$), so we expect that it is well defined and convergent for arbitrarily strong interactions. It may be interesting to show how it works in the Heisenberg picture since the evolution of the σ-operators is nonlinear in this picture. We show this in the following section.

The usual problem with a many-body Hamiltonian is that the nonlinear part containing interactions is very difficult to solve. Here the nonlinear part $H_0 = \Delta \sum\limits_{i=1}^{N} \hat{\sigma}^i_{ee} + \sum\limits_{i=1,j>i}^{N} \kappa_{ij}\hat{\sigma}^i_{ee}\hat{\sigma}^j_{ee}$ is exactly solvable. This Hamiltonian cannot change the number of excited atoms and thus any pure collective state with a fixed number of excited atoms is an eigenstate of H_0. This is essentially the reason that allows calculating any term in the Ω-expansion. Moreover, for a square laser pulse, all terms are expressed in a closed form.

To simplify the treatment, we assume that $f(t)$ is real, and we identify Δ with the diagonal interaction terms $\kappa_{ii} \equiv \Delta$. We also use only dimensionless variables $t/T \rightarrow t$, $HT \rightarrow H$, $\omega = \Omega T$ and $k_{ij} = \kappa_{ij}T$, where T is a pulse duration. It is convenient to factorize the wave function as follows

$$|\psi(t)\rangle = e^{-iH_0t}(|\varphi_0\rangle + \omega\,|\varphi_1(t)\rangle + \omega^2\,|\varphi_2(t)\rangle + \ldots)\,. \tag{4.1.4}$$

The state $|\varphi_0\rangle$ is the initial state and it is actually time-independent. It satisfies $\left(i\frac{\partial}{\partial t} - H_0\right)\exp(-iH_0t)\,|\varphi_0\rangle = 0$. The conditions that $|\psi(t)\rangle$ satisfies the Schrödinger equation is equivalent to the following set of equations (for $p \geq 1$).

$$\begin{aligned} i\frac{\partial}{\partial t}\,|\varphi_p\rangle &= \frac{1}{2}f(t)e^{iH_0t}\sum_{i=1}^{N}\left(\hat{\sigma}^i_{eg} + \hat{\sigma}^i_{ge}\right)e^{-iH_0t}\,|\varphi_{p-1}\rangle \\ &\equiv \frac{1}{2}f(t)U(t)\,|\varphi_{p-1}\rangle\,, \end{aligned} \tag{4.1.5}$$

where the operator $U(t)$ is introduced for convenience. This expression describes the evolution of states in the interaction picture. The form $U(t)$ can be simplified using the commutation relations of the σ-operators.

$$e^{iH_0t}\hat{\sigma}^i_{eg}e^{-iH_0t} = e^{it\sum_j k_{ij}\hat{\sigma}^j_{ee}}\sigma^i_{eg}, \tag{4.1.6}$$

$$e^{iH_0t}\hat{\sigma}^i_{ge}e^{-iH_0t} = \sigma^i_{ge}e^{-it\sum_j k_{ij}\hat{\sigma}^j_{ee}}. \tag{4.1.7}$$

The integral form of (4.1.5) is more useful

$$\begin{aligned} |\varphi_p\rangle &= \frac{-i}{2}\int_{t_0}^{t} dt_1 f(t_1)U(t)\,|\varphi_{p-1}\rangle \qquad (4.1.8) \\ &= \left(\frac{-i}{2}\right)^p \int_{t_0}^{t} dt_1 f(t_1)U(t_1)\int_{t_0}^{t_1} dt_2 f(t_2)U(t_2)\ldots\int_{t_0}^{t_{p-1}} dt_p f(t_p)U(t_p)\,|\varphi_0\rangle\,. \end{aligned}$$

For simplicity we assume that $|\varphi_0\rangle$ is the ground state $|G\rangle$.

The evaluation of the integrals (4.1.8) is greatly simplified by the fact that H_0 is exactly solvable. Its eigenstates are all pure states $|ij\ldots s\rangle = \hat{\sigma}^i_{eg}\hat{\sigma}^j_{eg}\ldots\hat{\sigma}^s_{eg}\,|G\rangle$. To avoid having too many indices, the following convention is used. In an arbitrary basis state, we numerate all excited states $|n\rangle$ from 1 to n so that $|n\rangle = \hat{\sigma}^1_{eg}\hat{\sigma}^2_{eg}\dots\hat{\sigma}^n_{eg}|G\rangle$. This should not cause confusion because we always consider only one $|n\rangle$ at a time. If $|n\rangle$ is an eigenstate of H_0, than $\hat{\sigma}^i_{eg}|n\rangle$ (and $\hat{\sigma}^i_{ge}|n\rangle$) is also an eigenstate of H_0 so that $U^i(t)|n\rangle \equiv \exp(iH_0t)\hat{\sigma}^i\exp(-iH_0t)|n\rangle = \exp(i\varepsilon_it)\hat{\sigma}^i|n\rangle$, where $\hat{\sigma}^i$ is $\hat{\sigma}^i_{eg}(\hat{\sigma}^i_{ge})$ and ε_i is directly proportional to the interaction energy of an atom being excited(de-excited). This feature is essential for calculating accurately $|\varphi_p\rangle$ and its components $\langle n|\varphi_p\rangle$. Note that $|\varphi_p\rangle$ contains only $|p\rangle$, $|p-2\rangle, \dots$ states.

First we calculate $\langle p|\varphi_p\rangle$ for an arbitrary $|p\rangle$. Since the operators $U(t)$ in (4.1.8) are just the sums of $U_i(t)$ (and $U_i{}^\dagger(t)$), the only non-vanishing terms contributing to $\langle n|\varphi_p\rangle$ are $\sim \langle p|e^{i\varepsilon_1t_1}\dots e^{i\varepsilon_pt_p}\hat{\sigma}^{\pi(1)}_{eg}\dots\hat{\sigma}^{\pi(p)}_{eg}|\varphi_0\rangle$, where π is a permutation of indices $(1,2\dots,p)$ and interaction energies are

$$\varepsilon_i = \sum_{j\neq\pi^{-1}(1),\dots,\pi^{-1}(i-1)}^{p} k_{j\pi^{-1}(i)}.$$

The meaning of this expression is the following. There are $p!$ ways to excite state $|p\rangle$. Each way corresponds to a certain permutation of atoms $(1,2\dots,p)$. The intermediate values ε_i of the interaction energy of the atoms that have been excited depends, of course, on which atoms are temporally excited and so depends on the permutation π. Consequently, the amplitudes of excitation $C^{(p)}_\pi$ corresponding to different ways of exciting $|p\rangle$ are different and to get $\langle p|\varphi_p\rangle$ we have to sum over all permutations

$$\langle p|\varphi_p\rangle = \left(\frac{-i}{2}\right)^p \sum_\pi C^{(p)}_\pi, \tag{4.1.9}$$

where $C_\pi^{(p)}$ is given by

$$C_\pi^{(p)} = \int_{t_0}^{t} dt_1 f(t_1) e^{i\varepsilon_1 t_1} \int_{t_0}^{t_1} dt_2 f(t_2) e^{i\varepsilon_2 t_2} \ldots \int_{t_0}^{t_{p-1}} dt_p f(t_p) e^{i\varepsilon_p t_p}. \tag{4.1.10}$$

For square pulses, $f(t_i) = 1$ (we set $t_0 = 0$), all $C^{(p)}$ can be expressed in a closed form; it is therefore interesting to analyze this case in detail. From the last equation it follows that $C_\pi^{(p)}$ can be characterized by its set of interaction energies $C_\pi^{(p)} = C_{\varepsilon_1,\ldots,\varepsilon_p}^{(p)}$. By rearranging the integrals in (4.1.10), one can find the following interesting relation for any $2 < q < p$

$$C_{\varepsilon_1,\ldots,\varepsilon_p}^{(p)} = \int_0^t dt_q e^{i\varepsilon_{1\uparrow q} t_q} C_{\varepsilon_1,\ldots,\varepsilon_{q-1}}^{(q-1)}(t-t_q) C_{\varepsilon_{q+1},\ldots,\varepsilon_p}^{(p-q)}(t_q), \tag{4.1.11}$$

where $\varepsilon_{i\uparrow j} = \sum_{s=i}^{j} \varepsilon_s$. For $p = 1$, we have $C_\varepsilon^{(1)}(t) = \int_0^t dt_1\, e^{i\varepsilon t_1} = i\left[1 - \exp(i\varepsilon t)\right]/\varepsilon$. Using repeatedly the simple formula $\int_0^t dt_1\, e^{i\varepsilon' t_1} C_\varepsilon^{(1)}(t_1) = i\left[C_{\varepsilon'}^{(1)}(t) - C_{\varepsilon+\varepsilon'}^{(1)}(t)\right]/\varepsilon$, the integral (4.1.10) for square pulses can be found to be

$$C_\pi^{(p)} = \sum_{s=1}^{p} \frac{i^{p-1}(-1)^{s-1}}{P_{s\downarrow} P_{(s+1)\uparrow}} C_{\varepsilon_{1\uparrow s}}^{(1)}, \tag{4.1.12}$$

where $P_{s\downarrow} = \prod_{i=2}^{s} \varepsilon_{i\uparrow s}$, $P_{s\uparrow} = \prod_{i=s}^{p} \varepsilon_{s\uparrow i}$ with the additional definitions $P_{1\downarrow} = P_{(p+1)\uparrow} = 1$. It is obvious that all $\langle p \geq 2|\varphi_p\rangle$ vanish in the limit $k_{ij} \to \infty$, as expected. Because all ε_i include the detuning, they are in general different from zero, but from Eq. (4.1.10) it is clear that $C_\pi^{(p)}$ are well defined even if for some "i" $\varepsilon_i \to 0$.

The next step is to find $\langle p-2|\varphi_p\rangle$ for an arbitrary $|p-2\rangle = \hat{\sigma}_{eg}^1 \hat{\sigma}_{eg}^2 \ldots \hat{\sigma}_{eg}^{p-2} |G\rangle$. In this case we need to consider all permutations $\pi^*(1,\ldots,p)$ of the σ-operators in the product $\hat{\sigma}_{eg}^1 \ldots \hat{\sigma}_{eg}^{(p-2)} \hat{\sigma}_{ge}^{(s)} \hat{\sigma}_{eg}^{(s)}$, where $s \neq (1,\ldots,p-2)$. Since $\langle p-2| \ldots \hat{\sigma}_{eg}^{(s)} \ldots \hat{\sigma}_{ge}^{(s)} \ldots = 0$

(atom "s" cannot deexcite if it has not been excited first), nonvanishing contributions come only from the permutations for which $\hat{\sigma}_{ge}^{(s)}$ precedes $\hat{\sigma}_{eg}^{(s)}$. In other words, $\pi^*(1,\ldots,p)$ are all permutations $\pi(1,\ldots,p)$ satisfying $\pi(p-1) < \pi(p)$. Collecting all contributions to $\langle p-2|\varphi_p\rangle$, one obtains

$$\langle p-2|\varphi_p\rangle = \left(\frac{-i}{2}\right)^p \sum_{s\neq(1,\ldots,p-2)} \sum_{\pi^*} C_{\pi^*}^{(p)}. \tag{4.1.13}$$

Most $C_{\pi^*}^{(p)}$ are also determined by Eq. (4.1.12), however this formula cannot be applied directly for p—1 sets of amplitudes. If the permutation $\pi_q^*(1,\ldots,p)$ leaves the operators $\hat{\sigma}_{ge}^{(s)}$ and $\hat{\sigma}_{eg}^{(s)}$ adjacent, i.e. $\pi_q^*(p)=\pi_q^*(p-1)+1 = q$, $q = 2,\ldots p$, then the energies ε_{q-1} and ε_q satisfy $\varepsilon_{q-1}+\varepsilon_q=\varepsilon_{(q-1)\uparrow q}=0$. The energy ε_{q-1} has opposite sign because it originates from $U_s{}^\dagger(t)$, not $U_i(t)$ like other ε_i. Since the products $P_{(q-1)\uparrow}$ and $P_{q\downarrow}$ contain $\varepsilon_{(q-1)\uparrow q}$ as a factor, there are two terms in Eq. (4.1.12) whose limits have to be determined when $\varepsilon_{(q-1)\uparrow q}\to 0$. Instead of finding these limits we transform $C_{\pi_q^*}^{(p)}$ using the following recurrence formula

$$C_{\varepsilon_1,\ldots,\varepsilon_p}^{(p)} = \frac{i}{\varepsilon_q} C_{\ldots,\varepsilon_{q-1},\varepsilon_q+\varepsilon_{q+1},\varepsilon_{q+2},\ldots}^{(p-1)} - \frac{i}{\varepsilon_q} C_{\ldots,\varepsilon_{q-2},\varepsilon_{q-1}+\varepsilon_q,\varepsilon_{q+1},\ldots}^{(p-1)}, \tag{4.1.14}$$

which is obtained using integration by parts. If $\varepsilon_{(q-1)\uparrow q}=0$, the second term in (4.1.14) needs to be determined. It is a simple task because the limit of (4.1.12) can be easily found when any $\varepsilon_i\to 0$. A compact formula for this limit (for $q > 1$) directly follows from Eq. (4.1.14) using the following transformation

$$\begin{aligned} C^{(p)}_{\varepsilon_1,\dots,\varepsilon_p} &= \frac{i}{\varepsilon_q} C^{(p-1)}_{\dots,\varepsilon_{q-1},\varepsilon_q+\varepsilon_{q+1},\varepsilon_{q+2},\dots} - \frac{i}{\varepsilon_q} C^{(p-1)}_{\dots,\varepsilon_{q-2},\varepsilon_{q-1}+\varepsilon_q,\varepsilon_{q+1},\dots} = \\ & \frac{i}{\varepsilon_q}\left(C^{(p-1)}_{\dots,\varepsilon_{q-1},\varepsilon_q+\varepsilon_{q+1},\varepsilon_{q+2},\dots} - C^{(p-1)}_{\dots,\varepsilon_{q-1},\varepsilon_{q+1},\dots}\right) \\ & - \frac{i}{\varepsilon_q}\left(C^{(p-1)}_{\dots,\varepsilon_{q-2},\varepsilon_{q-1}+\varepsilon_q,\varepsilon_{q+1},\dots} - C^{(p-1)}_{\dots,\varepsilon_{q-1},\varepsilon_{q+1},\dots}\right), \end{aligned} \tag{4.1.15}$$

which in the limit $\varepsilon_q \to 0$ gives

$$C^{(p)}_{\varepsilon_1,\dots,\varepsilon_p}\Big|_{\varepsilon_q=0} = i\left(\frac{\partial}{\partial\varepsilon_{q+1}} - \frac{\partial}{\partial\varepsilon_{q-1}}\right) C^{(p-1)}_{\varepsilon_1,\dots,\varepsilon_{q-1},\varepsilon_{q+1},\dots,\varepsilon_p}. \tag{4.1.16}$$

For $q=1$ the analog of (4.1.16) is $C^{(p)}_{\varepsilon_1,\dots,\varepsilon_p}\Big|_{\varepsilon_1=0} = (t + i\partial/\partial\varepsilon_2) C^{(p-1)}_{\varepsilon_2,\dots,\varepsilon_p}$. The comparison of this formula and the limit of (4.1.12) when $\varepsilon_1 \to 0$ gives the new relation

$$\sum_{s=1}^{p} \frac{i^{p-1}(-1)^{s-1}}{P_{s\downarrow} P_{(s+1)\uparrow}} = 0. \tag{4.1.17}$$

Although this formula is derived for $\varepsilon_1 = 0$, it is actually true for any set of energies $\varepsilon_1, \dots, \varepsilon_p$. Other components $\langle p-4|\varphi_p\rangle$, $\langle p-6|\varphi_p\rangle$, ...can be calculated in a similar fashion.

Calculating P_{exc} up to ω^4 is not very difficult in any of the two picture we consider. Higher orders are much more challenging. It is extremely difficult to evaluate higher orders in the Heisenberg picture because there are many more terms to calculate. The reason is essentially that the expectation values of the σ-operators are quadratic functions of excitation amplitudes, which are themselves polynomial functions of ω. In the next section we present the Ω-expansion in the the Heisenberg picture and give some concrete results of this approach.

4.2 Ω-Expansion in the Heisenberg picture

The evolution of the σ-operators in the Heisenberg picture, governed by Hamiltonian (4.1.1),is given by the following equations

$$\frac{d\hat{\sigma}^i_{ee}}{d\tau} = i\frac{\Omega}{2}\left[f(t)\hat{\sigma}^i_{eg} - f^*(t)\hat{\sigma}^i_{ge}\right], \tag{4.2.1}$$

$$\frac{d\hat{\sigma}^i_{eg}}{d\tau} = i\Delta\hat{\sigma}^i_{eg} + i\frac{\Omega}{2}f^*(t)\left[2\hat{\sigma}^i_{ee} - 1\right] + i\sum_{j\neq i}\kappa_{ij}\hat{\sigma}^i_{eg}\hat{\sigma}^j_{ee}. \tag{4.2.2}$$

These equations can be slightly simplified by removing the Δ term using new scaled (dimensionless) variables

$$\hat{\sigma}^j_{eg}e^{-i\Delta t} \to \hat{\sigma}^j_{eg}, \quad \tau = t/T, \quad \omega = \Omega T, \quad \delta = \Delta T, \quad k_{ij} = \kappa_{ij}T$$

where T is the pulse duration. The equations for the new σ-operators can then be rewritten as

$$\frac{d\hat{\sigma}^i_{ee}}{d\tau} = i\frac{\omega}{2}\left[g(\tau)\hat{\sigma}^i_{eg} - g^*(\tau)\hat{\sigma}^i_{ge}\right], \tag{4.2.3}$$

$$\frac{d\hat{\sigma}^i_{eg}}{d\tau} = i\frac{\omega}{2}g(t)^*\left[2\hat{\sigma}^i_{ee} - 1\right] + i\sum_{j\neq i}k_{ij}\hat{\sigma}^i_{eg}\hat{\sigma}^j_{ee}, \tag{4.2.4}$$

where $g(\tau) = f(\tau\sigma)e^{i\delta\tau}$.

We solve the equations of motion by expanding the σ-operators in power of ω.

$$\hat{\sigma}^i_{ee} = \hat{\sigma}^{i(0)}_{ee} + \omega\hat{\sigma}^{i(1)}_{ee} + \omega^2\hat{\sigma}^{i(2)}_{ee} + \ldots, \tag{4.2.5}$$

$$\hat{\sigma}^i_{eg} = \hat{\sigma}^{i(0)}_{eg} + \omega\hat{\sigma}^{i(1)}_{eg} + \omega^2\hat{\sigma}^{i(2)}_{eg} + \ldots. \tag{4.2.6}$$

The ω-expansion of $\langle\hat{\sigma}^i_{ee}(\tau)\rangle$ $(\langle\hat{\sigma}^i_{eg}(\tau)\rangle)$ contains only even (odd) power of ω if all the atoms are initially in their ground state. This statement is not true for arbitrary initial conditions or for the σ-operators themselves. This can be shown as follows. Assume that instead of $|g\rangle$ and $|e\rangle$ we use $|g'\rangle$ and $|e'\rangle$ defined as

$$|g'\rangle = e^{i\varphi_g}\,|g\rangle \;, \qquad |e'\rangle = e^{i\varphi_e}\,|e\rangle \;, \tag{4.2.7}$$

where the constant phase factors satisfy $\varphi_e - \varphi_g = \pm\pi$. This defines new operators $\hat{\sigma}_{e'e'}$ and $\hat{\sigma}_{e'g'}$. It follows from the definitions of these operators that, for any τ and ω, the following relations have to be satisfied

$$\hat{\sigma}_{e'e'}(\tau,\omega) = \hat{\sigma}_{ee}(\tau,\omega), \qquad \hat{\sigma}_{e'g'}(\tau,\omega) = -\hat{\sigma}_{eg}(\tau,\omega), \tag{4.2.8}$$

which gives

$$\langle\hat{\sigma}_{e'e'}(\tau,\omega)\rangle = \langle\hat{\sigma}_{ee}(\tau,\omega)\rangle, \qquad \langle\hat{\sigma}_{e'g'}(\tau,\omega)\rangle = -\langle\hat{\sigma}_{eg}(\tau,\omega)\rangle. \tag{4.2.9}$$

Similarly to Eqs. (4.2.3)-(4.2.4), we can write analogous evolution equations for the new operators $\hat{\sigma}_{e'e'}$ and $\hat{\sigma}_{e'g'}$. We can also write Eqs. (4.2.3)-(4.2.4) for the opposite sign of omega $\omega \to -\omega$. However, after the substitution $\omega' = -\omega$, the time evolution of the expectation values $\langle\hat{\sigma}_{ee}(t,\omega)\rangle$ and $\langle\hat{\sigma}_{eg}(t,\omega)\rangle$, and the time evolution of $\langle\hat{\sigma}_{e'e'}(t,\omega')\rangle$ and $\langle\hat{\sigma}_{e'g'}(t,\omega')\rangle$ are given by the same differential equations. Since the initial conditions are the same, the solutions have to be the same as well

$$\begin{aligned}\langle\hat{\sigma}_{ee}(\tau,\omega)\rangle &= \langle\hat{\sigma}_{e'e'}(\tau,\omega')\rangle = \langle\hat{\sigma}_{e'e'}(\tau,-\omega)\rangle,\\ \langle\hat{\sigma}_{eg}(\tau,\omega)\rangle &= \langle\hat{\sigma}_{e'g'}(\tau,\omega')\rangle = \langle\hat{\sigma}_{e'g'}(\tau,-\omega)\rangle.\end{aligned} \tag{4.2.10}$$

Combining Eq.(4.2.9) and Eq.(4.2.10) we conclude

$$\begin{aligned}\langle\hat{\sigma}_{ee}(\tau,\omega)\rangle &= \langle\hat{\sigma}_{ee}(\tau,-\omega)\rangle,\\ \langle\hat{\sigma}_{eg}(\tau,\omega)\rangle &= -\langle\hat{\sigma}_{eg}(\tau,-\omega)\rangle.\end{aligned} \tag{4.2.11}$$

Therefore, if all the atoms are initially in the ground state, $\langle\hat{\sigma}_{ee}(t,\omega)\rangle$ is an even function of ω and $\langle\hat{\sigma}_{eg}(t,\omega)\rangle$ is odd. All these symmetry properties can be checked against the explicit formulae below.

According to Eqs. (4.2.3)-(4.2.4), the differential equations for $\sigma_{ee}^{i(n)}$ and $\sigma_{eg}^{i(n)}$ are

$$\frac{d\hat{\sigma}_{ee}^{i(n)}}{d\tau} = i\frac{1}{2}\left[g(\tau)\hat{\sigma}_{eg}^{i(n-1)} - g^*(\tau)\hat{\sigma}_{ge}^{i(n-1)}\right], \tag{4.2.12}$$

$$\frac{d\hat{\sigma}_{eg}^{i(n)}}{d\tau} = i\frac{g^*(t)}{2}(2\hat{\sigma}_{ee}^{i(n-1)} - \delta_{n1}) + i\sum_{j\neq i} k_{ij}\sum_{p=0}^{n-1}\hat{\sigma}_{eg}^{i(p)}\hat{\sigma}_{ee}^{j(n-p)} + i\sum_{j\neq i} k_{ij}\hat{\sigma}_{eg}^{i(n)}\hat{\sigma}_{ee}^{j(0)}, \tag{4.2.13}$$

where δ_{n1} is the Kronecker delta function. To start the recurrence procedure, we need the initial operators $\hat{\sigma}_{ee}^{i(0)}$ and $\hat{\sigma}_{eg}^{i(0)}$. They are derived from Eqs. (4.2.3)-(4.2.4) for $\omega = 0$

$$\hat{\sigma}_{ee}^{i(0)}(\tau) = \hat{\sigma}_{ee}^{i(0)}(\tau_0), \quad \hat{\sigma}_{eg}^{i(0)}(\tau) = \hat{\sigma}_{eg}^{i(0)}(\tau_0)e^{-i(\tau-\tau_0)\sum_{s\neq i} k_{is}\hat{\sigma}_{ee}^{s(0)}(\tau_0)}, \tag{4.2.14}$$

where τ_0 is the initial time.

The equivalent integral form of Eq. (4.2.12) is

$$\hat{\sigma}_{ee}^{i(n)}(\tau) = \frac{i}{2}\int_{\tau_0}^{\tau} d\tau_1\left[g(\tau_1)\hat{\sigma}_{eg}^{i(n-1)}(\tau_1) - g^*(\tau_1)\hat{\sigma}_{ge}^{i(n-1)}(\tau_1)\right]. \tag{4.2.15}$$

We get an equivalent integral form of Eq. (4.2.13) in two steps. After multiplying this equation by $\exp(-i\tau\sum_{j\neq i} k_{ij}\hat{\sigma}_{ee}^{j(0)})$,. grouping terms with $\hat{\sigma}_{eg}^{i(n)}$ and utilizing the time independence of $\hat{\sigma}_{ee}^{s(0)}$, another differential equation is obtained

$$\frac{d}{d\tau}\left(\hat{\sigma}_{eg}^{i(n)}e^{-i\tau\sum\limits_{s\neq i} k_{is}\hat{\sigma}_{ee}^{s(0)}}\right) = \left[i\frac{g^*(\tau_1)}{2}(2\hat{\sigma}_{ee}^{i(n-1)} - \delta_{n1}) + i\sum_{j\neq i} k_{ij}\sum_{p=0}^{n-1}\hat{\sigma}_{eg}^{i(p)}\hat{\sigma}_{ee}^{j(n-p)}\right]e^{-i\tau\sum\limits_{s\neq i} k_{is}\hat{\sigma}_{ee}^{s(0)}}. \tag{4.2.16}$$

The corresponding integral equation is

$$\begin{aligned}\hat{\sigma}_{eg}^{i(n)}(\tau) = \int\limits_{\tau_0}^{\tau} d\tau_1 \Bigg[& i\frac{g^*(\tau_1)}{2}(2\hat{\sigma}_{ee}^{i(n-1)}(\tau_1) - \delta_{n1}) \\ & +i\sum_{j\neq i} k_{ij} \sum_{p=0}^{n-1} \hat{\sigma}_{eg}^{i(p)}(\tau_1)\hat{\sigma}_{ee}^{j(n-p)}(\tau_1)\Bigg] e^{-i(\tau-\tau_1)\sum\limits_{s\neq i} k_{is}\hat{\sigma}_{ee}^{s(0)}}\end{aligned} \tag{4.2.17}$$

In our approach the recurrence relations (4.2.15) and (4.2.17) provide the way of calculating any order of the expansions. To calculate $\hat{\sigma}_{eg}^{i(n)}$, one needs to calculate $\hat{\sigma}_{ee}^{i(n)}$ first. What we really want is the expectation values of the σ-operators, especially $\langle\hat{\sigma}_{ee}^{i}\rangle$. With the help of the recurrence relations, we express $\hat{\sigma}_{ee}^{i(n)}$ and $\hat{\sigma}_{eg}^{i(n)}$ in terms of $\hat{\sigma}_{ee}^{j(0)}$ and $\hat{\sigma}_{eg}^{j(0)}$. Since we can easily find the expectation values of any product of $\hat{\sigma}_{ee}^{j(0)}$ and $\hat{\sigma}_{eg}^{j(0)}$, in principle, we can find exactly any term in the expansions (4.2.5)-(4.2.6). In our calculation, we assume that all atoms are initially in the ground state. Consequently, the following expectation values are necessarily equal to zero for any atom i

$$\left\langle\hat{\sigma}_{eg}^{i(0)}\ldots\right\rangle = \left\langle\ldots\hat{\sigma}_{ge}^{i(0)}\right\rangle = \left\langle\hat{\sigma}_{ee}^{i(0)}\ldots\right\rangle = \left\langle\ldots\hat{\sigma}_{ee}^{i(0)}\right\rangle = 0. \tag{4.2.18}$$

Since in the Heisenberg picture the wave function is time-independent, the average $\langle\,\rangle$ can go through integrals contained in the recurrence relations. We find a new recurrence relation for $\left\langle\hat{\sigma}_{ee}^{i(n)}\right\rangle$ after substituting expression (4.2.17), for $\hat{\sigma}_{eg}^{i(n-1)}$, into Eq. (4.2.15)

$$\begin{aligned}\left\langle\hat{\sigma}_{ee}^{i(n)}(\tau)\right\rangle = & \int\limits_{\tau_0}^{\tau} d\tau_1 \left(\delta_{n2} - 2\left\langle\hat{\sigma}_{ee}^{i(n-2)}(\tau_1)\right\rangle\right) \int\limits_{\tau_1}^{\tau} d\tau_2 \frac{g(\tau_1)g^*(\tau_2)+g^*(\tau_1)g(\tau_2)}{4} \\ & -\sum_{j\neq i} k_{ij} \sum_{p=0}^{n-2} \mathrm{Re}\left[\int\limits_{\tau_0}^{\tau} d\tau_1 \left\langle\hat{\sigma}_{eg}^{i(p)}(\tau_1)\hat{\sigma}_{ee}^{j(n-p)}(\tau_1)\right\rangle \frac{F(\tau) - F(\tau_1)}{2}\right],\end{aligned} \tag{4.2.19}$$

where $F(\tau) = \int_{\tau_0}^{\tau} d\tau' g(\tau')$. For $n = 2$, this equation, together with expressions (4.2.18), leads to

$$\left\langle \hat{\sigma}_{ee}^{i(2)}(\tau) \right\rangle = \int_{\tau_0}^{\tau} d\tau_1 \int_{\tau_1}^{\tau} d\tau_2 \frac{g(\tau_1)g^*(\tau_2) + g^*(\tau_1)g(\tau_2)}{4}. \tag{4.2.20}$$

For any symmetric function $G(\tau_1, \tau_2) = G(\tau_2, \tau_1)$, the following relation is true (if the integrals exist)

$$\int_{\tau_0}^{\tau} d\tau_1 \int_{\tau_0}^{\tau_1} d\tau_2 G(\tau_1, \tau_2) = \int_{\tau_0}^{\tau} d\tau_1 \int_{\tau_1}^{\tau} d\tau_2 G(\tau_1, \tau_2) = \frac{1}{2} \int_{\tau_0}^{\tau} d\tau_1 \int_{\tau_0}^{\tau} d\tau_2 G(\tau_1, \tau_2). \tag{4.2.21}$$

Using this property we get instantly the final formula for $\left\langle \hat{\sigma}_{e}^{i(2)}(\tau) \right\rangle$

$$\left\langle \hat{\sigma}_{ee}^{i(2)}(\tau) \right\rangle = \frac{|F(\tau)|^2}{4}. \tag{4.2.22}$$

The last relation shows that the effects of interactions comes through higher orders than $n = 2$. This, of course, would not be true if the initial conditions were different. In the beginning there are no excited atoms and so there are no effects due to interactions. For these initial conditions, the excitation always starts as isolated atom excitation. Calculating $\left\langle \hat{\sigma}_{ee}^{i(4)}(\tau) \right\rangle$ takes more effort, so we split all its contributions, given by Eq. (4.2.19), into three parts

$$\left\langle \hat{\sigma}_{ee}^{i(4)}(\tau) \right\rangle = -I_{41} - I_{42} - I_{43}. \tag{4.2.23}$$

The integrals are defined as follows

$$\begin{aligned} I_{41} &= \int_{\tau_0}^{\tau} d\tau_1 \left\langle \hat{\sigma}_{ee}^{i(2)}(\tau_1) \right\rangle \int_{\tau_1}^{\tau} d\tau_2 \frac{g(\tau_1)g^*(\tau_2) + g^*(\tau_1)g(\tau_2)}{2}, \\ I_{42} &= \sum_{j \neq i} k_{ij} \mathrm{Re} \left[\int_{\tau_0}^{\tau} d\tau_1 \int_{\tau_1}^{\tau} d\tau_2 g(\tau_2) \left\langle \hat{\sigma}_{eg}^{i(1)}(\tau_1) \hat{\sigma}_{ee}^{j(2)}(\tau_1) \right\rangle \right], \end{aligned} \tag{4.2.24}$$

$$I_{43} = \sum_{j\neq i} k_{ij}\mathrm{Re}\left[\int_{\tau_0}^{\tau} d\tau_1 \int_{\tau_1}^{\tau} d\tau_2 g(\tau_2)\left\langle \hat{\sigma}_{eg}^{i(2)}(\tau_1)\hat{\sigma}_{ee}^{j(1)}(\tau_1)\right\rangle\right] . \tag{4.2.25}$$

The integral I_{41} can be calculated easily since $\left\langle \hat{\sigma}_{eg}^{i(2)}(\tau)\right\rangle$ is given by Eq. (4.2.22). After integration over τ_2, we obtain

$$\begin{aligned} I_{41} &= \frac{1}{4}\mathrm{Re}\left[\int_{\tau_0}^{\tau} d\tau_1 \left|F(\tau_1)\right|^2 g(\tau_1)\left(F^*(\tau) - F^*(\tau_1)\right)\right] \\ &= \frac{\left|F(\tau)\right|^4}{16} - \frac{1}{8}\mathrm{Re}\left[F(\tau)\int_{\tau_0}^{\tau} d\tau_1 g^*(\tau_1)F^2(\tau_1)\right] . \end{aligned} \tag{4.2.26}$$

Only I_{42} and I_{43} include interactions. The calculation procedure is to apply Eqs. (4.2.15) and (4.2.17) repeatedly until the only operators left are $\hat{\sigma}_{eg}^{i(0)}$ and $\hat{\sigma}_{ee}^{i(0)}$, whose expectation values are trivial to calculate.

The result for I_{42} is

$$I_{42} = \sum_{j\neq i}\frac{k_{ij}}{16i}\int_{\tau_0}^{\tau} d\tau_1 \left|F(\tau_1)\right|^2\left(F(\tau)F^*(\tau_1) - F^*(\tau)F(\tau_1)\right) . \tag{4.2.27}$$

This term is zero on resonance. Actually, this integral is canceled out by one of the I_{43} terms, so there is no need to consider it in detail.

It is convenient to have k_{ij} in the exponential (phase) factors only. This can be done for the sum $\mathcal{I}_4 = I_{42} + I_{43}$. After several partial integrations, the simplified form of $\mathcal{I}_4$ is

$$\begin{aligned} \mathcal{I}_4 = \frac{1}{4}\sum_{j\neq i}\mathrm{Re}\Bigg[&\int_{\tau_0}^{\tau} d\tau_1 g(\tau_1)\left(F(\tau) - 2F(\tau_1)\right) \\ &\times \int_{\tau_0}^{\tau_1} d\tau_2 g^*(\tau_2)F^*(\tau_2)\left(e^{i(\tau_1-\tau_2)k_{ij}} - 1\right)\Bigg] . \end{aligned} \tag{4.2.28}$$

For a system of N atoms, one just needs to calculate these integrals for given k_{ij}.

The derived expressions for I_{41} and $\mathcal{I}_4$ are formally sufficient but they might not be very convenient in the limit of a large number of atoms N, where we replace the sum $\sum_{j\neq i}$ by the integral $\int \rho d^3R$, where ρ is the atom density. It can be shown by direct calculation, for the terms we explicitely consider in the expansion, this replacement is equivalent to averaging over all posible spatial distribution of atoms. For a large sample and an arbitrary pulse shape, a better way is to first find the sum in Eq. (4.2.29) (i.e. the integral $\int \rho d^3R$). As an example, we give the result for the excitation probabilities in large systems (surface effects are ignored) with uniform densities. For simplicity, we assume that the system is on resonance. The last form of $I_{42}+I_{43}$ is very convenient to account for any angular dependence of k_{ij}. For large homogeneous systems and $k_{ij} \sim C_s/R^s$, we obtain

$$\begin{aligned}\mathcal{I}_4 = \lambda\, \rho\, (C_sT)^{3/s}\mathrm{Re}\Bigg[\int_{\tau_0}^{\tau} & d\tau_1 f(\tau_1)\,(F(\tau)-2F(\tau_1)) \\ & \times \int_{\tau_0}^{\tau_1} d\tau_2 g^*(\tau_2)F^*(\tau_2)(\tau_1-\tau_2)^{3/s}\,(1-i\,\mathrm{sgn}(C_6))\Bigg]\,,\end{aligned} \tag{4.2.29}$$

where λ is a parameter which depends on the spatial integral $\int d^3R\,\rho\,\left(e^{i(\tau_1-\tau_2)k_{ij}}-1\right)$. For resonant excitation and real $f(t)$, the ensemble averaged expansion of excitation probabilities is

$$P_{\text{exc}} = \frac{\pi^2}{4}\frac{I}{I_{\text{sat}}} - \frac{\pi^4}{48}\left(1+\gamma\rho\,|(C_s|\,T)^{3/s}\right)\frac{I^2}{I_{\text{sat}}^2} + \dots\,. \tag{4.2.30}$$

where I_{sat} is the saturation laser intensity (for isolated atoms) and T is the pulse duration. For $s=6$ we have the van der Waals interactions and for $s=3$ the dipole-dipole interactions. The values of the parameter γ in various cases of laser pulses and interactions are presented in Table 4.1. We note that the parameter γ for the angular dependent dipole-dipole interactions (with aligned dipole moments) $V(R) = \frac{U_3}{R^3}(1 - \cos^2\theta)$ is $\gamma = 4\gamma'/3\sqrt{3}$, where γ' corresponds to the isotropic interaction U_3/R^3.

These formulae have the first contributions of interactions to excitation probabilities. Note that we never assumed that the interactions were weak. Actually Eq. (4.2.29) is consistent with the limit $k_{ij} \to \infty$ for any i, j. In this limit, there is no contribution from the exponential terms since they oscillate infinitely fast. The remaining part reproduces exactly what one gets when the exact solution (4.1.3) in the limit $k_{ij} \to \infty$ is expanded.

One can use Eq. (4.2.30) to find the first approximation to the suppression of excitation, i.e. N_D introduced in the previous chapter. For large systems, I assume this N_D refers only to the suppression factor. The collective oscillations in large systems have not been seen in the experiments [11–13], and the simulation [60] does not support it. Our calculation presented in the previous chapter also suggests that these oscillations are hard to observe in disordered systems unless the system is almost fully blockaded.

Table 4.1: The parameter γ in the expansion (4.2.30) of excitation probabilities for various interaction potentials and excitation pulses. The pulse envelope for a Gaussian pulse is $g(\tau) = e^{-\tau^2}$ and for a rectangular one is $g(\tau) = \Theta(1 - \tau)$.

γ	C_3/R^3	$\frac{U_3}{R^3}(1 - 3\cos^2\theta)$	C_6/R^6
Gauss. pulse	32.1138	24.7212	10.8627
Square pulse	$\frac{2\pi^3}{5}$	$\frac{8\pi^3}{15\sqrt{3}}$	$\frac{128\pi^2}{189}$

4.3 Conclusion

I have shown that the equations of motion can be solved by expanding the wavefunction $|\psi\rangle$ or the σ-operators in powers of Ω. For square pulses, I have derived a closed formula for the terms in the expansion of many-body excitation amplitudes. Since this expansion is exact, it can also be used to test approximate methods. We derived the first two terms in the omega expansion of excitation probabilities for homogeneous systems with dipole-dipole and van der Waals interactions for square and Gaussian pulses.

Appendix A

Asymptotic Molecular States and the Dispersion Expansion

A.1 Asymptotic form of molecular states in Hund's case (a)

Since we only consider nonrotating molecules, there is no significant difference between Hund's case (a) and (b). The good quantum numbers are the projection Λ of the total electronic orbital angular momentum along the internuclear axis, the value S of the total electronic spin angular momentum and its projection Σ. In this section, we construct symmetrized asymptotic molecular states with the spin state $|S\rangle$ factorized out. A similar procedure was used in [80]. Assuming that atomic fine structure can be ignored, at least initially, such states are convenient to use for a molecular basis because Rydberg-Rydberg interactions are spin independent. The effects of atomic fine structure can be accounted for retroactively, if it needed. However, if the atomic fine-structure splitting is comparable with the energy separation between nearby $n\ell + n'\ell'$ asymptotes, this is not a good choice for a molecular basis, as explained in Chapter 1. We assume that atoms have only one valence electron, and so the following constructions of molecular states is appropriate for alkali elements. In addition, we consider the case of nonoverlapping electronic distributions. This means that the probability that both electrons are located around the same atom is negligible. In the asymptotic region, we use atomic states $\varphi^{a(b)}_{n\ell m}(\mathbf{r})$, where $a(b)$ indicates the ion core and $\mathbf{r}$ is the position of the surrounding valence electron relative to the corresponding ion core. The general asymptotic form of the electronic wave function is

$$\begin{aligned}\psi = \big[&c_1\varphi^a_{n_1\ell_1m_1}(\mathbf{r}_1)\varphi^b_{n_2\ell_2(\Lambda-m_1)}(\mathbf{r}_2) + c_2\varphi^b_{n_1\ell_1m_1}(\mathbf{r}_1)\varphi^a_{n_2\ell_2(\Lambda-m_1)}(\mathbf{r}_2) + \\ &c_3\varphi^a_{n_2\ell_2(\Lambda-m_1)}(\mathbf{r}_1)\varphi^b_{n_1\ell_1m_1}(\mathbf{r}_2) + c_4\varphi^b_{n_2\ell_2(\Lambda-m_1)}(\mathbf{r}_1)\varphi^a_{n_1\ell_1m_1}(\mathbf{r}_2)\big]\,|S\rangle\,.\end{aligned} \tag{A.1.1}$$

Under the exchange of the electrons ψ must be antisymmetric, i.e. $P_{12}\psi = -\psi$. The spin state $|S\rangle$ is symmetric under P_{12} if $S = 1$ and antisymmetric if $S = 0$

$$\begin{aligned}-\psi = \sigma\big[&c_1\varphi^a_{n_1\ell_1m_1}(\mathbf{r}_2)\varphi^b_{n_2\ell_2(\Lambda-m_1)}(\mathbf{r}_1) + c_2\varphi^b_{\ell_1m_1}(\mathbf{r}_2)\varphi^a_{n_2\ell_2(\Lambda-m_1)}(\mathbf{r}_1) \\ &+ c_3\varphi^a_{n_2\ell_2(\Lambda-m_1)}(\mathbf{r}_2)\varphi^b_{n_1\ell_1m_1}(\mathbf{r}_1) + c_4\varphi^b_{n_2\ell_2(B;\Lambda-m_1)}(\mathbf{r}_2)\varphi^a_{n_1\ell_1m_1}(\mathbf{r}_1)\big]\,|S\rangle\,,\end{aligned} \tag{A.1.2}$$

where $\sigma = (-1)^{S+1}$. Comparing Eqs. (A.1.1) and (A.1.2) we find

$$c_4 = (-1)^S c_1, \qquad c_3 = (-1)^S c_2. \tag{A.1.3}$$

Now Eq. (A.1.1) can be rewritten as

$$\begin{aligned}\psi = \big[&c_1\left(\varphi^a_{n_1\ell_1m_1}(\mathbf{r}_1)\varphi^b_{n_2\ell_2(\Lambda-m_1)}(\mathbf{r}_2) + \sigma\varphi^b_{n_2\ell_2(\Lambda-m_1)}(\mathbf{r}_1)\varphi^a_{n_1\ell_1m_1}(\mathbf{r}_2)\right) + \\ &c_2\left(\varphi^b_{n_1\ell_1m_1}(\mathbf{r}_1)\varphi^a_{n_2\ell_2(\Lambda-m_1)}(\mathbf{r}_2) + \sigma\varphi^a_{n_2\ell_2(\Lambda-m_1)}(\mathbf{r}_1)\varphi^b_{n_1\ell_1m_1}(\mathbf{r}_2)\right)\big]\,|S\rangle\,.\end{aligned} \tag{A.1.4}$$

The inversion symmetry i, by definition, operates only in the orbital part of the molecular state. Gerade (ungerade) states are symmetric (antisymmetric) under this operation. This operation transfers a single electronic state located around one nucleus to the same state located around the other nucleus but with inversion of all the coordinates

$$
\begin{aligned}
i[\varphi^{a}_{n_1\ell_1 m_1}(\mathbf{r}_1)\varphi^{b}_{n_2\ell_2(\Lambda-m_1)}(\mathbf{r}_2)] = \varphi^{b}_{n_1\ell_1 m_1}(-\mathbf{r}_1)\varphi^{a}_{n_2\ell_2(A;\Lambda-m_1)}(-\mathbf{r}_2) = \\
(-1)^{n_1\ell_1+n_2\ell_2}\varphi^{b}_{n_1\ell_1 m_1}(\mathbf{r}_1)\varphi^{a}_{n_2\ell_2(\Lambda-m_1)}(\mathbf{r}_2)
\end{aligned}
\tag{A.1.5}
$$

The effect of i on ψ is

$$
\begin{aligned}
i\psi = (-1)^{\ell_1+\ell_2}[c_1\left(\varphi^{b}_{n_1\ell_1 m_1}(\mathbf{r}_1)\varphi^{a}_{n_2\ell_2(\Lambda-m_1)}(\mathbf{r}_2) + \sigma\varphi^{a}_{n_2\ell_2(A;\Lambda-m_1)}(\mathbf{r}_1)\varphi^{b}_{n_1\ell_1 m_1}(\mathbf{r}_2)\right) \\
c_1\left(\varphi^{a}_{n_1\ell_1 m_1}(\mathbf{r}_1)\varphi^{b}_{n_2\ell_2(\Lambda-m_1)}(\mathbf{r}_2) + \sigma\varphi^{b}_{n_2\ell_2(B;\Lambda-m_1)}(\mathbf{r}_1)\varphi^{a}_{n_1\ell_1 m_1}(\mathbf{r}_2 1)\right)]|S\rangle.
\end{aligned}
\tag{A.1.6}
$$

To satisfy the symmetry condition $i\psi = p\psi$, where p is the eigenvalue of i, we have to impose

$$
c_2 = p(-1)^{\ell_1+\ell_2}c_1. \tag{A.1.7}
$$

The symmetrized form of asymptotic molecular states is

$$
\begin{aligned}
\psi = c_1[\varphi^{a}_{n_1\ell_1 m_1}(\mathbf{r}_1)\varphi^{b}_{n_2\ell_2(\Lambda-m_1)}(\mathbf{r}_2) + p\sigma(-1)^{\ell_1+\ell_2}\varphi^{a}_{n_2\ell_2(\Lambda-m_1)}(\mathbf{r}_1)\varphi^{b}_{n_1\ell_1 m_1}(\mathbf{r}_2) + \\
p(-1)^{\ell_1+\ell_2}\left(\varphi^{b}_{n_1\ell_1 m_1}(\mathbf{r}_1)\varphi^{a}_{n_2\ell_2(\Lambda-m_1)}(\mathbf{r}_2) + p\sigma(-1)^{\ell_1+\ell_2}\varphi^{b}_{n_2\ell_2(\Lambda-m_1)}(\mathbf{r}_1)\varphi^{a}_{n_1\ell_1 m_1}(\mathbf{r}_2)\right)]|S\rangle.
\end{aligned}
\tag{A.1.8}
$$

For homonuclear diatomic molecules the last two terms are physically the same as the first two terms so their contribution to the molecular potentials are also the same. There are no mutual contributions of these two pairs in any order of perturbation theory because the electronic distributions of electrons 1 and 2 are non-overlapping. This means that without losing any generality we can keep only one of these pairs as the asymptotic form of the molecular wave function for a given symmetry. Dropping the spin part, we can write the symmetric form of the molecular state as follows

$$\psi = \frac{1}{\sqrt{2}} \left[\varphi^a_{n_1\ell_1 m_1}(\mathbf{r}_1)\varphi^b_{n_2\ell_2(\Lambda-m_1)}(\mathbf{r}_2) + \beta\varphi^a_{n_2\ell_2(\Lambda-m_1)}(\mathbf{r}_1)\varphi^b_{n_1\ell_1 m_1}(\mathbf{r}_2) \right]. \tag{A.1.9}$$

where $\beta = p\sigma(-1)^{\ell_1+\ell_2}$. States with $\Lambda = 0$ will be characterized additionally with the eigenvalue of the reflection operator $\hat{\sigma}$.

A.2 Asymptotic form of molecular states in Hund's case (c)

This symmetrization is similar to the previous one but the good quantum number here is the projection of the total electronic angular momentum $\mathbf{L}+\mathbf{S}$ along the molecular axis. We construct the asymptotic basis using atomic $\varphi_{njm}(\mathbf{r})$ functions. Because of ℓs-coupling, atomic functions are also described by the quantum number ℓ, but we omit this in our notation. This information will be important wjen we apply the inversion operator i. Assuming nonoverlapping electronic distributions, we start with the general asymptotic form of the electronic wave function

$$\begin{aligned} \psi =& c_1\varphi^a_{n_1j_1m_1}(\mathbf{r}_1)\varphi^b_{n_2j_2(\Omega-m_1)}(\mathbf{r}_2) + c_2\varphi^a_{n_1j_1m_1}(\mathbf{r}_2)\varphi^b_{n_2j_2(\Omega-m_1)}(\mathbf{r}_1) \\ & c_3\varphi^b_{n_1j_1m_1}(\mathbf{r}_1)\varphi^a_{n_2j_2(\Omega-m_1)}(\mathbf{r}_2) + c_4\varphi^b_{n_1j_1m_1}(\mathbf{r}_1)\varphi^a_{n_2j_2(\Omega-m_1)}(\mathbf{r}_2). \end{aligned} \tag{A.2.1}$$

This ψ must be antisymmetric under the exchange of electrons $P_{12}\psi = -\psi$.

$$\begin{aligned} -\psi =& c_1\varphi^a_{n_1j_1m_1}(\mathbf{r}_2)\varphi^b_{n_2j_2(\Omega-m_1)}(\mathbf{r}_1) + c_2\varphi^a_{n_1j_1m_1}(\mathbf{r}_1)\varphi^b_{n_2j_2(\Omega-m_1)}(\mathbf{r}_2) \\ & c_3\varphi^b_{n_1j_1m_1}(\mathbf{r}_2)\varphi^a_{n_2j_2(\Omega-m_1)}(\mathbf{r}_1) + c_4\varphi^b_{n_1j_1m_1}(\mathbf{r}_2)\varphi^a_{n_2j_2(\Omega-m_1)}(\mathbf{r}_1). \end{aligned} \tag{A.2.2}$$

Comparing Eqs. (1.1) and (1.2) we find

$$c_1 = -c_2, \qquad c_3 = -c_4. \tag{A.2.3}$$

Now ψ reads

$$\begin{aligned}\psi = & c_1 \left(\varphi^a_{n_1j_1m_1}(\mathbf{r}_1)\varphi^b_{n_2j_2(\Omega-m_1)}(\mathbf{r}_2) - \varphi^a_{n_1j_1m_1}(\mathbf{r}_2)\varphi^b_{n_2j_2(\Omega-m_1)}(\mathbf{r}_1)\right) + \\ & c_4 \left(\varphi^b_{n_1j_1m_1}(\mathbf{r}_2)\varphi^a_{n_2j_2(\Omega-m_1)}(\mathbf{r}_1) - \varphi^b_{n_1j_1m_1}(\mathbf{r}_1)\varphi^a_{n_2j_2(\Omega-m_1)}(\mathbf{r}_2)\right).\end{aligned} \tag{A.2.4}$$

There is no essential difference in the action of the inversion transformation i on the new asymptotic states

$$i[\varphi^a_{n_1j_1m_1}(\mathbf{r}_1)\varphi^b_{n_2j_2(\Omega-m_1)}(\mathbf{r}_2)] = (-1)^{\ell_1+\ell_2}\varphi^b_{n_1j_1m_1}(\mathbf{r}_1)\varphi^a_{n_2j_2(\Omega-m_1)}(\mathbf{r}_2) \tag{A.2.5}$$

From the symmetry condition $i\psi = p\psi$ we derive

$$c_4 = -p(-1)^{\ell_1+\ell_2}c_1. \tag{A.2.6}$$

The symmetrized form of asymptotic molecular states is

$$\begin{aligned}\psi = c_1 \big[& \varphi^a_{n_1j_1m_1}(\mathbf{r}_1)\varphi^b_{n_2j_2(\Omega-m_1)}(\mathbf{r}_2) - p(-1)^{\ell_1+\ell_2}\varphi^a_{n_2j_2(\Omega-m_1)}(\mathbf{r}_1)\varphi^b_{n_1j_1m_1}(\mathbf{r}_2) + \\ & p(-1)^{\ell_1+\ell_2}\left(\varphi^b_{n_1j_1m_1}(\mathbf{r}_1)\varphi^a_{n_2j_2(\Omega-m_1)}(\mathbf{r}_2) - p(-1)^{\ell_1+\ell_2}\varphi^b_{n_2j_2(\Omega-m_1)}(\mathbf{r}_1)\varphi^a_{n_1j_1m_1}(\mathbf{r}_2)\right)\big].\end{aligned} \tag{A.2.7}$$

For the same reason as before, the last two terms are physically the same as the first two terms so their contributions to the molecular potentials are also the same. Consequently, we can keep only one of these pairs as the asymptotic form of the molecular wave function for a given symmetry.

$$\psi = \frac{1}{\sqrt{2}}\left(\varphi^a_{n_1j_1m_1}(\mathbf{r}_1)\varphi^b_{n_2j_2(\Omega-m_1)}(\mathbf{r}_2) - p(-1)^{\ell_1+\ell_2}\varphi^a_{n_2j_2(\Omega-m_1)}(\mathbf{r}_1)\varphi^b_{n_1j_1m_1}(\mathbf{r}_2)\right) \tag{A.2.8}$$

States with $\Omega = 0$ will be characterized additionally with the eigenvalue of the reflection operator $\hat{\sigma}$.

A.3 Expressions for C coefficients

In order to obtain the expressions for the C coefficients, perturbation theory is applied. The interaction potential $V(\mathbf{r}_1, \mathbf{r}_2)$ out of equation (1.2.1) is taken as perturbation to H_0 which is the Hamiltonian of a noninteracting atom pair. The total Hamiltonian H has the following form

$$H = H_0 + V(\mathbf{r}_1, \mathbf{r}_2). \tag{A.3.1}$$

As unperturbed zero-order molecular wave functions, the asymptotic expressions (1.1.1) of the preceding sections are used. The first order energy shift for nondegenerate states is obtained by calculating the expectation values of V defined in equation (1.2.1) with respect to the selected state and is

$$\Delta E^{(1)} = \left\langle {}^{n_1\ell_1,m_1}_{n_2\ell_2,m2}, \Lambda\sigma; p \right| V \left| {}^{n_1\ell_1,m_1}_{n_2\ell_2,m_2}, \Lambda\sigma; p \right\rangle, \tag{A.3.2}$$

where

$$\left| {}^{n_1\ell_1 m_1}_{n_2\ell_2 m_2} \right\rangle \equiv |n_1\ell_1 m_1\rangle \, |n_2\ell_2 m_2\rangle \, . \tag{A.3.3}$$

Due to symmetry, Λ, σ and p are good quantum numbers. If $R > R_{LR}$ the electron wave functions for each atom do not overlap so that mutual terms between the first square bracket and the second square bracket of equation (A.1.8) are zero. Additionally perturbation terms evaluated for the first square bracket are the same as for the second square bracket since the only difference in the states is a permutation of the position vectors of the two nuclei. As a consequence, the expressions for the unperturbed zero-order wavefunction are further simplified by using only the properly normalized first square bracket Eq. (A17). This greatly simplifies the evaluation and therefore Eq. (A.3.2) can be rewritten as

$$\frac{1}{2}\left[\left\langle {}^{n_1\ell_1m_1}_{n_2\ell_2m_2}\right| + \sigma p(-1)^{\ell_1+\ell_2}\left\langle {}^{n_2\ell_2m_2}_{n_1\ell_1m_1}\right|\right] V \left[\left| {}^{n_1\ell_1m_1}_{n_2\ell_2m_2}\right\rangle + \sigma p(-1)^{\ell_1+\ell_2}\left| {}^{n_2\ell_2m_2}_{n_1\ell_1m_1}\right\rangle\right], \tag{A.3.4}$$

with $\Lambda = m_1 + m_2$. From Eq. (A.3.4) we can see a two-fold degeneracy between singlet gerade and tripled ungerade and between singlet ungerade and tripled gerade as the Hamiltonian (A.3.1) is spin independent and the matrix elements depend only on the product σp. This degeneracy is removed at shorter distances for which the electronic wavefunctions overlap. For such distances the mutual contributions of the two square brackets in (A.1.8) are not negligible.

In the long-range region the interaction matrix elements of $V_{\ell L}$ have the following form

$$\begin{aligned}\left\langle {}^{n_1'\ell_1'm_1'}_{n_2'\ell_2'm_2'}\right| V_{\ell L}\left| {}^{n_1\ell_1m_1}_{n_2\ell_2m_2}\right\rangle &= \frac{(-1)^L 4\pi}{\sqrt{(2\ell+1)(2L+1)}}\left\langle n_1'\ell_1'||r^\ell||n_1\ell_1\right\rangle\left\langle n_2'\ell_2'||r^L||n_2\ell_2\right\rangle \\ &\sum_m \sqrt{\binom{\ell+L}{\ell+m}\binom{\ell+L}{L+m}}\left\langle \ell_1'm_1'||Y_{\ell m}||\ell_1m_1\right\rangle\left\langle \ell_2'm_2'||Y_{L-m}||\ell_2m_2\right\rangle .\end{aligned} \tag{A.3.5}$$

where $\langle n'\ell'||r^x||n\ell\rangle$ is the radial matrix element of r^x. The matrix elements of the spherical harmonics expressed in terms of 3j-symbols are

$$\begin{aligned}\langle \ell'm'|\, Y_{LM}\, |\ell m\rangle =& (-1)^{m'}\sqrt{\frac{(2\ell'+1)(2L+1)(2\ell+1)}{4\pi}} \\ &\times \begin{pmatrix} \ell' & L & \ell \\ 0 & 0 & 0 \end{pmatrix}\begin{pmatrix} \ell' & L & \ell \\ -m' & M & m \end{pmatrix}.\end{aligned} \tag{A.3.6}$$

For degenerate zero-order molecular states $|\Lambda, i\rangle$, where $i = 1, 2, \ldots,$ degenerate perturbation theory has to be applied. In order to find the right eigenvectors, the matrix

$V^{(0)}$ with elements $V_{\mathrm{ij}}^{(0)} = \langle\Lambda, i|V|\Lambda, j\rangle$ has to be diagonalized. The eigenvalues are the first-order energy shifts and the eigenvectors are the zero-order basis states.

In the first-order of perturbation theory, the C_5 coefficients originate from the quadrupole interactions. Consequently, the *ns-ns* potentials cannot have this dispersion term according to the quadrupole selection rules. Some of the *nd-nd* symmetries have also a C_7 coefficient arising from the first-order correction to the energy. The determination of C_5 and C_7 coefficients, as well as the higher order corrections, is facing additional difficulties because even the zeroth-order wavefunctions depend on the internuclear distance R if the C_7 does not vanish. In order to obtain the C_5 and C_7 for those states one should diagonalize the matrix of the first-order correction to the energy and then expand its eigenvalues in powers of $1/R$. The matrix is of the following type

$$R^{-5}(M_0 + R^{-2}M_1), \tag{A.3.7}$$

where Eq. (A.3.7) represent (1.2.1) in the set of the degenerate asymptotic states. The C_5 and C_7 in these cases are

$$C_5 = \langle n_i|\, M_0\, |n_i\rangle\,, \tag{A.3.8}$$

$$C_7 = \langle n_i|\, M_1\, |n_i\rangle\,,$$

where $|n_i\rangle$ are the eigenstates of M_0. These expressions are valid if the $1/R^5$ term is much larger than the $1/R^7$ term. This additionally limits the region of validity of these relations.

The energy correction in the second-order perturbation has the form

$$\Delta E^{(2)} = \sum_{\phi_i} \frac{\left\langle \begin{smallmatrix} n_1\ell_1m_1 \\ n_2\ell_2m_2 \end{smallmatrix}, \Lambda\sigma; p \right| V \left|\phi_i\right\rangle \left\langle\phi_i\right| V \left| \begin{smallmatrix} n_1\ell_1m_1 \\ n_2\ell_2m_2 \end{smallmatrix}, \Lambda\sigma; p \right\rangle}{E_M - E_{M_i}}, \tag{A.3.9}$$

where the sum is over a complete orthogonal basis set. As in the first-order case, we have to sum matrix elements of the following form

$$\sum_{\substack{n_il_im_i \\ n_jl_jm_j}} \frac{\left\langle \begin{smallmatrix} n_1'l_1'm_1' \\ n_2'l_2'm_2' \end{smallmatrix} \right| V \left| \begin{smallmatrix} n_il_im_i \\ n_jl_jm_j \end{smallmatrix} \right\rangle \left\langle \begin{smallmatrix} n_jl_jm_j \\ n_il_im_i \end{smallmatrix} \right| V \left| \begin{smallmatrix} n_1l_1m_1 \\ n_2l_2m_2 \end{smallmatrix} \right\rangle}{(E_{n_1l_1} + E_{n_2l_2}) - (E_{n_il_i} + E_{n_jl_j})} \tag{A.3.10}$$

$$= \sum_{l,L,l',L'=1}^{\infty} \frac{1}{R^{l+L+l'+L'+2}} \times \sum_{\substack{n_il_im_i \\ n_jl_jm_j}} \frac{\left\langle \begin{smallmatrix} n_1'l_1'm_1' \\ n_2'l_2'm_2' \end{smallmatrix} \right| V_{l'L'} \left| \begin{smallmatrix} n_il_im_i \\ n_jl_jm_j \end{smallmatrix} \right\rangle \left\langle \begin{smallmatrix} n_il_im_i \\ n_jl_jm_j \end{smallmatrix} \right| V_{lL} \left| \begin{smallmatrix} n_1l_1m_1 \\ n_2l_2m_2 \end{smallmatrix} \right\rangle}{(E_{n_1l_1} + E_{n_2l_2}) - (E_{n_il_i} + E_{n_jl_j})},$$

and the sum is over all possible intermediate states. For simplicity, we define the following matrix notation

$$\left\langle \begin{smallmatrix} n_1'l_1'm_1' \\ n_2'l_2'm_2' \end{smallmatrix} \right| W_{lL}^{l'L'} \left| \begin{smallmatrix} n_1l_1m_1 \\ n_2l_2m_2 \end{smallmatrix} \right\rangle \equiv \sum_{\substack{n_il_im_i \\ n_jl_jm_j}} \frac{\left\langle \begin{smallmatrix} n_1'l_1'm_1' \\ n_2'l_2'm_2' \end{smallmatrix} \right| V_{l'L'} \left| \begin{smallmatrix} n_il_im_i \\ n_jl_jm_j \end{smallmatrix} \right\rangle \left\langle \begin{smallmatrix} n_il_im_i \\ n_jl_jm_j \end{smallmatrix} \right| V_{lL} \left| \begin{smallmatrix} n_1l_1m_1 \\ n_2l_2m_2 \end{smallmatrix} \right\rangle}{(E_{n_1l_1} + E_{n_2l_2}) - (E_{n_il_i} + E_{n_jl_j})}. \tag{A.3.11}$$

The calculational effort is simplified by the following symmetry properties:

$$\left\langle \begin{smallmatrix} n_1'\ell_1'm_1' \\ n_2'\ell_2'm_2' \end{smallmatrix} \right| V_{\ell L} \left| \begin{smallmatrix} n_1\ell_1m_1 \\ n_2\ell_2m_2 \end{smallmatrix} \right\rangle = (-1)^{\ell+L} \left\langle \begin{smallmatrix} n_2'\ell_2'm_2' \\ n_1'\ell_1'm_1' \end{smallmatrix} \right| V_{L\ell} \left| \begin{smallmatrix} n_2\ell_2m_2 \\ n_1\ell_1m_1 \end{smallmatrix} \right\rangle \tag{A.3.12}$$

$$= \left\langle \begin{smallmatrix} n_1'\ell_1'-m_1' \\ n_2'\ell_2'-m_2' \end{smallmatrix} \right| V_{\ell L} \left| \begin{smallmatrix} n_1\ell_1-m_1 \\ n_2\ell_2-m_2 \end{smallmatrix} \right\rangle \tag{A.3.13}$$

$$= \left\langle \begin{smallmatrix} n_1\ell_1m_1 \\ n_2\ell_2m_2 \end{smallmatrix} \right| V_{\ell L} \left| \begin{smallmatrix} n_1'\ell_1'm_1' \\ n_2'\ell_2'm_2' \end{smallmatrix} \right\rangle. \tag{A.3.14}$$

Also, $\left\langle \begin{smallmatrix} n_1'\ell_1'm_1' \\ n_2'\ell_2'm_2' \end{smallmatrix} \right| V_{\ell L} \left| \begin{smallmatrix} n_1\ell_1m_1 \\ n_2\ell_2m_2 \end{smallmatrix} \right\rangle = 0$ if at least one of the following conditions is true:

$$\begin{array}{lll} \ell < |\ell_1' - \ell_1|, & \ell_2' + \ell_2 + L = (\text{odd}), & L < |\ell_2' - \ell_2|, \\ \ell > \ell_1' + \ell_1, & \ell_1' + \ell_1 + \ell = (\text{odd}), & m_1' + m_2' \neq m_1 + m_2, \\ L > \ell_2' + \ell_2. & & \end{array} \tag{A.3.15}$$

The symmetry properties of $\left\langle \substack{n_1'\ell_1'm_1' \\ n_2'\ell_2'm_2'} \right| W_{\ell L}^{\ell' L'} \left| \substack{n_1\ell_1m_1 \\ n_2\ell_2m_2} \right\rangle$ are

$$\begin{aligned}
\left\langle \substack{n_1'\ell_1'm_1' \\ n_2'\ell_2'm_2'} \right| W_{\ell L}^{\ell' L'} \left| \substack{n_1\ell_1m_1 \\ n_2\ell_2m_2} \right\rangle &= (-1)^{\ell+\ell'+L+L'} \left\langle \substack{n_2'\ell_2'm_2' \\ n_1'\ell_1'm_1'} \right| W_{L\ell}^{L'\ell'} \left| \substack{n_2\ell_2m_2 \\ n_1\ell_1m_1} \right\rangle && \text{(A.3.16)} \\
&= \left\langle \substack{n_1'\ell_1'-m_1' \\ n_2'\ell_2'-m_2'} \right| W_{\ell L}^{\ell' L'} \left| \substack{n_1\ell_1-m_1 \\ n_2\ell_2-m_2} \right\rangle && \text{(A.3.17)} \\
&= \left\langle \substack{n_1\ell_1m_1 \\ n_2\ell_2m_2} \right| W_{\ell' L'}^{\ell L} \left| \substack{n_1'\ell_1'm_1' \\ n_2'\ell_2'm_2'} \right\rangle . && \text{(A.3.18)}
\end{aligned}$$

Again, $\left\langle \substack{n_1'\ell_1'm_1' \\ n_2'\ell_2'm_2'} \right| W_{\ell L}^{\ell' L'} \left| \substack{n_1\ell_1m_1 \\ n_2\ell_2m_2} \right\rangle = 0$ if at least one of the following conditions is true:

$$\begin{array}{ll}
\ell_1 + \ell_1' + \ell + \ell' = (\text{odd}), & \ell_2 + \ell_2' + L + L' = (\text{odd}), \\
m_1' + m_2' \neq m_1 + m_2, & |\ell_1' - \ell'| > \ell_1 + \ell, \\
|\ell_1 - \ell| > \ell_1' + \ell', & |\ell_2' - L'| > \ell_2 + L, \\
|\ell_2 - L| > \ell_2' + L'. &
\end{array} \qquad \text{(A.3.19)}$$

Table A.1: The zeroth-order molecular states for different symmetries. States with equal $|\Lambda|$ and the same symmetry are asymptotically degenerate and are obtained by degenerate perturbation theory.

$\lvert\Lambda\rvert$	Symmetry	Representation for the *ns*-*ns* asymptote
0	${}^1\Sigma_g^+$, ${}^3\Sigma_u^+$	$\left\lvert\begin{smallmatrix}n00\\n00\end{smallmatrix}\right\rangle$
$\lvert\Lambda\rvert$	Symmetry	Representation for the *np*-*np* asymptote
2	${}^1\Delta_g$, ${}^3\Delta_u$	$\left\lvert\begin{smallmatrix}n11\\n11\end{smallmatrix}\right\rangle$
1	${}^1\Pi_u$, ${}^3\Pi_g$	$\frac{1}{\sqrt{2}}\left(\left\lvert\begin{smallmatrix}n11\\n10\end{smallmatrix}\right\rangle - \left\lvert\begin{smallmatrix}n10\\n11\end{smallmatrix}\right\rangle\right)$
1	${}^1\Pi_g$, ${}^3\Pi_u$	$\frac{1}{\sqrt{2}}\left(\left\lvert\begin{smallmatrix}n11\\n10\end{smallmatrix}\right\rangle + \left\lvert\begin{smallmatrix}n10\\n11\end{smallmatrix}\right\rangle\right)$
0	${}^1\Sigma_u^-$, ${}^3\Sigma_g^-$	$\frac{1}{\sqrt{2}}\left(\left\lvert\begin{smallmatrix}n11\\n1-1\end{smallmatrix}\right\rangle - \left\lvert\begin{smallmatrix}n1-1\\n11\end{smallmatrix}\right\rangle\right)$
0	${}^1\Sigma_g^+$, ${}^3\Sigma_u^+$	$\sqrt{\frac{2}{3}}\left\lvert\begin{smallmatrix}n10\\n10\end{smallmatrix}\right\rangle + \frac{1}{\sqrt{6}}\left\lvert\begin{smallmatrix}n11\\n1-1\end{smallmatrix}\right\rangle + \frac{1}{\sqrt{6}}\left\lvert\begin{smallmatrix}n1-1\\n11\end{smallmatrix}\right\rangle$
	degenerate	$-\frac{1}{\sqrt{3}}\left\lvert\begin{smallmatrix}n10\\n10\end{smallmatrix}\right\rangle + \frac{1}{\sqrt{3}}\left\lvert\begin{smallmatrix}n11\\n1-1\end{smallmatrix}\right\rangle + \frac{1}{\sqrt{3}}\left\lvert\begin{smallmatrix}n1-1\\n11\end{smallmatrix}\right\rangle$
$\lvert\Lambda\rvert$	Symmetry	Representation for the *nd*-*nd* asymptote
4	${}^1\Gamma_g$, ${}^3\Gamma_u$	$\left\lvert\begin{smallmatrix}n22\\n22\end{smallmatrix}\right\rangle$
3	${}^1\Phi_u$, ${}^3\Phi_g$	$\frac{1}{\sqrt{2}}\left(\left\lvert\begin{smallmatrix}n22\\n21\end{smallmatrix}\right\rangle - \left\lvert\begin{smallmatrix}n21\\n22\end{smallmatrix}\right\rangle\right)$
3	${}^1\Phi_g$, ${}^3\Phi_u$	$\frac{1}{\sqrt{2}}\left(\left\lvert\begin{smallmatrix}n22\\n21\end{smallmatrix}\right\rangle + \left\lvert\begin{smallmatrix}n21\\n22\end{smallmatrix}\right\rangle\right)$
2	${}^1\Delta_u$, ${}^3\Delta_g$	$\frac{1}{\sqrt{2}}\left(\left\lvert\begin{smallmatrix}n22\\n20\end{smallmatrix}\right\rangle - \left\lvert\begin{smallmatrix}n20\\n22\end{smallmatrix}\right\rangle\right)$
2	${}^1\Delta_g$, ${}^3\Delta_u$	$\sqrt{\frac{8}{19}}\left\lvert\begin{smallmatrix}n22\\n20\end{smallmatrix}\right\rangle + \sqrt{\frac{8}{19}}\left\lvert\begin{smallmatrix}n20\\n22\end{smallmatrix}\right\rangle + \sqrt{\frac{3}{19}}\left\lvert\begin{smallmatrix}n21\\n21\end{smallmatrix}\right\rangle$
	degenerate	$-\sqrt{\frac{3}{38}}\left\lvert\begin{smallmatrix}n22\\n20\end{smallmatrix}\right\rangle - \sqrt{\frac{3}{38}}\left\lvert\begin{smallmatrix}n20\\n22\end{smallmatrix}\right\rangle + \frac{4}{\sqrt{19}}\left\lvert\begin{smallmatrix}n21\\n21\end{smallmatrix}\right\rangle$
1	${}^1\Pi_u$, ${}^3\Pi_g$	$\sqrt{\frac{1}{4}+\frac{7}{4\sqrt{55}}}\left(\left\lvert\begin{smallmatrix}n21\\n20\end{smallmatrix}\right\rangle - \left\lvert\begin{smallmatrix}n20\\n21\end{smallmatrix}\right\rangle\right) + \sqrt{\frac{1}{4}-\frac{7}{4\sqrt{55}}}\left(\left\lvert\begin{smallmatrix}n22\\n2-1\end{smallmatrix}\right\rangle - \left\lvert\begin{smallmatrix}n2-1\\n22\end{smallmatrix}\right\rangle\right)$
	degenerate	$\sqrt{\frac{1}{4}-\frac{7}{4\sqrt{55}}}\left(-\left\lvert\begin{smallmatrix}n21\\n20\end{smallmatrix}\right\rangle + \left\lvert\begin{smallmatrix}n20\\n21\end{smallmatrix}\right\rangle\right) + \sqrt{\frac{1}{4}+\frac{7}{4\sqrt{55}}}\left(\left\lvert\begin{smallmatrix}n22\\n2-1\end{smallmatrix}\right\rangle - \left\lvert\begin{smallmatrix}n2-1\\n22\end{smallmatrix}\right\rangle\right)$
1	${}^1\Pi_g$, ${}^3\Pi_u$	$\sqrt{\frac{1}{4}-\frac{5}{4\sqrt{79}}}\left(-\left\lvert\begin{smallmatrix}n21\\n20\end{smallmatrix}\right\rangle - \left\lvert\begin{smallmatrix}n20\\n21\end{smallmatrix}\right\rangle\right) + \sqrt{\frac{1}{4}+\frac{5}{4\sqrt{79}}}\left(\left\lvert\begin{smallmatrix}n22\\n2-1\end{smallmatrix}\right\rangle + \left\lvert\begin{smallmatrix}n2-1\\n22\end{smallmatrix}\right\rangle\right)$
	degenerate	$\sqrt{\frac{1}{4}+\frac{5}{4\sqrt{79}}}\left(\left\lvert\begin{smallmatrix}n21\\n20\end{smallmatrix}\right\rangle + \left\lvert\begin{smallmatrix}n20\\n21\end{smallmatrix}\right\rangle\right) + \sqrt{\frac{1}{4}-\frac{5}{4\sqrt{79}}}\left(\left\lvert\begin{smallmatrix}n22\\n2-1\end{smallmatrix}\right\rangle + \left\lvert\begin{smallmatrix}n2-1\\n22\end{smallmatrix}\right\rangle\right)$
0	${}^1\Sigma_u^-$, ${}^3\Sigma_g^-$	$\frac{-1+\sqrt{5}}{2\sqrt{5-\sqrt{5}}}\left(\left\lvert\begin{smallmatrix}n21\\n2-1\end{smallmatrix}\right\rangle - \left\lvert\begin{smallmatrix}n2-1\\n21\end{smallmatrix}\right\rangle\right) + \frac{1}{\sqrt{5-\sqrt{5}}}\left(\left\lvert\begin{smallmatrix}n22\\n2-2\end{smallmatrix}\right\rangle - \left\lvert\begin{smallmatrix}n2-2\\n22\end{smallmatrix}\right\rangle\right)$
	degenerate	$\frac{1+\sqrt{5}}{2\sqrt{5+\sqrt{5}}}\left(-\left\lvert\begin{smallmatrix}n21\\n2-1\end{smallmatrix}\right\rangle + \left\lvert\begin{smallmatrix}n2-1\\n21\end{smallmatrix}\right\rangle\right) + \frac{1}{\sqrt{5+\sqrt{5}}}\left(\left\lvert\begin{smallmatrix}n22\\n2-2\end{smallmatrix}\right\rangle - \left\lvert\begin{smallmatrix}n2-2\\n22\end{smallmatrix}\right\rangle\right)$
0	${}^1\Sigma_g^+$, ${}^3\Sigma_u^+$	$0.4121\left(\left\lvert\begin{smallmatrix}n21\\n2-1\end{smallmatrix}\right\rangle + \left\lvert\begin{smallmatrix}n2-1\\n21\end{smallmatrix}\right\rangle\right) + 0.5204\left(\left\lvert\begin{smallmatrix}n22\\n2-2\end{smallmatrix}\right\rangle + \left\lvert\begin{smallmatrix}n2-2\\n22\end{smallmatrix}\right\rangle\right) + 0.3445\left\lvert\begin{smallmatrix}n20\\n20\end{smallmatrix}\right\rangle$
	degenerate	$-0.1316\left(\left\lvert\begin{smallmatrix}n21\\n2-1\end{smallmatrix}\right\rangle + \left\lvert\begin{smallmatrix}n2-1\\n21\end{smallmatrix}\right\rangle\right) - 0.2064\left(\left\lvert\begin{smallmatrix}n22\\n2-2\end{smallmatrix}\right\rangle + \left\lvert\begin{smallmatrix}n2-2\\n22\end{smallmatrix}\right\rangle\right) + 0.9382\left\lvert\begin{smallmatrix}n20\\n20\end{smallmatrix}\right\rangle$
	degenerate	$-0.5593\left(\left\lvert\begin{smallmatrix}n21\\n2-1\end{smallmatrix}\right\rangle + \left\lvert\begin{smallmatrix}n2-1\\n21\end{smallmatrix}\right\rangle\right) + 0.4320\left(\left\lvert\begin{smallmatrix}n22\\n2-2\end{smallmatrix}\right\rangle + \left\lvert\begin{smallmatrix}n2-2\\n22\end{smallmatrix}\right\rangle\right) + 0.0331\left\lvert\begin{smallmatrix}n20\\n20\end{smallmatrix}\right\rangle$

Table A.2: Dispersion coefficients of high Rydberg states for the *ns-ns*, *np-np* and *nd-nd* asymptotes of Li-Li. The coefficients are scaled by their major dependence on n and the residual dependence is fitted using three fitting parameters as indicated in the table.

ns-ns	$C_6 = n^{11}(c_0 + c_1 n + c_2 n^2)$			$C_8 = n^{15}(c_0 + c_1 n + c_2 n^2)$			$C_{10} = n^{22}(c_0 + c_1 n + c_2 n^2)$		
	c_0	c_1	c_2	c_0	c_1	c_2	c_0	c_1	c_2
symmetry	$(\times 10^{1})$	$(\times 10^{-1})$	$(\times 10^{-4})$	$(\times 10^{1})$	$(\times 10^{-2})$	$(\times 10^{-4})$	$(\times 10^{-3})$	$(\times 10^{-5})$	$(\times 10^{-7})$
$^1\Sigma_g$, $^3\Sigma_u$	-1.594	-1.045	5.690	5.039	-2.935	1.207	-2.501	4.376	-2.189[1]
np-np	$C_5 = n^{8}(c_0 + c_1 n + c_2 n^2)$			$C_6 = n^{11}(c_0 + c_1 n + c_2 n^2)$			$C_8 = n^{15}(c_0 + c_1 n + c_2 n^2)$		
symmetry	$(\times 10^{0})$	$(\times 10^{-2})$	$(\times 10^{-4})$	$(\times 10^{0})$	$(\times 10^{-1})$	$(\times 10^{-3})$	$(\times 10^{1})$	$(\times 10^{0})$	$(\times 10^{-2})$
$^1\Delta_g$,$^3\Delta_u$	-1.190	-0.539	0.293	-2.806	-1.220	0.623	-0.669	-0.721	0.365
$^1\Pi_u$,$^3\Pi_g$		Vanishes		-2.147	-1.264	0.648	-5.381	-3.450	1.750
$^1\Pi_g$,$^3\Pi_u$	4.778	2.128	-1.167	-6.177	-2.193	1.123	3.187	-0.979	0.476[2]
$^1\Sigma_u^-$,$^3\Sigma_g^-$		Vanishes		-4.763	-1.692	0.862	-2.789	-1.518	0.768
$^1\Sigma_g^+$,$^3\Sigma_u^+$	-7.168	-3.192	1.750	9.326	-1.852	0.932	7.914	-3.963	1.953[3]
$^1\Sigma_g^+$,$^3\Sigma_u^+$		Vanishes		-2.105	-1.161	0.599	-0.166	-0.990	0.506
nd-nd	$C_5 = n^{8}(c_0 + c_1 n + c_2 n^2)$			$C_6 = n^{11}(c_0 + c_1 n + c_2 n^2)$			$C_7 = n^{12}(c_0 + c_1 n + c_2 n^2)$		
	c_0	c_1	c_2	c_0	c_1	c_2	c_0	c_1	c_2
symmetry	$(\times 10^{0})$	$(\times 10^{-4})$	$(\times 10^{-5})$	$(\times 10^{2})$	$(\times 10^{-1})$	$(\times 10^{-3})$	$(\times 10^{1})$	$(\times 10^{-2})$	$(\times 10^{-4})$
$^1\Gamma_g$,$^3\Gamma_u$	-3.011	-11.670	0.710	1.307	0.716	-0.448	0.787	0.382	-0.232
$^1\Phi_u$,$^3\Phi_g$	-1.506	-5.836	0.355	1.356	0.722	-0.453	-0.197	-0.095	0.058
$^1\Phi_g$,$^3\Phi_u$	4.517	17.510	-1.064	2.973	1.707	-1.062	-3.345	-1.622	0.985
$^1\Delta_u$,$^3\Delta_g$	3.513	13.620	-0.828	2.719	1.545	-0.962	1.181	0.572	-0.348
$^1\Delta_g$,$^3\Delta_u$	3.262	12.650	-0.769	4.229	0.391	-0.298	4.226	2.048	-1.244
$^1\Delta_g$,$^3\Delta_u$	-1.506	-5.829	0.353	2.043	-0.022	-0.021	0.104	0.050	-0.030
$^1\Pi_u$,$^3\Pi_g$	-2.112	-8.186	0.498	2.835	-0.685	0.361	-1.675	-0.812	0.493
$^1\Pi_u$,$^3\Pi_g$	1.610	6.241	-0.379	2.785	0.858	-0.554	-1.277	-0.619	0.376
$^1\Pi_g$,$^3\Pi_u$	2.481	9.618	-0.585	2.464	1.384	-0.863	0.508	0.246	-0.150
$^1\Pi_g$,$^3\Pi_u$	-1.979	-7.673	0.466	6.314	-2.499	1.390	-0.311	-0.151	0.092
$^1\Sigma_u$,$^3\Sigma_g$	-4.872	-18.890	1.148	4.772	-1.749	0.968	2.848	1.381	-0.838
$^1\Sigma_u$,$^3\Sigma_g$	1.861	7.214	-0.439	2.476	1.139	-0.717	1.088	0.527	-0.320
$^1\Sigma_g$,$^3\Sigma_u$	-5.728	-22.200	1.350	5.951	-3.028	1.711	0.887	0.430	-0.261
$^1\Sigma_g$,$^3\Sigma_u$	-2.650	-10.270	0.624	3.500	-1.182	0.647	-3.751	-1.818	1.104
$^1\Sigma_g$,$^3\Sigma_u$	0.850	3.293	-0.200	2.403	0.643	-0.421	-1.071	-0.519	0.315

[1] The following resonance term is added: $C_{10} = n^{22}(c_0 + c_1 n + c_2 n^2 + 0.01493/(n - 22.91))$.

[2] The following resonance term is added: $C_8 = n^{15}(c_0 + c_1 n + c_2 n^2 + 33.77/(n - 38.50) + 8.523/(n - 44.49))$.

[3] The following resonance term is added: $C_8 = n^{15}(c_0 + c_1 n + c_2 n_2 + 101.2/(n - 38.50) + 25.61/(n - 44.49))$.

Table A.3: Dispersion coefficients of high Rydberg states for the *ns-ns*, *np-np* and *nd-nd* asymptotes of Na-Na. The coefficients are scaled by their major dependence on n and the residual dependence is fitted using three fitting parameters as indicated in the table.

ns-ns	$C_6 = n^{11}(c_0 + c_1 n + c_2 n^2)$			$C_8 = n^{15}(c_0 + c_1 n + c_2 n^2)$			$C_{10} = n^{22}(c_0 + c_1 n + c_2 n^2)$		
	c_0	c_1	c_2	c_0	c_1	c_2	c_0	c_1	c_2
symmetry	$(\times 10^0)$	$(\times 10^0)$	$(\times 10^{-3})$	$(\times 10^0)$	$(\times 10^0)$	$(\times 10^{-3})$	$(\times 10^{-2})$	$(\times 10^{-4})$	$(\times 10^{-6})$
$^1\Sigma_g$, $^3\Sigma_u$	8.5861	-1.4641	5.8201	-5.3151	-1.3571	6.7571	-1.4351	3.3431	-2.022
np-np	$C_5 = n^8(c_0 + c_1 n + c_2 n^2)$			$C_6 = n^{11}(c_0 + c_1 n + c_2 n^2)$			$C_8 = n^{15}(c_0 + c_1 n + c_2 n^2)$		
symmetry	$(\times 10^0)$	$(\times 10^{-2})$	$(\times 10^{-4})$	$(\times 10^0)$	$(\times 10^{-2})$	$(\times 10^{-4})$	$(\times 10^1)$	$(\times 10^0)$	$(\times 10^{-3})$
$^1\Delta_g$,$^3\Delta_u$	-0.974	-0.895	0.483	-0.014	-1.999	1.053	-1.325	-0.520	2.726
$^1\Pi_u$,$^3\Pi_g$	Vanishes			1.267	-1.177	0.608	-3.427	-1.510	7.896
$^1\Pi_g$,$^3\Pi_u$	3.895	3.582	-1.931	-1.672	-4.771	2.527	-1.556	-0.624	3.261
$^1\Sigma_u^-$,$^3\Sigma_g^-$	Vanishes			-1.483	-3.796	2.013	-0.987	-0.463	2.416
$^1\Sigma_g^+$,$^3\Sigma_u^+$	-5.819	-5.484	2.995	138.905	4.101	-2.313[1]	-1.238	-1.414	7.436
$^1\Sigma_g^+$,$^3\Sigma_u^+$	Vanishes			1.090	-1.175	0.617	-2.118	-0.953	5.049
nd-nd	$C_5 = n^8(c_0 + c_1 n + c_2 n^2)$			$C_6 = n^{11}(c_0 + c_1 n + c_2 n^2)$			$C_7 = n^{12}(c_0 + c_1 n + c_2 n^2)$		
	c_0	c_1	c_2	c_0	c_1	c_2	c_0	c_1	c_2
symmetry	$(\times 10^0)$	$(\times 10^{-4})$	$(\times 10^{-5})$	$(\times 10^1)$	$(\times 10^{-1})$	$(\times 10^{-3})$	$(\times 10^1)$	$(\times 10^{-2})$	$(\times 10^{-4})$
$^1\Gamma_g$,$^3\Gamma_u$	-2.993	-14.930	0.888	2.571	0.522	-0.503	0.780	0.509	-0.301
$^1\Phi_u$,$^3\Phi_g$	-1.496	-7.464	0.444	3.164	0.540	-0.522	-0.195	-0.127	0.075
$^1\Phi_g$,$^3\Phi_u$	4.489	22.390	-1.331	4.005	1.193	-1.145	-3.314	-2.162	1.280
$^1\Delta_u$,$^3\Delta_g$	3.492	17.410	-1.035	4.062	1.090	-1.047	1.170	0.763	-0.452
$^1\Delta_g$,$^3\Delta_u$	3.242	16.170	-0.961	5.527	1.645	-1.573	4.187	2.731	-1.617
$^1\Delta_g$,$^3\Delta_u$	-1.496	-7.464	0.444	4.369	0.786	-0.756	0.103	0.067	-0.040
$^1\Pi_u$,$^3\Pi_g$	-2.099	-10.470	0.622	5.349	1.075	-1.031	-1.659	-1.082	0.641
$^1\Pi_u$,$^3\Pi_g$	1.600	7.981	-0.475	4.148	1.098	-1.053	-1.265	-0.825	0.489
$^1\Pi_g$,$^3\Pi_u$	2.466	12.300	-0.731	3.908	0.987	-0.949	0.503	0.328	-0.194
$^1\Pi_g$,$^3\Pi_u$	-1.967	-9.812	0.583	8.193	2.376	-2.265	-0.308	-0.201	0.119
$^1\Sigma_u$,$^3\Sigma_g$	-4.842	-24.150	1.436	6.051	1.800	-1.716	2.822	1.841	-1.090
$^1\Sigma_u$,$^3\Sigma_g$	1.850	9.225	-0.549	4.076	0.985	-0.946	1.078	0.703	-0.416
$^1\Sigma_g$,$^3\Sigma_u$	-5.693	-28.390	1.688	7.510	2.223	-2.117	0.878	0.573	-0.339
$^1\Sigma_g$,$^3\Sigma_u$	-2.633	-13.130	0.781	6.032	1.320	-1.263	-3.716	-2.424	1.435
$^1\Sigma_g$,$^3\Sigma_u$	0.844	4.211	-0.250	4.065	0.944	-0.906	-1.061	-0.692	0.410

[1] The following resonance term is added: $C_6 = n^{11}(c_0 + c_1 n + c_2 n^2 + 6736/(n - 55.49))$.

Table A.4: Dispersion coefficients of high Rydberg states for the *ns-ns*, *np-np* and *nd-nd* asymptotes of K-K. The coefficients are scaled by their major dependence on n and the residual dependence is fitted using three fitting parameters as indicated in the table.

ns-ns	$C_6 = n^{11}(c_0 + c_1 n + c_2 n^2)$			$C_8 = n^{15}(c_0 + c_1 n + c_2 n^2)$			$C_{10} = n^{22}(c_0 + c_1 n + c_2 n^2)$		
	c_0	c_1	c_2	c_0	c_1	c_2	c_0	c_1	c_2
symmetry	($\times10^0$)	($\times10^{-1}$)	($\times10^{-3}$)	($\times10^0$)	($\times10^{-1}$)	($\times10^{-3}$)	($\times10^{-3}$)	($\times10^{-4}$)	($\times10^{-6}$)
$^1\Sigma_g$, $^3\Sigma_u$	1.827	-4.352	2.054	2.955	3.950	-2.016	-9.594	2.115	-1.234
np-np	$C_5 = n^8(c_0 + c_1 n + c_2 n^2)$			$C_6 = n^{11}(c_0 + c_1 n + c_2 n^2)$			$C_8 = n^{15}(c_0 + c_1 n + c_2 n^2)$		
symmetry	($\times10^0$)	($\times10^{-2}$)	($\times10^{-4}$)	($\times10^1$)	($\times10^{-1}$)	($\times10^{-3}$)	($\times10^1$)	($\times10^0$)	($\times10^{-2}$)
$^1\Delta_g$,$^3\Delta_u$	-0.571	-1.508	0.794	-0.012	-3.592	1.680	0.610	1.704	-0.811
$^1\Pi_u$,$^3\Pi_g$	Vanishes			0.015	-7.296	3.388	1.950	-0.358	0.139
$^1\Pi_g$,$^3\Pi_u$	2.284	6.031	-3.177	-0.056	-1.910	0.923	0.716	3.082	-1.456
$^1\Sigma_u^-$,$^3\Sigma_g^-$	Vanishes			-0.047	-0.900	0.447	1.165	0.662	-0.342
$^1\Sigma_g^+$,$^3\Sigma_u^+$	-3.426	-9.046	4.766	2.698	-4.285	2.154	6.016	-5.126	2.227
$^1\Sigma_g^+$,$^3\Sigma_u^+$	Vanishes			0.012	-6.510	3.024	1.509	0.763	-0.396
nd-nd	$C_5 = n^8(c_0 + c_1 n + c_2 n^2)$			$C_6 = n^{11}(c_0 + c_1 n + c_2 n^2)$			$C_7 = n^{12}(c_0 + c_1 n + c_2 n^2)$		
	c_0	c_1	c_2	c_0	c_1	c_2	c_0	c_1	c_2
symmetry	($\times10^0$)	($\times10^{-3}$)	($\times10^{-5}$)	($\times10^1$)	($\times10^{-1}$)	($\times10^{-4}$)	($\times10^1$)	($\times10^{-1}$)	($\times10^{-4}$)
$^1\Gamma_g$,$^3\Gamma_u$	-2.645	-7.505	4.154	-0.381	-0.423	2.301	0.646	0.279	-1.537
$^1\Phi_u$,$^3\Phi_g$	-1.322	-3.753	2.077	-0.628	-0.643	3.497	-0.162	-0.070	0.384
$^1\Phi_g$,$^3\Phi_u$	3.967	11.260	-6.231	-0.004	-0.207	1.115	-2.747	-1.187	6.531
$^1\Delta_u$,$^3\Delta_g$	3.086	8.756	-4.846	-0.190	-0.353	1.911	0.970	0.419	-2.305
$^1\Delta_g$,$^3\Delta_u$	2.865	8.131	-4.500	0.412	-0.396	2.206	3.471	1.500	-8.249
$^1\Delta_g$,$^3\Delta_u$	-1.322	-3.753	2.077	-0.574	-0.901	4.933	0.085	0.037	-0.202
$^1\Pi_u$,$^3\Pi_g$	-1.855	-5.264	2.913	-0.349	-1.014	5.584	-1.376	-0.594	3.270
$^1\Pi_u$,$^3\Pi_g$	1.414	4.013	-2.221	-0.069	-0.417	2.285	-1.049	-0.453	2.493
$^1\Pi_g$,$^3\Pi_u$	2.179	6.184	-3.423	-0.277	-0.413	2.241	0.417	0.180	-0.992
$^1\Pi_g$,$^3\Pi_u$	-1.739	-4.934	2.731	1.152	-0.827	4.674	-0.256	-0.110	0.608
$^1\Sigma_u$,$^3\Sigma_g$	-4.280	-12.140	6.721	0.914	-0.556	3.154	2.339	1.011	-5.560
$^1\Sigma_u$,$^3\Sigma_g$	1.635	4.638	-2.567	-0.309	-0.497	2.707	0.893	0.386	-2.124
$^1\Sigma_g$,$^3\Sigma_u$	-5.031	-14.280	7.902	1.297	-0.750	4.267	0.728	0.315	-1.731
$^1\Sigma_g$,$^3\Sigma_u$	-2.327	-6.604	3.655	-0.104	-1.048	5.793	-3.081	-1.331	7.323
$^1\Sigma_g$,$^3\Sigma_u$	0.746	2.117	-1.172	-0.275	-0.566	3.096	-0.880	-0.380	2.091

Table A.5: Dispersion coefficients of high Rydberg states for the *ns-ns*, *np-np* and *nd-nd* asymptotes of Rb-Rb. The coefficients are scaled by their major dependence on n and the residual dependence is fitted using three fitting parameters as indicated in the table.

ns-ns	$C_6 = n^{11}(c_0 + c_1 n + c_2 n^2)$			$C_8 = n^{15}(c_0 + c_1 n + c_2 n^2)$			$C_{10} = n^{22}(c_0 + c_1 n + c_2 n^2)$		
	c_0	c_1	c_2	c_0	c_1	c_2	c_0	c_1	c_2
symmetry	($\times 10^{1}$)	($\times 10^{-1}$)	($\times 10^{-3}$)	($\times 10^{0}$)	($\times 10^{-1}$)	($\times 10^{-3}$)	($\times 10^{-4}$)	($\times 10^{-6}$)	($\times 10^{-9}$)
$^1\Sigma_g$, $^3\Sigma_u$	1.197	-8.486	3.385	-7.303	8.068	-3.792	-5.546	5.242	-3.154
np-np	$C_5 = n^{8}(c_0 + c_1 n + c_2 n^2)$			$C_6 = n^{11}(c_0 + c_1 n + c_2 n^2)$			$C_8 = n^{15}(c_0 + c_1 n + c_2 n^2)$		
symmetry	($\times 10^{0}$)	($\times 10^{-2}$)	($\times 10^{-2}$)	($\times 10^{-1}$)	($\times 10^{-1}$)	($\times 10^{-4}$)	($\times 10^{1}$)	($\times 10^{0}$)	($\times 10^{-2}$)
$^1\Delta_g$,$^3\Delta_u$	-0.231	-1.976	0.010	3.620	-0.579	2.778	1.199	-0.624	0.250
$^1\Pi_u$,$^3\Pi_g$	Vanishes			6.070	-1.273	6.157	1.173	0.010	-0.069
$^1\Pi_g$,$^3\Pi_u$	0.922	7.903	-0.041	3.575	-0.183	0.816	2.973	-2.281	0.990
$^1\Sigma_u^-$,$^3\Sigma_g^-$	Vanishes			2.373	-0.034	0.107	2.176	-1.711	0.747
$^1\Sigma_g^+$,$^3\Sigma_u^+$	-1.383	-11.850	0.061	43.010	3.575	-1.714[1]	5.359	-3.984	1.729
$^1\Sigma_g^+$,$^3\Sigma_u^+$	Vanishes			5.461	-1.133	5.476	0.712	0.244	-0.162
nd-nd	$C_5 = n^{8}(c_0 + c_1 n + c_2 n^2)$			$C_6 = n^{11}\left(c_0 + c_1 n + \frac{c_{-1}}{n-n_0}\right)$			$C_7 = n^{12}(c_0 + c_1 n + c_2 n^2)$		
	c_0	c_1	c_2	c_0	c_1	c_{-1}	c_0	c_1	c_2
symmetry	($\times 10^{0}$)	($\times 10^{-2}$)	($\times 10^{-4}$)	($\times 10^{1}$)	($\times 10^{-2}$)	($\times 10^{0}$)	($\times 10^{1}$)	($\times 10^{-1}$)	($\times 10^{-1}$)
$^1\Gamma_g$,$^3\Gamma_u$	-1.445	-2.731	1.477	2.603	1.454	66.310	0.235	0.920	-0.487
$^1\Phi_u$,$^3\Phi_g$	-0.722	-1.366	0.738	4.124	2.475	105.000	-0.059	-0.230	0.122
$^1\Phi_g$,$^3\Phi_u$	2.167	4.097	-2.215	0.643	-0.273	16.570	-0.997	-3.911	2.069
$^1\Delta_u$,$^3\Delta_g$	1.686	3.186	-1.723	1.730	0.525	44.200	0.352	1.380	-0.730
$^1\Delta_g$,$^3\Delta_u$	1.565	2.959	-1.600	0.571	-0.584	14.650	1.260	4.940	-2.614
$^1\Delta_g$,$^3\Delta_u$	-0.722	-1.366	0.738	5.157	3.032	131.200	0.031	0.121	-0.064
$^1\Pi_u$,$^3\Pi_g$	-1.013	-1.915	1.036	5.157	2.864	131.200	-0.499	-1.958	1.036
$^1\Pi_u$,$^3\Pi_g$	0.773	1.460	-0.789	1.789	0.563	45.640	-0.381	-1.493	0.790
$^1\Pi_g$,$^3\Pi_u$	1.191	2.250	-1.217	2.217	0.916	56.570	0.151	0.594	-0.314
$^1\Pi_g$,$^3\Pi_u$	-0.950	-1.795	0.971	0.907	-0.779	22.990	-0.093	-0.364	0.193
$^1\Sigma_u$,$^3\Sigma_g$	-2.338	-4.419	2.389	0.274	-0.870	6.928	0.849	3.330	-1.762
$^1\Sigma_u$,$^3\Sigma_g$	0.893	1.688	-0.913	2.676	1.229	68.210	0.324	1.272	-0.673
$^1\Sigma_g$,$^3\Sigma_u$	-2.748	-5.195	2.809	0.298	-1.100	7.455	0.264	1.037	-0.548
$^1\Sigma_g$,$^3\Sigma_u$	-1.271	-2.403	1.299	4.755	2.449	120.900	-1.118	-4.386	2.320
$^1\Sigma_g$,$^3\Sigma_u$	0.408	0.771	-0.417	2.942	1.436	74.940	-0.319	-1.252	0.663

[1] The following resonance term is added: $C_6 = n^{11}(c_0 + c_1 n + c_2 n^2 + 693.1/(n - 29.5))$.

Table A.6: Dispersion coefficients of high Rydberg states for the *ns-ns*, *np-np* and *nd-nd* asymptotes of Cs-Cs. The coefficients are scaled by their major dependence on n and the residual dependence is fitted using three fitting parameters as indicated in the table.

ns-ns	$C_6 = n^{11}(c_0 + c_1 n + c_2 n^2)$			$C_8 = n^{15}(c_0 + c_1 n + c_2 n^2)$			$C_{10} = n^{22}(c_0 + c_1 n + c_2 n^2)$		
	c_0	c_1	c_2	c_0	c_1	c_2	c_0	c_1	c_2
symmetry	$(\times 10^1)$	$(\times 10^{-1})$	$(\times 10^{-3})$	$(\times 10^1)$	$(\times 10^0)$	$(\times 10^{-2})$	$(\times 10^{-3})$	$(\times 10^{-5})$	$(\times 10^{-7})$
$^1\Sigma_g, {}^3\Sigma_u$	1.064	-6.249	2.330	-3.019	3.777	-1.581	3.190	-5.920	3.022
np-np	$C_5 = n^8(c_0 + c_1 n + c_2 n^2)$			$C_6 = n^{11}(c_0 + c_1 n + c_2 n^2)$			$C_8 = n^{15}(c_0 + c_1 n + c_2 n^2)$		
symmetry	$(\times 10^0)$	$(\times 10^{-2})$	$(\times 10^{-4})$	$(\times 10^{-1})$	$(\times 10^{-1})$	$(\times 10^{-3})$	$(\times 10^1)$	$(\times 10^0)$	$(\times 10^{-2})$
$^1\Delta_g, {}^3\Delta_u$	-0.070	-1.973	0.940	-2.886	0.571	-0.268	-0.774	1.044	-0.445
$^1\Pi_u, {}^3\Pi_g$		Vanishes		-0.738	0.346	-0.168	-4.270	4.239	-1.793
$^1\Pi_g, {}^3\Pi_u$	0.279	7.893	-3.759	-8.121	1.349	-0.625	0.402	-0.093	0.031
$^1\Sigma_u^-, {}^3\Sigma_g^-$		Vanishes		-6.577	1.072	-0.496	0.031	0.088	-0.042
$^1\Sigma_g^+, {}^3\Sigma_u^+$	-0.418	-11.840	5.638	133.400	6.850	-3.074	-1.569	1.747	-0.765
$^1\Sigma_g^+, {}^3\Sigma_u^+$		Vanishes		-0.839	0.337	-0.163	-2.671	3.045	-1.289
nd-nd	$C_5 = n^8(c_0 + c_1 n + c_2 n^2)$			$C_6 = n^{11}(c_0 + c_1 n + c_2 n^2)$			$C_7 = n^{12}(c_0 + c_1 n + c_2 n^2)$		
	c_0	c_1	c_2	c_0	c_1	c_2	c_0	c_1	c_2
symmetry	$(\times 10^0)$	$(\times 10^{-2})$	$(\times 10^{-4})$	$(\times 10^0)$	$(\times 10^{-1})$	$(\times 10^{-3})$	$(\times 10^0)$	$(\times 10^{-1})$	$(\times 10^{-3})$
$^1\Gamma_g, {}^3\Gamma_u$	-0.710	-3.483	1.725	0.712	-0.257	0.108	0.271	1.062	-0.504
$^1\Phi_u, {}^3\Phi_g$	-0.355	-1.742	0.863	1.003	-0.151	0.053	-0.068	-0.266	0.126
$^1\Phi_g, {}^3\Phi_u$	1.065	5.225	-2.588	0.641	-1.013	0.460	-1.151	-4.515	2.143
$^1\Delta_u, {}^3\Delta_g$	0.828	4.064	-2.013	0.798	-0.834	0.374	0.406	1.593	-0.756
$^1\Delta_g, {}^3\Delta_u$	0.769	3.774	-1.869	0.569	-1.834	0.845	1.454	5.703	-2.707
$^1\Delta_g, {}^3\Delta_u$	-0.355	-1.742	0.863	1.161	-0.515	0.221	0.036	0.140	-0.066
$^1\Pi_u, {}^3\Pi_g$	-0.498	-2.443	1.210	1.147	-0.999	0.448	-0.576	-2.260	1.073
$^1\Pi_u, {}^3\Pi_g$	0.380	1.862	-0.922	0.721	-0.982	0.445	-0.439	-1.723	0.818
$^1\Pi_g, {}^3\Pi_u$	0.585	2.870	-1.422	0.843	-0.704	0.313	0.175	0.686	-0.325
$^1\Pi_g, {}^3\Pi_u$	-0.467	-2.290	1.134	0.439	-3.284	1.527	-0.107	-0.420	0.199
$^1\Sigma_u, {}^3\Sigma_g$	-1.149	-5.636	2.792	0.274	-2.491	1.159	0.980	3.844	-1.825
$^1\Sigma_u, {}^3\Sigma_g$	0.439	2.153	-1.066	0.896	-0.715	0.318	0.374	1.468	-0.697
$^1\Sigma_g, {}^3\Sigma_u$	-1.350	-6.626	3.282	0.217	-3.262	1.521	0.305	1.197	-0.568
$^1\Sigma_g, {}^3\Sigma_u$	-0.625	-3.065	1.518	1.068	-1.428	0.650	-1.290	-5.063	2.403
$^1\Sigma_g, {}^3\Sigma_u$	0.200	0.983	-0.487	0.872	-0.747	0.334	-0.368	-1.446	0.686

Appendix B

Molecular Basis Transformations

We have to consider these transformations because the optical field and molecular states are naturally defined in different coordinate systems. The optical field is simply defined in the space-fixed frame (SFF) and the quantization axis for single atoms is usually the polarization axis. Molecular states are normally defined in the molecule-fixed frame (MFF) and their quantization axis here is the molecular axis. We, in general, consider nonrotating molecules, which means that only the electronic part of the molecular states is of interest. Since the nuclear part is not involved, the dealing with the anomalous commutation relations and the coupling between electronic and nuclear angular momenta are not subjects of this analysis. Fortunately, we do not have to transform all molecular states from one reference frame to the other because, in the problems we have considered, only *np* states can be directly excited by the optical field. As a consequence, we only transform $np + np$ states.

B.1 Orthogonal transformations of atomic states

The basis of asymptotic molecular states was built in Appendix A using atomic states. Therefore, we can derive transformations between molecular states from the transformations of atomic states. It would be sufficient to consider the representation of general angular momentum $\hat{\mathbf{K}}$ for $K = 1$. For the quantization axis $\mathbf{z}$, the eigenstates of $\mathbf{z} \cdot \hat{\mathbf{K}} = \hat{K}_z$ are $|\mathbf{z}; K = 1, M\rangle$ $(M = -1, 0, 1)$. For another quantization axis $\boldsymbol{\eta}$, we have the eigenstates $|\boldsymbol{\eta}; K = 1, M\rangle$ of $\boldsymbol{\eta} \cdot \hat{\mathbf{K}} = \hat{K}_\eta$. We want to express all $|\boldsymbol{\eta}; K = 1, M\rangle$ in the basis of $|\mathbf{z}; K = 1, M\rangle$ states. For that purpose we just need to diagonalize $\boldsymbol{\eta} \cdot \hat{\boldsymbol{K}}$. For simplicity, we choose $\boldsymbol{\eta} = (\eta_x, \eta_y, \eta_z) = (\cos\theta, 0, \sin\theta)$, where θ is the angle between the two quantization axes. Using the standard representation of $\hat{K}_x$, $\hat{K}_y$, and $\hat{K}_z$ for $K = 1$, we easily find the following connection

$$\begin{pmatrix} |\boldsymbol{\eta}; M = 1\rangle \\ |\boldsymbol{\eta}; M = 0\rangle \\ |\boldsymbol{\eta}; M = -1\rangle \end{pmatrix} = \begin{pmatrix} \cos^2\frac{\theta}{2} & \frac{\sin\theta}{\sqrt{2}} & \sin^2\frac{\theta}{2} \\ -\frac{\sin\theta}{\sqrt{2}} & \cos\theta & \frac{\sin\theta}{\sqrt{2}} \\ \sin^2\frac{\theta}{2} & -\frac{\sin\theta}{\sqrt{2}} & \cos^2\frac{\theta}{2} \end{pmatrix} \begin{pmatrix} |\mathbf{z}; M = 1\rangle \\ |\mathbf{z}; M = 0\rangle \\ |\mathbf{z}; M = -1\rangle \end{pmatrix}. \tag{B.1.1}$$

The last formula is sufficient for our purposes because we only transform $np_j + np_{j'}$ molecular states. The transformation matrices for atomic states with $\ell = 1$ and the total spin state $S = 1$, corresponding to different quantization axes, are the same and given by the last formula. We know that states with $S = 0$ are invariant under rotations. Therefore, all the transformation of $np_j + np_{j'}$ can be derived from the last expression for general angular momentum $K = 1$.

B.2 Transformations between molecular basis states

We basically have to find out how to project certain np+np states, defined in the SFF, onto molecular bases of different symmetries. As showed in the section on molecular resonances, if a pair of ground-state atoms is excited by a linearly polarized optical field, the doubly-xcited diatomic states are

$$
\begin{aligned}
|\mathrm{SFF}, A, 1\rangle &= \left|np_{3/2}, m\right\rangle \left|np_{3/2}, m\right\rangle, && \text{(B.2.1)}\\
|\mathrm{SFF}, A, 2\rangle &= \frac{1}{\sqrt{2}}\left[\left|np_{3/2}, m\right\rangle \left|np_{1/2}, m\right\rangle + \left|np_{1/2}, m\right\rangle \left|np_{3/2}, m\right\rangle\right], && \text{(B.2.2)}\\
|\mathrm{SFF}, A, 3\rangle &= \left|np_{1/2}, m\right\rangle \left|np_{1/2}, m\right\rangle, && \text{(B.2.3)}
\end{aligned}
$$

for the initial projections $m_1 = m_2$, or

$$
\begin{aligned}
|\mathrm{SFF}, B, 1\rangle &= \frac{1}{\sqrt{2}}\left[\left|np_{3/2}, m\right\rangle \left|np_{3/2}, -m\right\rangle + q\left|np_{3/2}, -m\right\rangle \left|np_{3/2}, m\right\rangle\right] && \text{(B.2.4)}\\
|\mathrm{SFF}, B, 2\rangle &= \frac{1}{\sqrt{2}}\left[\left|np_{3/2}, m\right\rangle \left|np_{1/2}, -m\right\rangle + q\left|np_{3/2}, -m\right\rangle \left|np_{1/2}, m\right\rangle\right] && \text{(B.2.5)}\\
|\mathrm{SFF}, B, 3\rangle &= \frac{1}{\sqrt{2}}\left[\left|np_{1/2}, m\right\rangle \left|np_{3/2}, -m\right\rangle + q\left|np_{1/2}, -m\right\rangle \left|np_{3/2}, m\right\rangle\right] && \text{(B.2.6)}\\
|\mathrm{SFF}, B, 4\rangle &= \frac{1}{\sqrt{2}}\left[\left|np_{1/2}, m\right\rangle \left|np_{3/2}, -m\right\rangle + q\left|np_{1/2}, -m\right\rangle \left|np_{3/2}, m\right\rangle\right] && \text{(B.2.7)}
\end{aligned}
$$

for the initial projections $m_1 = -m_2$ $(q = \pm 1)$. For all these states the quantization axis is the polarization axis of the optical field. It is sufficient to consider the $m = 1/2$ case.

Now we list asymptotic $np + np$ basis states corresponding to 0_g^+, 0_u^- and 1_u symmetries. All these states are in the MFF and the molecular axis is the quantization axis.

$$\begin{aligned}
|\mathrm{MFF}, 0_g^+, 1\rangle &= \frac{1}{\sqrt{2}}\left[\left|np_{3/2}, 3/2\right\rangle \left|np_{3/2}, -3/2\right\rangle - \left|np_{3/2}, -3/2\right\rangle \left|np_{3/2}, 3/2\right\rangle\right], \\
|\mathrm{MFF}, 0_g^+, 2\rangle &= \frac{1}{\sqrt{2}}\left[\left|np_{3/2}, 1/2\right\rangle \left|np_{3/2}, -1/2\right\rangle - \left|np_{3/2}, -1/2\right\rangle \left|np_{3/2}, 1/2\right\rangle\right], \\
|\mathrm{MFF}, 0_g^+, 3\rangle &= \frac{1}{2}\left[\left|np_{3/2}, 1/2\right\rangle \left|np_{1/2}, -1/2\right\rangle - \left|np_{1/2}, -1/2\right\rangle \left|np_{1/2}, 3/2\right\rangle\right] + \\
&\quad \frac{1}{2}\left[\left|np_{3/2}, -1/2\right\rangle \left|np_{1/2}, 1/2\right\rangle - \left|np_{1/2}, -1/2\right\rangle \left|np_{1/2}, 3/2\right\rangle\right], \\
|\mathrm{MFF}, 0_g^+, 4\rangle &= \frac{1}{\sqrt{2}}\left[\left|np_{1/2}, 1/2\right\rangle \left|np_{1/2}, -1/2\right\rangle - \left|np_{1/2}, -1/2\right\rangle \left|np_{1/2}, 1/2\right\rangle\right].
\end{aligned}$$

Only $|\mathrm{SFF}, B, i\rangle$ states for $q = -1$ have nonvanishing projections onto 0_g^+ states. These projections are given by the matrix $U1$ defined as $W_{0_g^+}(i,j) = \langle \mathrm{SFF}, B, i | \mathrm{MFF}, 0_g^+, j\rangle$

$$W_{0_g^+} = \begin{pmatrix} -\frac{3}{4}\sin^2\theta & \frac{1}{8}(5 + 3\cos 2\theta) & 0 & 0 \\ 0 & 0 & \frac{1+3\cos 2\theta}{4\sqrt{2}} & 0 \\ 0 & 0 & -\frac{1+3\cos 2\theta}{4\sqrt{2}} & 0 \\ 0 & 0 & 0 & 1 \end{pmatrix}.$$

The $np + np$ basis states of 0_u^- symmetry are.

$$\begin{aligned}
|\mathrm{MFF}, 0_u^-, 1\rangle &= \frac{1}{\sqrt{2}}\left[\left|np_{3/2}, 3/2\right\rangle \left|np_{3/2}, -3/2\right\rangle + \left|np_{3/2}, -3/2\right\rangle \left|np_{3/2}, 3/2\right\rangle\right], \\
|\mathrm{MFF}, 0_u^-, 2\rangle &= \frac{1}{\sqrt{2}}\left[\left|np_{3/2}, 1/2\right\rangle \left|np_{3/2}, -1/2\right\rangle + \left|np_{3/2}, -1/2\right\rangle \left|np_{3/2}, 1/2\right\rangle\right], \\
|\mathrm{MFF}, 0_u^-, 3\rangle &= \frac{1}{2}\left[\left|np_{3/2}, 1/2\right\rangle \left|np_{1/2}, -1/2\right\rangle + \left|np_{1/2}, -1/2\right\rangle \left|np_{1/2}, 3/2\right\rangle\right] - \\
&\quad \frac{1}{2}\left[\left|np_{3/2}, -1/2\right\rangle \left|np_{1/2}, 1/2\right\rangle + \left|np_{1/2}, -1/2\right\rangle \left|np_{1/2}, 3/2\right\rangle\right], \\
|\mathrm{MFF}, 0_u^-, 4\rangle &= \frac{1}{\sqrt{2}}\left[\left|np_{1/2}, 1/2\right\rangle \left|np_{1/2}, -1/2\right\rangle + \left|np_{1/2}, -1/2\right\rangle \left|np_{1/2}, 1/2\right\rangle\right].
\end{aligned}$$

In this case, both $|\mathrm{SFF}, A, i\rangle$ and $|\mathrm{SFF}, B, j\rangle$ (for $q = 1$) states have nonzero projections. We define two matrices $V_{0_u^-}(i,j) = \langle \mathrm{SFF}, A, i | \mathrm{MFF}, 0_u^-, j\rangle$ and $W_{0_u^-}(i,j) =$

$\langle \mathrm{MFF}, B, i | \mathrm{MFF}, 0_u^-, j\rangle$. These matrices are

$$V_{0_u^-} = \begin{pmatrix} \frac{3\sin^3\theta}{4\sqrt{2}} & -\frac{5\sin\theta+9\sin 3\theta}{16\sqrt{2}} & 0 & 0 \\ 0 & 0 & -\frac{\sin\theta}{2\sqrt{2}} & 0 \\ 0 & 0 & 0 & -\frac{\sin\theta}{\sqrt{2}} \end{pmatrix},$$

and

$$W_{0_u^-} = \begin{pmatrix} -\frac{3}{4}\cos\theta\sin^2\theta & \frac{7\cos\theta+9\cos 3\theta}{16} & 0 & 0 \\ 0 & 0 & -\frac{\cos\theta}{\sqrt{2}} & 0 \\ 0 & 0 & \frac{\cos\theta}{\sqrt{2}} & 0 \\ 0 & 0 & 0 & \cos\theta \end{pmatrix}.$$

The $np + np$ basis states of 1_u symmetry are

$$\begin{aligned} |\mathrm{MFF}, 1_u, 1\rangle &= \left|np_{3/2}, 1/2\right\rangle \left|np_{3/2}, 1/2\right\rangle, \\ |\mathrm{MFF}, 1_u, 2\rangle &= \frac{1}{\sqrt{2}}\left[\left|np_{3/2}, 3/2\right\rangle \left|np_{3/2}, -1/2\right\rangle + \left|np_{3/2}, -1/2\right\rangle \left|np_{3/2}, 3/2\right\rangle\right], \\ |\mathrm{MFF}, 1_u, 3\rangle &= \frac{1}{2}\left[\left|np_{3/2}, 3/2\right\rangle \left|np_{1/2}, -1/2\right\rangle + \left|np_{1/2}, -1/2\right\rangle \left|np_{1/2}, 3/2\right\rangle\right], \\ |\mathrm{MFF}, 1_u, 4\rangle &= \frac{1}{\sqrt{2}}\left[\left|np_{3/2}, 1/2\right\rangle \left|np_{1/2}, 1/2\right\rangle + \left|np_{1/2}, 1/2\right\rangle \left|np_{3/2}, 1/2\right\rangle\right], \\ |\mathrm{MFF}, 1_u, 5\rangle &= \left|np_{1/2}, 1/2\right\rangle \left|np_{1/2}, 1/2\right\rangle. \end{aligned}$$

For these states we also define two matrices $V_{1_u}(i,j) = \langle \mathrm{SFF}, A, i | \mathrm{MFF}, 1_u, j\rangle$ and $W_{1_u}(i,j) = \langle \mathrm{SFF}, B, i | \mathrm{MFF}, 1_u, j\rangle$ (for $q = 1$). These matrices are

$$V_{1_u} = \begin{pmatrix} \frac{\left(\cos\frac{\theta}{2}+3\cos\frac{3\theta}{2}\right)^3}{16} & -\frac{\sqrt{3}(1+3\cos\theta)\sin^2\theta}{4\sqrt{2}} & 0 & 0 & 0 \\ 0 & 0 & -\frac{\sqrt{3}}{4}\sin^2\theta & \frac{(3\cos\theta-1)\cos^2\frac{\theta}{2}}{2} & 0 \\ 0 & 0 & 0 & 0 & \cos^2\frac{\theta}{2} \end{pmatrix}$$

and

$$W_{1_u} = \begin{pmatrix} \frac{5\cos\theta+9\sin 3\theta}{16\sqrt{2}} & -\frac{\sqrt{3}(\sin\theta-3\sin 3\theta)}{16} & 0 & 0 & 0 \\ 0 & 0 & \sqrt{3}\cos^3\frac{\theta}{2}\sin\frac{\theta}{2} & \frac{(3\cos\theta-1)\sin\theta}{4} & 0 \\ 0 & 0 & -\sqrt{3}\cos\frac{\theta}{2}\sin^3\frac{\theta}{2} & \frac{(1+3\cos\theta)\sin\theta}{4} & 0 \\ 0 & 0 & 0 & 0 & \frac{\sin\theta}{\sqrt{2}} \end{pmatrix}.$$

All these transformation formulae are needed to find the average of ω_{eff}^2 over all possible orientations of the molecular axis. This quantity is important for the calculation of probabilities. Because ω_{eff}^2 is a quadratic function of the components which are transformed via the above listed matrices, there are all together more than a hundred angular integrals to evaluate. However, one can derive a formula which can be implemented in *Mathematica* to give a fast and efficient way to calculate all of them. Angular averaging is performed in addition to the averaging of ω_{eff}^2 over initial states. Both types of averaging are done for each symmetry individually.

First, we define some auxiliary vectors:

$$|\beta_{\text{v}}\rangle \equiv \left(\frac{1}{\Delta}, \sqrt{f/2}\frac{\Delta+\Delta'}{\Delta\Delta'}, f\frac{1}{\Delta'}\right), \tag{B.2.8}$$

$$|\beta_{\text{w}}\rangle \equiv \left(\frac{1}{\Delta}, \sqrt{f}\frac{\Delta+\Delta'}{2\Delta\Delta'}, \sqrt{f}\frac{\Delta+\Delta'}{2\Delta\Delta'}, f\frac{1}{\Delta'}\right), \tag{B.2.9}$$

$$|\mathbf{a}_{\text{v}}\rangle \equiv (a_{ee}, a_{ee'}, a_{e'e'}), \tag{B.2.10}$$

$$|\mathbf{a}_{\text{w}}\rangle \equiv (a_{ee}, a_{ee'}, a_{e'e}, a_{e'e'}), \tag{B.2.11}$$

where f is the ratio of oscillator strengths $f_{1/2}/f_{3/2}$. Indices v and w correspond to the initial conditions $m_1 = m_2$ and $m_1 = -m_2$, respectively. Note that the components of $|\mathbf{a}_{\text{v(w)}}\rangle$ are defined differently in these cases (section 1.3.1). These vectors can be rewritten more formally

$$\begin{aligned} |\mathbf{a}_{\mathrm{v}}\rangle &= \sum_i{}' \langle \mathrm{SFF}, A, i|\varphi_\lambda\rangle \; |\mathrm{SFF}, A, i\rangle && \text{(B.2.12)} \\ |\mathbf{a}_{\mathrm{w}}\rangle &= \sum_j{}' \langle \mathrm{SFF}, B, j|\varphi_\lambda\rangle \; |\mathrm{SFF}, B, i\rangle, && \text{(B.2.13)} \end{aligned}$$

where $|\varphi_\lambda\rangle$ is an eigenstate of $U(R)$ defined by (1.2.8). These vectors are used to find $\omega_{\text{eff}} = \omega^2 \langle \boldsymbol{\beta}_{\mathrm{v(w)}} | \mathbf{a}_{\mathrm{v(w)}} \rangle$. The difficulty is that the components of the vectors $|\mathbf{a}_{\mathrm{v(w)}}\rangle$ are scalar products of states defined in different reference frames. To compute them, we also need to define a new vector $|\boldsymbol{\alpha}\rangle$ as $\alpha_i = \langle \mathrm{MFF}, i|\varphi_\lambda\rangle$, where $|\mathrm{MFF}, i\rangle$ are asymptotic $np + np$ basis states we have defined in this appendix for each symmetry. This means that $|\boldsymbol{\alpha}\rangle$ is different for different molecular states (and thus for different symmetries as well). These α_i are just components of the eigenstates of $U(R)$ in the asymptotic basis so they are calculated together with molecular potentials. The connection between $|\mathbf{a}_{\mathrm{v(w)}}\rangle$ and $|\boldsymbol{\alpha}\rangle$ is

$$\begin{aligned} |\mathbf{a}_{\mathrm{v}}\rangle &= V|\boldsymbol{\alpha}\rangle && \text{(B.2.14)} \\ |\mathbf{a}_{\mathrm{w}}\rangle &= W|\boldsymbol{\alpha}\rangle, && \text{(B.2.15)} \end{aligned}$$

where V is one of the $V_{0_u^-}$, V_{1_u} matrices, and similarly W is one of the $W_{0_g^+}$, $W_{0_u^-}$, W_{1_u} matrices. For the initial conditions $m_1 = m_2$ we have

$$\omega_{\text{eff}}^2 = \omega^4 \langle \boldsymbol{\alpha}|V^T|\boldsymbol{\beta}_{\mathrm{v}}\rangle\langle\boldsymbol{\beta}_{\mathrm{v}}|V|\boldsymbol{\alpha}\rangle = \omega^4 \mathrm{Tr}\left\{\mathrm{V^T}|\boldsymbol{\beta}_{\mathrm{v}}\rangle\langle\boldsymbol{\beta}_{\mathrm{v}}|\mathrm{V}|\boldsymbol{\alpha}\rangle\langle\boldsymbol{\alpha}|\right\}. \qquad \text{(B.2.16)}$$

Similarly, for the initial conditions $m_1 = -m_2$ we find

$$\omega_{\text{eff}}^2 = \omega^4 \langle \boldsymbol{\alpha}|W^T|\boldsymbol{\beta}_{\mathrm{w}}\rangle\langle\boldsymbol{\beta}_{\mathrm{w}}|W|\boldsymbol{\alpha}\rangle = \omega^4 \mathrm{Tr}\left\{\mathrm{W^T}|\boldsymbol{\beta}_{\mathrm{w}}\rangle\langle\boldsymbol{\beta}_{\mathrm{w}}|\mathrm{W}|\boldsymbol{\alpha}\rangle\langle\boldsymbol{\alpha}|\right\}. \qquad \text{(B.2.17)}$$

From the last two equations we conclude that the averaging over all possible orientations of the molecular axis is reduced to averaging the matrices $V^T|\boldsymbol{\beta}_\mathrm{v}\rangle\langle\boldsymbol{\beta}_\mathrm{v}|V$ and $W^T|\boldsymbol{\beta}_\mathrm{w}\rangle\langle\boldsymbol{\beta}_\mathrm{w}|W$. These matrices are not related to $U(R)$ and its eigenproblem so this averaging can be done first. As a result, we get two matrices $\langle\langle V^T|\boldsymbol{\beta}_\mathrm{v}\rangle\langle\boldsymbol{\beta}_\mathrm{v}|V\rangle\rangle$ and $\langle\langle W^T|\boldsymbol{\beta}_\mathrm{w}\rangle\langle\boldsymbol{\beta}_\mathrm{w}|W\rangle\rangle$ with no angular dependence (here $\langle\langle\,\rangle\rangle$ refers to angular averaging only). We just use these matrices in (B.2.16) and (B.2.17) instead of the angle-dependent ones. Such average matrices have to be found for $V = V_{0_u^-}, V_{1_u}$ and $W = W_{0_g^+}, W_{0_u^-}, W_{1_u}$, which is a straightforward task in *Mathematica*.

Appendix C

The Analysis of $(n-1)p_{3/2}+(n+1)p_{3/2}$ Molecular Resonances

C.1 The role of fine structure

Here, we focus on resonances at energies corresponding to excited atom pairs $(n-1)p_{3/2}+(n+1)p_{3/2}$. The simplest treatment described in the Chapter 2 and given by Eq. (1.3.18) is sufficient to reproduce very well the main features of the resonance. In this appendix, we present the results of our theory applied to these resonances. We also show some technical details which were not previously included in the main text.

The $(n-1)p_{3/2}+(n+1)p_{3/2}$ resonances are relatively close to the atomic np resonance, which means that they occur at small interaction energies and thus large internuclear separations R; in this range of R, the most important interactions are the dipole-dipole terms. Importantly, np states cannot be coupled directly via dipole-dipole interaction, and so significant ℓ-mixing is required. The matrix elements of the dipole interaction $V_{\rm dip}(R)$ can be calculated using Eq. (1.2.10) for $L=1$.

Because of the proximity of these resonances to the atomic resonance, we do not

0_u^- state	Symmetrization $\left((1-\sigma_\nu)/\sqrt{2}\right)\ \lvert 0_u\rangle$
$\lvert 70s71s, 0_u^-\rangle$	$\frac{1}{\sqrt{2}}\left\{\lvert 70s_{\frac{1}{2}}, \frac{1}{2}; 71s_{\frac{1}{2}}, -\frac{1}{2}; 0_u\rangle + \lvert 70s_{\frac{1}{2}}, -\frac{1}{2}; 71s_{\frac{1}{2}}, \frac{1}{2}; 0_u\rangle\right\}$
$\lvert 70p_{\frac{3}{2}}70p_{\frac{3}{2}}, 0_u^-\rangle$	$\lvert 70p_{\frac{3}{2}}, \frac{3}{2}; 70p_{\frac{3}{2}}, -\frac{3}{2}; 0_u\rangle$
degenerate	$\lvert 70p_{\frac{3}{2}}, \frac{1}{2}; 70p_{\frac{3}{2}}, -\frac{1}{2}; 0_u\rangle$
$\lvert 70p_{\frac{3}{2}}70p_{\frac{1}{2}}, 0_u^-\rangle$	$\frac{1}{\sqrt{2}}\left\{\lvert 70p_{\frac{3}{2}}, -\frac{1}{2}; 70p_{\frac{1}{2}}, \frac{1}{2}; 0_u\rangle - \lvert 70p_{\frac{3}{2}}, \frac{1}{2}; 70p_{\frac{1}{2}}, -\frac{1}{2}; 0_u\rangle\right\}$
$\lvert 70p_{\frac{1}{2}}70p_{\frac{1}{2}}, 0_u^-\rangle$	$\lvert 70p_{\frac{1}{2}}, \frac{1}{2}; 70p_{\frac{1}{2}}, -\frac{1}{2}; 0_u\rangle$
$\lvert 69p_{\frac{3}{2}}71p_{\frac{3}{2}}, 0_u^-\rangle$	$\frac{1}{\sqrt{2}}\left\{\lvert 69p_{\frac{3}{2}}, \frac{3}{2}; 71p_{\frac{3}{2}}, -\frac{3}{2}; 0_u\rangle + \lvert 69p_{\frac{3}{2}}, -\frac{3}{2}; 71p_{\frac{3}{2}}, \frac{3}{2}; 0_u\rangle\right\}$
degenerate	$\frac{1}{\sqrt{2}}\left\{\lvert 69p_{\frac{3}{2}}, \frac{1}{2}; 71p_{\frac{3}{2}}, -\frac{1}{2}; 0_u\rangle + \lvert 69p_{\frac{3}{2}}, -\frac{1}{2}; 71p_{\frac{3}{2}}, \frac{1}{2}; 0_u\rangle\right\}$
$\lvert 69p_{\frac{3}{2}}71p_{\frac{1}{2}}, 0_u^-\rangle$	$\frac{1}{\sqrt{2}}\left\{\lvert 69p_{\frac{3}{2}}, \frac{1}{2}; 71p_{\frac{1}{2}}, -\frac{1}{2}; 0_u\rangle - \lvert 69p_{\frac{3}{2}}, -\frac{1}{2}; 71p_{\frac{1}{2}}, \frac{1}{2}; 0_u\rangle\right\}$
$\lvert 69p_{\frac{1}{2}}71p_{\frac{3}{2}}, 0_u^-\rangle$	$\frac{1}{\sqrt{2}}\left\{\lvert 69p_{\frac{1}{2}}, \frac{1}{2}; 71p_{\frac{3}{2}}, -\frac{1}{2}; 0_u\rangle - \lvert 69p_{\frac{1}{2}}, -\frac{1}{2}; 71p_{\frac{3}{2}}, \frac{1}{2}; 0_u\rangle\right\}$
$\lvert 69p_{\frac{1}{2}}71p_{\frac{1}{2}}, 0_u^-\rangle$	$\frac{1}{\sqrt{2}}\left\{\lvert 69p_{\frac{1}{2}}, \frac{1}{2}; 71p_{\frac{1}{2}}, -\frac{1}{2}; 0_u\rangle + \lvert 69p_{\frac{1}{2}}, -\frac{1}{2}; 71p_{\frac{1}{2}}, \frac{1}{2}; 0_u\rangle\right\}$
$\lvert 69s72s, 0_u^-\rangle$	$\frac{1}{\sqrt{2}}\left\{\lvert 69s_{\frac{1}{2}}, \frac{1}{2}; 72s_{\frac{1}{2}}, -\frac{1}{2}; 0_u\rangle + \lvert 69s_{\frac{1}{2}}, -\frac{1}{2}; 72s_{\frac{1}{2}}, \frac{1}{2}; 0_u\rangle\right\}$

Table C.1: Asymptotic 0_u^- molecular states. All of the 0_u^- states used to calculate the lineshape of the $69p + 71p$ resonance are listed. The $\Omega = 0$ states have to be additionally symmetrized with respect to σ_ν. Both m_j and $m_2 = \Omega - m_j$ change sign under σ_ν, but the phase factors resulting from the symmetrization $(1 \pm \sigma_\nu)/\sqrt{2}$ are not obvious. The result of this symmetrization is presented explicitly. We assume that all $\lvert n\ell_j, m_j; n'\ell'_{j'}, m_{j'}; 0_u\rangle$ states are symmetrized according to (1.1.2).

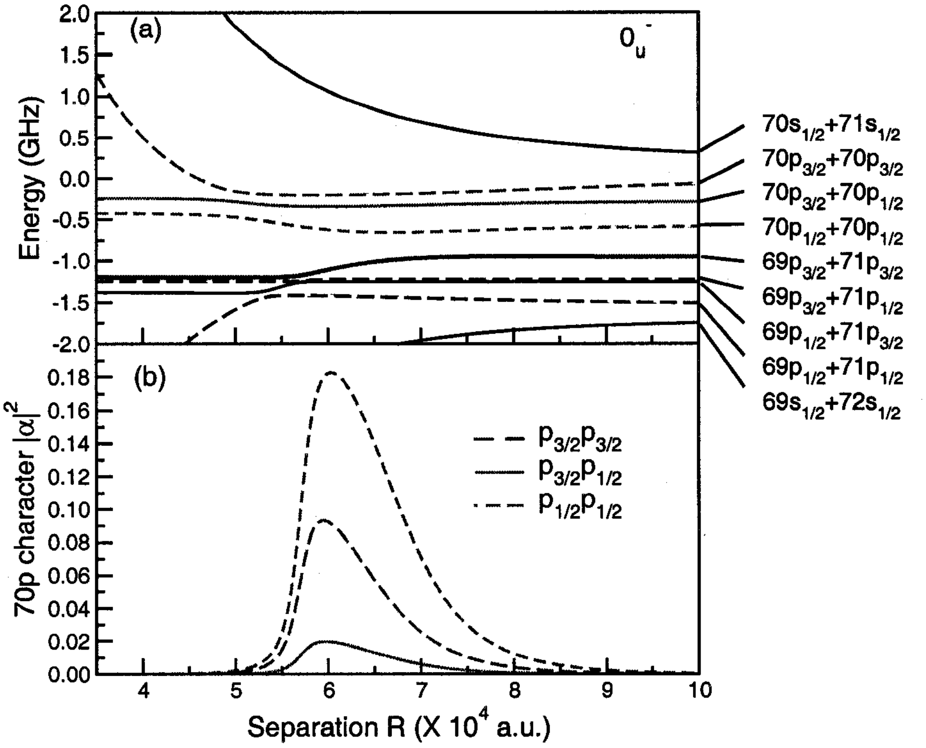

Fig. C.1: (a) Potential curves for the 0_u^- symmetry corresponding to asymptotes from $70s_{1/2}+71s_{1/2}$ to $69s_{1/2}+72s_{1/2}$ centered around $69p_{3/2}+71p_{3/2}$. This latter curve is indicated by a thicker line. The zero of energy is set at the $70p_{3/2}+70p_{3/2}$ asymptote. Only curves that are not flat (within our approximations) are shown; at separation $R < 45000$ a.u., they become less reliable. (b) The fraction of $70p$ character $|\alpha|^2$ for $p_{3/2}p_{3/2}$, $p_{3/2}p_{1/2}$, and $p_{1/2}p_{1/2}$ mixtures corresponding to the potential correlated to the $69p_{3/2}+71p_{3/2}$ asymptote. These different fractions are given by the components α_i of the vector $|\alpha\rangle$ defined in Appendix B.

need to use a large basis set. To diagonalize $U(R)$, we select all states correlated with the $np+np$ and $(n-1)p+(n+1)p$ asymptotes, as well as all states correlated to the asymptotes in between. Nearby states having significant dipole-dipole couplings with these aforementioned states are also included. In the basis (1.1.2), dipole-dipole interactions give off-diagonal elements and asymptotic separations between states give diagonal terms. In the R-range relevant for the $(n-1)p+(n+1)p$ resonances, the coupling due to dipole matrix elements $R_{nn'}$ decays rapidly with $\Delta n \equiv |n - n'|$; for $\Delta n = 2$, it is roughly 100 times weaker than for $\Delta n = 0$, and since the interaction matrix elements $\langle 1,2|V_{\rm dip}|3,4,\rangle$ are quadratic in $R_{nn'}$, we neglected states corresponding to $\Delta n \geq 3$. Specifically, we have included all states correlated to the following asymptotes: $ns+(n+1)s$, $np+np$, $(n-1)p+(n+1)p$ and $(n-1)s+(n+2)s$. As an illustration, in Tables C.1-C.2, we list all asymptotic states of 0_u^- and 0_g^+ symmetry,respectively, used in our calculation of the $69p + 71p$ resonance. The excitation probabilities are dominated by the contributions from 0_u^- and 1_u states. In Figs. C.1-C.3, we show the potential curves for the three relevant symmetries (0_g^+, 0_u^- and 0_g^+) for the resonance located near the $69p_{3/2} + 71p_{3/2}$ asymptote.

The selection rule $\Delta m = 0$ for the laser polarization determines the polarization of the intermediate states. We label excited Rydberg states as $|e,m\rangle$ and $|e',m\rangle$, where e and e' correspond to $np_{3/2}$ and $np_{1/2}$ respectively. We have considered in detail the $m_1 = -m_2$ case for the atom pairs in their ground states. For this case we just give the final results. However, we give more technical details about the $m_1 = m_2 = \pm 1/2$ case, which has not been fully analyzed. We introduce a simplified notation for diatomic states. We define $|gg\rangle \equiv |g,m\rangle|g,m\rangle$, where $m = \pm 1/2$, and similar definitions are used for $|ee\rangle$ and $|e'e'\rangle$. States $|ge\rangle$, $|ge'\rangle$ and $|ee'\rangle$ are defined as symmetric superpositions; *e.g.*, $|ge\rangle = \{|g,m\rangle|e,m\rangle + |e,m\rangle|g,m\rangle\}/\sqrt{2}$.

The actual doubly-excited states, labeled as $|\varphi_\lambda(R)\rangle$, correspond to the molecular

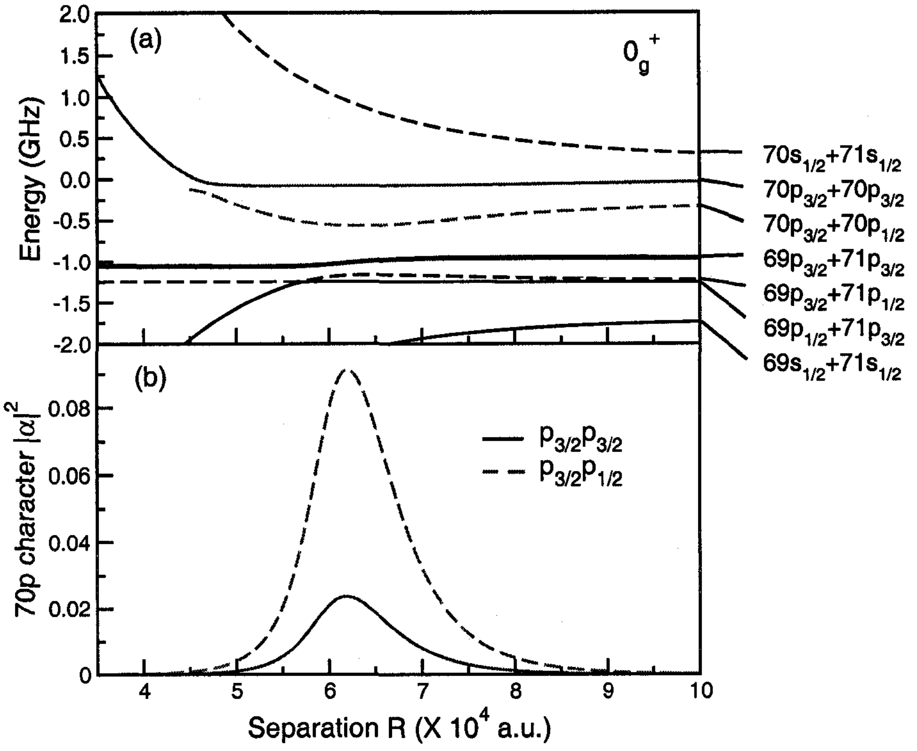

Fig. C.2: Same as Fig.C.1 but for the 0_g^+ symmetry. In (b), $|\alpha|^2$ for the $p_{1/2}p_{1/2}$ mixture is negligible and hence not shown.

potential curves $\epsilon_\lambda(R)$; they are eigenvectors and eigenvalues of (1.2.8), respectively. Many potential curves λ contribute, to various degrees, to the population of excited pairs of atoms.

To solve for the excitation probability, we solve the coupled time-dependent Schrödinger equation. The Hamiltonian of an interacting pair of atoms is ($\hbar = 1$)

$$\begin{aligned} H &= \sum_{i=1}^{2} \left[\Delta\sigma^i_{ee} + \Delta'\sigma^i_{e'e'}\right] + \sum_{i=1}^{2} \left[\frac{\omega}{2}\sigma^i_{eg} + \frac{\omega'}{2}\sigma^i_{e'g} + \text{h.c.}\right] \\ &\quad + \left[\Delta_\lambda + \epsilon_\lambda(R)\right] |\varphi_\lambda\rangle\langle\varphi_\lambda| \, . \end{aligned} \qquad \text{(C.1.1)}$$

All physical variables in this H have been defined before. The operators σ^i_{eg} and σ^i_{ee}

0_g^+ state	Symmetrization $\left((1+\sigma_\nu)/\sqrt{2}\right)\ \|0_g\rangle$
$\|70s71s, 0_g^+\rangle$	$\frac{1}{\sqrt{2}}\left\{\|70s_{\frac{1}{2}}, \frac{1}{2}; 71s_{\frac{1}{2}}, -\frac{1}{2}; 0_g\rangle - \|70s_{\frac{1}{2}}, -\frac{1}{2}; 71s_{\frac{1}{2}}, \frac{1}{2}; 0_g\rangle\right\}$
$\|70p_{\frac{3}{2}}70p_{\frac{3}{2}}, 0_g^+\rangle$	$\|70p_{\frac{3}{2}}, \frac{3}{2}; 70p_{\frac{3}{2}}, -\frac{3}{2}; 0_g\rangle$
degenerate	$\|70p_{\frac{3}{2}}, \frac{1}{2}; 70p_{\frac{3}{2}}, -\frac{1}{2}; 0_g\rangle$
$\|70p_{\frac{3}{2}}70p_{\frac{1}{2}}, 0_g^+\rangle$	$\frac{1}{\sqrt{2}}\left\{\|70p_{\frac{3}{2}}, -\frac{1}{2}; 70p_{\frac{1}{2}}, \frac{1}{2}; 0_g\rangle + \|70p_{\frac{3}{2}}, \frac{1}{2}; 70p_{\frac{1}{2}}, -\frac{1}{2}; 0_g\rangle\right\}$
$\|70p_{\frac{1}{2}}70p_{\frac{1}{2}}, 0_g^+\rangle$	$\|70p_{\frac{1}{2}}, \frac{1}{2}; 70p_{\frac{1}{2}}, -\frac{1}{2}; 0_g\rangle$
$\|69p_{\frac{3}{2}}71p_{\frac{3}{2}}, 0_g^+\rangle$	$\frac{1}{\sqrt{2}}\left\{\|69p_{\frac{3}{2}}, \frac{3}{2}; 71p_{\frac{3}{2}}, -\frac{3}{2}; 0_g\rangle - \|69p_{\frac{3}{2}}, -\frac{3}{2}; 71p_{\frac{3}{2}}, \frac{3}{2}; 0_g\rangle\right\}$
degenerate	$\frac{1}{\sqrt{2}}\left\{\|69p_{\frac{3}{2}}, \frac{1}{2}; 71p_{\frac{3}{2}}, -\frac{1}{2}; 0_g\rangle - \|69p_{\frac{3}{2}}, -\frac{1}{2}; 71p_{\frac{3}{2}}, \frac{1}{2}; 0_g\rangle\right\}$
$\|69p_{\frac{3}{2}}71p_{\frac{1}{2}}, 0_g^+\rangle$	$\frac{1}{\sqrt{2}}\left\{\|69p_{\frac{3}{2}}, \frac{1}{2}; 71p_{\frac{1}{2}}, -\frac{1}{2}; 0_g\rangle + \|69p_{\frac{3}{2}}, -\frac{1}{2}; 71p_{\frac{1}{2}}, \frac{1}{2}; 0_g\rangle\right\}$
$\|69p_{\frac{1}{2}}71p_{\frac{3}{2}}, 0_g^+\rangle$	$\frac{1}{\sqrt{2}}\left\{\|69p_{\frac{1}{2}}, \frac{1}{2}; 71p_{\frac{3}{2}}, -\frac{1}{2}; 0_g\rangle + \|69p_{\frac{1}{2}}, -\frac{1}{2}; 71p_{\frac{3}{2}}, \frac{1}{2}; 0_g\rangle\right\}$
$\|69p_{\frac{1}{2}}71p_{\frac{1}{2}}, 0_g^+\rangle$	$\frac{1}{\sqrt{2}}\left\{\|69p_{\frac{1}{2}}, \frac{1}{2}; 71p_{\frac{1}{2}}, -\frac{1}{2}; 0_g\rangle - \|69p_{\frac{1}{2}}, -\frac{1}{2}; 71p_{\frac{1}{2}}, \frac{1}{2}; 0_g\rangle\right\}$
$\|69s72s, 0_g^+\rangle$	$\frac{1}{\sqrt{2}}\left\{\|69s_{\frac{1}{2}}, \frac{1}{2}; 72s_{\frac{1}{2}}, -\frac{1}{2}; 0_g\rangle - \|69s_{\frac{1}{2}}, -\frac{1}{2}; 72s_{\frac{1}{2}}, \frac{1}{2}; 0_g\rangle\right\}$

Table C.2: Same as Table. C.1 but for the 0_g^+ symmetry.

are now

$$\sigma_{eg}^i = \sum_m |e_i, m\rangle\langle g_i, m| \,, \qquad \sigma_{ee}^i = \sum_m |e_i, m\rangle\langle e_i, m| \,. \tag{C.1.2}$$

Our wave function is the superposition

$$|\psi\rangle = c_0\,|gg\rangle + c_1\,|ge\rangle + +c_1'\,|ge'\rangle + c_2\,|\varphi_\lambda\rangle \,. \tag{C.1.3}$$

Solving the Schrödinger equation $i\partial\psi/\partial t = H\psi$, we obtain four equations for the excitation amplitudes $c(t)$,

$$\begin{aligned}
i\frac{dc_0}{dt} &= \frac{\omega^*}{\sqrt{2}}c_1 + \frac{\omega'^*}{\sqrt{2}}c_1', && \text{(C.1.4)}\\
i\frac{dc_1}{dt} &= \Delta c_1 + \frac{\omega}{\sqrt{2}}c_0 + \frac{\omega^*}{\sqrt{2}}\langle ee|\varphi_\lambda\rangle c_2 + \frac{\omega'^*}{2}\langle ee'|\varphi_\lambda\rangle c_2, && \text{(C.1.5)}\\
i\frac{dc_1'}{dt} &= \Delta' c_1' + \frac{\omega'}{\sqrt{2}}c_0 + \frac{\omega'^*}{\sqrt{2}}\langle e'e'|\varphi_\lambda\rangle c_2 + \frac{\omega^*}{2}\langle ee'|\varphi_\lambda\rangle c_2, && \text{(C.1.6)}\\
i\frac{dc_2}{dt} &= (\Delta_\lambda + \epsilon_\lambda(R))c_2 + \frac{\omega}{\sqrt{2}}\langle\varphi_\lambda|ee\rangle c_1 + \frac{\omega'}{\sqrt{2}}\langle\varphi_\lambda|e'e'\rangle c_1'\\
&\quad + \frac{\omega'}{2}\langle\varphi_\lambda|ee'\rangle c_1 + \frac{\omega}{2}\langle\varphi_\lambda|ee'\rangle c_1'. && \text{(C.1.7)}
\end{aligned}$$

For the $69p_{3/2} + 71p_{3/2}$ resonance, the one-photon detunings Δ and Δ' (defined in Section 1.3.1) are large, about $2\pi \cdot 480$ MHz and $2\pi \cdot 195$ MHz from resonance, respectively, while the Rabi frequencies ω and ω' are about 250 MHz and 110 MHz, respectively (using the experimental parameters, see next section). Over the range of the experimental scan, $\Delta/2\pi = 400 - 900$ MHz, and we have $\Delta \gg \omega$ and $\Delta' \gg \omega'$. We can adiabatically eliminate c_1 and c_1' using Eqs.(C.1.5) and (C.1.6), to obtain

$$\begin{aligned}
c_1 &\approx -\frac{\omega}{\sqrt{2}\Delta}c_0 - \left[\frac{\omega^*}{\sqrt{2}\Delta}\langle ee|\varphi_\lambda\rangle + \frac{\omega'^*}{2\Delta}\langle ee'|\varphi_\lambda\rangle\right]c_2,\\
c_1' &\approx -\frac{\omega'}{\sqrt{2}\Delta'}c_0 - \left[\frac{\omega'^*}{\sqrt{2}\Delta'}\langle e'e'|\varphi_\lambda\rangle + \frac{\omega^*}{2\Delta'}\langle ee'|\varphi_\lambda\rangle\right]c_2.
\end{aligned}$$

Substituting these two expressions in the formulae (C.1.4) and (C.1.7) for c_0 and c_2, we formally obtain the Bloch equations of a two-level system

$$\begin{aligned}
i\frac{dc_0}{dt} &= -\frac{\omega^*_{\text{eff}}}{2}c_2 && \text{(C.1.8)}\\
i\frac{dc_2}{dt} &= [\Delta_\lambda + \epsilon_\lambda(R)]\,c_2 - \frac{\omega_{\text{eff}}}{2}c_0. && \text{(C.1.9)}
\end{aligned}$$

The effective two-photon Rabi frequency is

$$\omega_{\text{eff}} = \frac{\omega^2}{\Delta} a_{ee}(\lambda) + \frac{\omega\,\omega'}{\sqrt{2}\frac{\Delta\Delta'}{\Delta+\Delta'}} a_{ee'}(\lambda) + \frac{\omega'^2}{\Delta'} a_{e'e'}(\lambda), \tag{C.1.10}$$

where $a_{ee}(\lambda) = \langle ee|\varphi_\lambda\rangle$, $a_{ee'}(\lambda) = \langle ee'|\varphi_\lambda\rangle$ and $a_{e'e'}(\lambda) = \langle e'e'|\varphi_\lambda\rangle$. We assumed here that all of the a_{ij} coefficients are real. In Eqs.(C.1.8) and (C.1.9), we neglect all AC-Stark shifts and terms proportional to a^2.

We can eliminate ω' using the known ratio of oscillator strength $\omega/\omega' = \sqrt{f_{3/2}/f_{1/2}}$. We write $\omega_{\text{eff}}(t) = \beta_1(\lambda)\omega^2(t)$, where $\beta_1(\lambda)$ is defined as the time-independent factor of ω_{eff}

$$\beta_1(\lambda) = \frac{a_{ee}(\lambda)}{\Delta} + \sqrt{\frac{f_{1/2}}{2f_{3/2}}}\frac{\Delta+\Delta'}{\Delta\Delta'} a_{ee'}(\lambda) + \frac{f_{1/2}/f_{3/2}}{\Delta'} a_{e'e'}(\lambda). \tag{C.1.11}$$

If we perform the phase transformation $c_2 \equiv \exp[-i(\Delta_\lambda + \epsilon_\lambda(R))t]\bar{c}_2$, our Bloch equations take the simpler form

$$\begin{aligned} i\frac{dc_0}{dt} &= -\frac{\omega^*_{\text{eff}}}{2} e^{-i(\Delta_\lambda+\epsilon_\lambda(R))t}\bar{c}_2, && \text{(C.1.12)}\\ i\frac{d\bar{c}_2}{dt} &= -\frac{\omega_{\text{eff}}}{2} e^{i(\Delta_\lambda+\epsilon_\lambda(R))t} c_0. && \text{(C.1.13)} \end{aligned}$$

The processes considered are far from (atomic) resonance. This means that $c_0 \approx 1$. Using this approximation and $\omega_{\text{eff}}(t) = \beta_1(\lambda)\omega^2(t)$, we get our final formula for $\bar{c}_2$,

$$\begin{aligned} \bar{c}_2(t\to\infty) &= -\frac{i\,\beta_1(\lambda)}{2}\int_{\infty}^{-\infty} \omega^2(t')e^{i(\Delta_\lambda+\epsilon_m(R))t'}dt' \\ &= -i\,\beta_1(\lambda)\sqrt{\pi/2}\,F_{(\Delta_\varphi+\epsilon_\lambda(R))}[\omega^2(t')], && \text{(C.1.14)} \end{aligned}$$

where $F_\nu[h(t)]$ is the Fourier transform of $h(t)$ with respect to ν. Although the Fourier transform of $\omega^2(t)$ is not equal to the Fourier transform of the optical field, they are

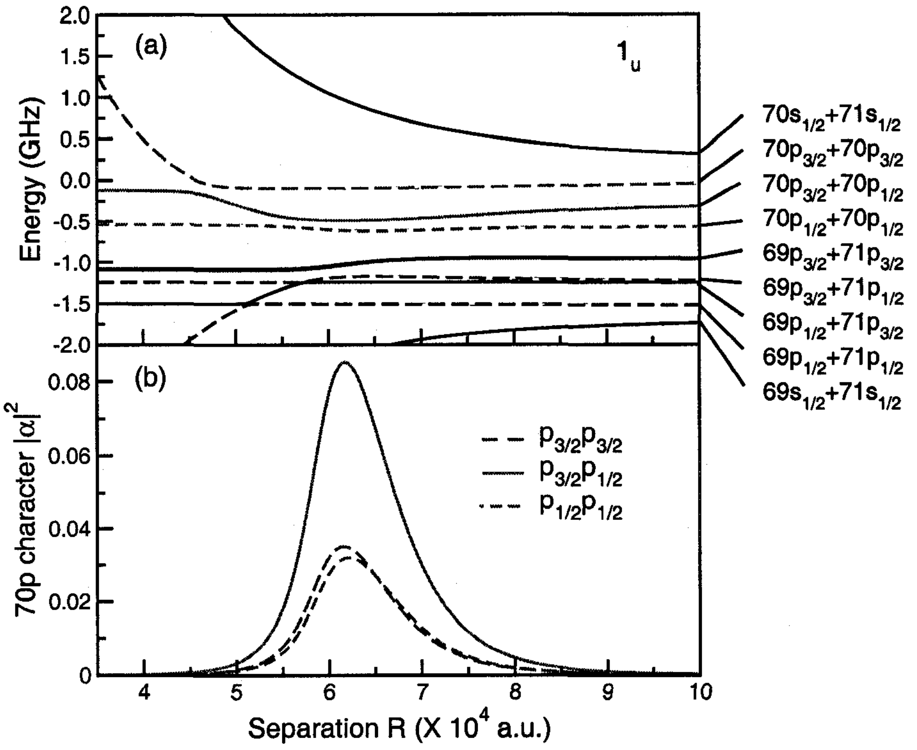

Fig. C.3: Same as Fig.C.1 for the 1_u symmetry.

related. The probability $P_1(\lambda)$ to excite the doubly-excited state $|\varphi_\lambda(R)\rangle$ is

$$P_1(\lambda) = \mathrm{Abs}\left[\tilde{c}_2^2(t \to \infty)\right] = \frac{\beta_1^2(\lambda)\pi}{2}\,\mathrm{Abs}\left[F^2_{(\Delta_\lambda+\epsilon_\lambda(R))}(\omega^2(t))\right]. \tag{C.1.15}$$

The previous analysis assumed that $m_1 = m_2$ for a pair of atoms in the ground state. For the $m_1 = -m_2$ case, the excitation probability can be derived in a similar way

$$P_2(\lambda) = \frac{\beta_2^2(\lambda)\pi}{2}\,\mathrm{Abs}\left[F^2_{(\Delta_\lambda+\epsilon_\lambda(R))}(\omega^2(t))\right], \tag{C.1.16}$$

where β_2 is given by

$$\beta_2(\lambda) = \frac{\tilde{a}_{ee}(\lambda)}{\Delta} + \frac{f_{1/2}/f_{3/2}}{\Delta'}\tilde{a}_{e'e'}(\lambda) + \frac{\sqrt{f_{1/2}/f_{3/2}}}{\frac{2\Delta\Delta'}{\Delta+\Delta'}}\left[\tilde{a}_{ee'}(\lambda) + \tilde{a}_{e'e}(\lambda)\right]. \tag{C.1.17}$$

To calculate the lineshape in the vicinity of a molecular resonance, P_1 and P_2 are averaged over initial diatomic states and all possible orientations of the internuclear axis, which gives $\langle \beta^2 \rangle$. Finally, we sum the pair excitation probabilities of different doubly-excited states $|\varphi_\lambda(R)\rangle$ to get the average excitation probability of a pair of atoms at internuclear separation R. The excitation probability per atom is the sum of all excitation probabilities of pairs that include a given atom,

$$P_{\text{exc}} = \sum_\lambda 2\pi^2 \int_0^\infty dR\, R^2 \rho \, \langle \beta^2(\lambda) \rangle \, \text{Abs} \left[F^2_{(\Delta_\lambda + \epsilon_\lambda(R))}(\omega^2(t)) \right], \tag{C.1.18}$$

where ρ is the sample density. Figs. C.1-C.3 illustrate the relevant α-coefficients (components of $|\boldsymbol{\alpha}\rangle$ defined in the previous appendix) for the signal corresponding to the $69p + 71p$ resonance. Although the relative phase between them is important, their square is plotted. Note that all averaging over angles is included in $\langle \beta^2 \rangle$.

For a Gaussian pulse of duration τ (FWHM) and bandwidth Γ (FWHM), the Fourier transform of ω^2 is given by (with $\epsilon_\lambda(R)$ and Δ_λ in angular frequencies)

$$\text{Abs} \left[F^2_{(\Delta_\lambda + \epsilon_\lambda(R))}(\omega^2(t)) \right] = \frac{I^2}{I^2_{\text{sat}}} \frac{\pi \ln^2 2}{\tau^3 \Gamma} \, 2^{-[\Delta_\lambda + \epsilon_\lambda(R)]^2 / 2\pi^2 \Gamma^2}. \tag{C.1.19}$$

This formula shows the expected quadratic dependence on the laser intensity I. We do not assume in Eq.(C.1.19) that Γ is equal to the Fourier transform limit, but the saturation intensity I_{sat} for isolated $np_{3/2}$ atoms is defined using this ideal pulse. Fig. C.4 shows P_{exc} in the vicinity of the $69p_{3/2} + 71p_{3/2}$ energy. The contributions of the three symmetries and the resulting lineshape are plotted in terms of the single-photon detuning from the $70p_{3/2}$ atomic resonance.

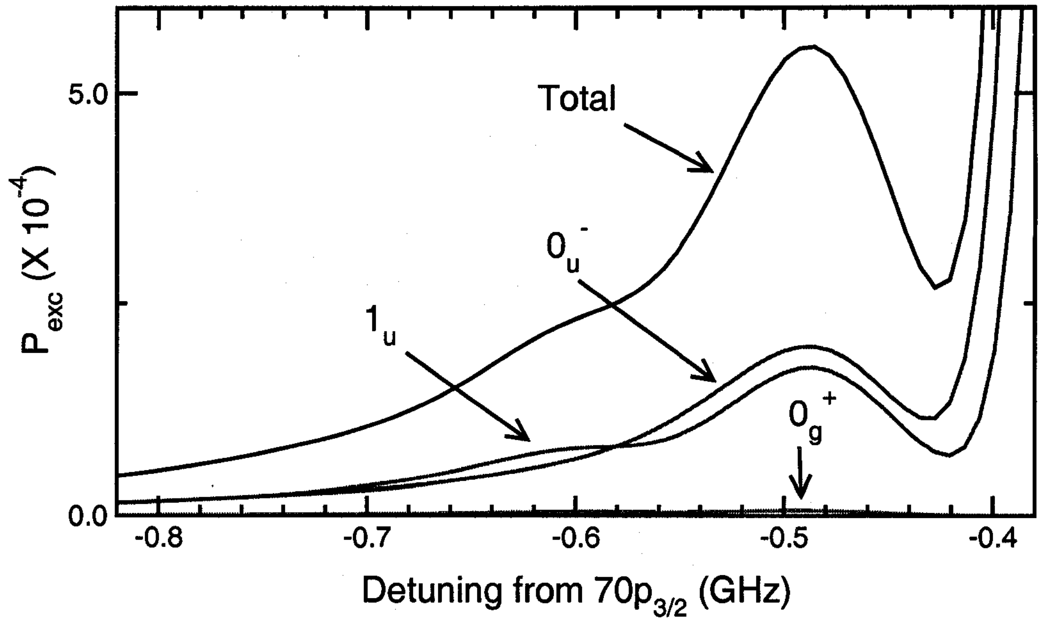

Fig. C.4: Convolutions for the three symmetries and the total lineshape, in the vicinity of the $69p_{3/2}$+$71p_{3/2}$ asymptote, using $I/I_{\text{sat}} = 0.354$ and a density of 6×10^{10} cm^{-3}. The total lineshape includes twice the contribution of 1_u since that state is two-fold degenerate (as opposed to 0_g^+ and 0_u^-). The horizontal axis is the single-photon detuning from the $70p_{3/2}$ atomic resonance.

C.2 Results and comparison with theoretical lineshapes

In Fig. C.5, we show a laser scan in the vicinity of the 70*p* atomic resonance. A significant broadening of the main *np* atomic resonances, predominantly to the red, is consistent with strong attractive Rydberg-Rydberg interactions. Both the $70p_{3/2}$ and $70p_{1/2}$ lines are visible, separated by the 285 MHz fine-structure splitting, and despite possible saturation, their relative sizes ($\sim 5-10$) illustrate the expected non-statistical character of $f_{3/2}/f_{1/2}$ for high Rydberg states of rubidium atoms. On this scan, a molecular resonance is seen as a small peak in the ion signal about 480 MHz to the red of the $70p_{3/2}$ line, its position being near the average energy of Rydberg atoms in the $69p_{3/2}$ and $71p_{3/2}$ states. Other apparent features, with linewidths less than that of the laser, do not reproduce from scan to scan and are attributed to experimental fluctuations. In [46], we showed that the signal size varies quadratically with the laser intensity, as predicted for a molecular resonance. Similar scans were obtained for other values of n over the range 50-70 [46].

In Fig. C.5, we also compare the experimental and theoretical lineshapes for the $69p_{3/2}+71p_{3/2}$ resonance. The theoretical curve was computed using the experimental parameters: for $5s \rightarrow 70p_{3/2}$, the saturation irradiance I_{sat} (defined by $\omega\tau = \sqrt{2\pi \ln 2}$) is about 1.5×10^7 W/cm^{-2}, the irradiance is $I/I_{\text{sat}} \sim 0.354$, the pulse duration is 5 nsec., and the bandwidth Γ (FWHM) is 120 MHz. The average MOT density used was 6×10^{10} cm^{-3}. The theoretical curve shown in Fig. C.5 has been scaled to match the experimental data, and a global background (corresponding to $\sim$ 20 % of the peak of the resonance) has been added to it. Finally, it was shifted by 35 MHz to the blue (within the experimental uncertainty). We find good overall agreement, although there are obvious differences in the details. In both cases, we observe a slight red-detuned wing in the molecular resonance. The lineshape for the broad red wing of the main atomic resonance is also well modeled by the theoretical lineshape, implying that our theoretical values of the potential curves describe the interaction reasonably well. Regarding the absolute signal size, uncertainties in the experimental parameters, such as ion detector response, laser intensity, and atomic

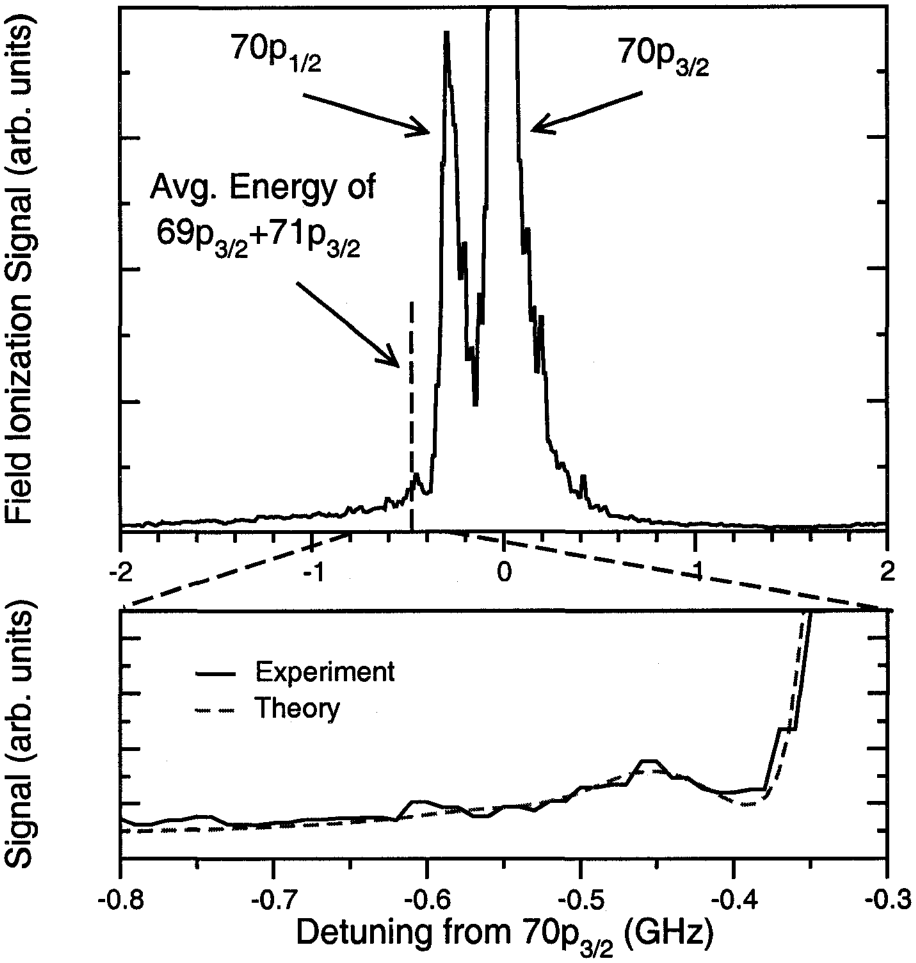

Fig. C.5: (a), Experimental Rydberg spectrum near the molecular resonance red-detuned from the 70p atomic resonance. Both 70$p_{1/2}$ and 70$p_{3/2}$ fine-structure components are shown. The resonance position roughly coincides with the average energy of the 69$p_{3/2}$ + 71$p_{3/2}$ asymptote. (b) Comparison of the experimental (solid line) and theoretical (dashed line). The theoretical spectrum has been shifted by 35 MHz (roughly one standard deviation) to the blue and the theoretical lineshape assumes a 120 MHz laser bandwidth.

density, prevent a precise comparison with theory. Possible detector saturation and blockading of atomic excitation [11,12] are further complications. Nevertheless, the calculated and measured signals are in reasonable agreement, although the calculated signal of $\sim$ 300 ions per shot (using the experimental parameters) is smaller by a factor 5-10. Note that the position of the theoretical signal is located only 5-6 MHz to the red of the average energy of the atom pair $69p_{3/2} + 71p_{3/2}$.

It is remarkable that the effect of the ℓ-mixing takes place almost entirely at the energy corresponding to the $(n-1)p_{3/2} + (n+1)p_{3/2}$ asymptote, even though several asymptotes are involved. This is in part due to the non-statistical $f_{3/2}/f_{1/2}$ ratio. In addition, from Figs. C.1-C.3, we find that the $|\alpha|^2$ 70p-characters peak around $R_0 \sim 62\,000\ a_0$ (a_0: bohr radius), with $\Delta R \sim 15\,000\ a_0$ (chosen as the FWHM of $|\alpha|^2$). The $|\alpha|^2$ 70p-characters for the other potential curves also exhibit maxima in the same range, but are much smaller, hence their weaker contribution to the total lineshape.

C.3 Conclusion

We have presented a theoretical treatment to evaluate possible molecular resonances due to avoided crossings and ℓ-mixings between long-range potential curves of pairs of excited Rydberg atoms.The calculated lineshape for the $69p_{3/2} + 71p_{3/2}$ resonance compares well with experimental observations. The detection of spectral features due to avoided crossings and ℓ-mixings will help in describing the long-range interaction between Rydberg atoms, and possibly lead to the detection of molecular bound levels with ultra-long equilibrium separations, the so-called "macrodimers" [45].

Bibliography

[1] T. F. Gallagher, Rep. Prog. Phys. **30**, 143002 (1988).

[2] T. F. Gallagher, *Rydberg Atoms*, Cambridge University Press, Cambridge, (1994).

[3] See the Special Issue on Rydberg Physics, J. Phys. B **38** N2, S1-S436 (2005) and references therein.

[4] See the Special Issue of Eur. Phys. J. D **40** N1, 1-156 (2006).

[5] 5 T. Calarco, H. J. Briegel, D. Jaksch, J. I. Cirac, P. Zoller, J. Mod. Opt. **47**, 2137 (2000).

[6] G. K. Brennen, I. H. Deutsch, P. S. Jessen, Phys. Rev. A **61**, 062309 (2000).

[7] K. G. Vollbrecht, E. Solano, and J. I. Cirac, Phys. Rev. Lett. **93**, 220502 (2004).

[8] D. Jaksch, J. I. Cirac, P. Zoller, S. L. Rolston, R. Côté, and M. D. Lukin, Phys. Rev. Lett. **85**, 2208 (2000).

[9] I. E. Protsenko, G. Reymond, N. Schlosser, and P. Grangier, Phys. Rev. A **65**, 052301 (2002).

[10] M. D. Lukin, M. Fleischhauer, R. Côté, L. M. Duan, D. Jaksch, J. I. Cirac, and P. Zoller, Phys. Rev. Lett. **87**, 037901 (2001).

[11] D. Tong, S. M. Farooqi, J. Stanojevic, S. Krishnan, Y. P. Zhang, R. Côté, E. E. Eyler, and P. L. Gould, Phys. Rev. Lett. **93**, 063001 (2004).

[12] K. Singer, M. Reetz-Lamour, T. Amthor, L. G. Marcassa, and M. Weidemüller, Phys. Rev. Lett. **93**, 163001 (2004).

[13] T. Cubel Liebisch, A. Reinhard, P. R. Berman, and G. Raithel, Phys. Rev. Lett. **95** 253002 (2005).

[14] C. Ates, T. Pohl, T. Pattard, and J.M. Rost, J. Phys. B **39**, L233 (2006)

[15] T. Vogt, M. Viteau, J. Zhao, A. Chotia, D. Comparat, and P. Pillet, Phys. Rev. Lett. **97**, 083003 (2006).

[16] C. Ates, T. Pohl, T. Pattard, and J.M. Rost, Phys. Rev. Lett. **98**, 023002 (2007).

[17] C. Ates, T. Pohl, T. Pattard, and J.M. Rost, Phys. Rev. A **76**, 013413 (2007).

[18] B. Knuffman and G. Raithel, Phys. Rev. A **73**, 020704(R) (2006).

[19] F. Robicheaux, J. Phys. B 38, S333 (2005).

[20] T. C. Killian, S. Kulin, S. D. Bergeson , L. A. Orozco, C. Orzel, and S. L. Rolston, Phys. Rev. Lett. **83**, 4776 (1999).

[21] P. L. Gould, S. M. Farooqi, J. Stanojevic, S. Krishnan, D. Tong, Y. P. Zhang, J. R. Ensher, A. Estrin, C. H. Cheng, and E. E. Eyler, in Proceedings of: "Interactions in Ultracold Gasses: from atoms to molecules", Editors: M. Weidemüller and C. Zimmermann, WILEY-VCH Verlag Berlin GmbH, 270 (2002).

[22] M. P. Robinson *et al.*, Phys. Rev. Lett. **85**, 4466 (2000).

[23] T. F. Gallagher, *et al.*, J. Opt. Soc. Am. B **20**, 1091 (2003).

[24] S. K. Dutta, D. Feldbaum, A. Walz-Flannigan, J. R. Guest, G. Raithel, Phys. Rev. Lett. **86**, 3993 (2001).

[25] T. Amthor, M. Reetz-Lamour, S. Westermann, J. Denskat, and M. Weidemüller, Phys. Rev. Lett. **98**, 023004 (2007).

[26] T. Amthor, M. Reetz-Lamour, C. Giese, and M. Weidemüller, arXiv:0705.3302v2 (2007).

[27] R. A. D. Zanon, K. M. F. Magalhaes, A. L. Oliveira, and L.G. Marcassa, Phys. Rev. A **65**, 023405 (2002).

[28] A. L. Oliveira, M. W. Mancini, V. S. Bagnato, and L.G. Marcassa, Phys. Rev. Lett. **30**, 143002 (2003).

[29] L.G. Marcassa, A. L. Oliveira, M. Weidemüller, and V. S. Bagnato, Phys. Rev. A **71**, 054701 (2005).

[30] J. M. Raimond, G. Vitrant, and S. Haroche, J. Phys. B **14**, L655 (1981).

[31] W. R. Anderson, J. R. Veale, and T. F. Gallagher, Phys. Rev. Lett. **80**, 249 (1998).

[32] I. Mourachko, D. Comparat, F. de Tomasi, A. Fioretti, P. Nosbaum, V. M. Akulin, P. and Pillet, Phys. Rev. Lett. **80** 253 (1998).

[33] J. S. Frasier, V. Celli, and T. Blum, Rev. Lett. **59**, 4358 (1999).

[34] R. C. Stoneman, M. D. Adams, and T. F. Gallagher, Phys. Rev. Lett. **58**, 1324 (1987).

[35] C. S. E. van Ditzhuijzen, A. F. Koenderink, J. V. Hernández, F. Robicheaux, L. D. Noordam and H. B. van Linden van den Heuvell, arXiv:0706.0110 (June 2007).

[36] J.-H. Choi, J. R. Guest, A. P. Povilus, E. Hansis, and G. Raithel, Phys. Rev. Lett. **95**, 243001 (2005).

[37] W. C. Stwalley, Contemp. Phys. **19** 65 (1978)

[38] b R. J. LeRoy and R. B. Bernstein, Chem. Phys. Lett. **5** 42 (1970).

[39] W. C. Stwalley, Chem. Phys. Lett. **6** 241 (1970).

[40] C. H. Greene, A. S. Dickinson, and H. R. Sadeghpour, Phys. Rev. Lett. **85**, 2458 (2000).

[41] B. E. Granger, E. L. Hamilton, and C. H. Greene, Phys. Rev. A **64**, 042508 (2001).

[42] E. L. Hamilton, C. H. Greene, and H. R. Sadeghpour, J. Phys. B **35**, L199 (2002).

[43] M. I. Chibisov, A. A. Khuskivadze, and I. I. Fabrikant, Phys. Rev. A **66**, 042709 (2002).

[44] M. I. Chibisov, A. A. Khuskivadze, and I. I. Fabrikant, J. Phys. B **35**, L193 (2002).

[45] C. Boisseau, I. Simbotin, and R. Côté, Phys. Rev. Lett. **88**, 133004 (2002).

[46] S. M. Farooqi, D. Tong, S. Krishnan, J. Stanojevic, Y. P. Zhang, J. R. Ensher, A. S. Estrin, C. Boisseau, R. Côté, E. E. Eyler, and P. L. Gould, Phys. Rev. Lett. **91**, 183002 (2003).

[47] A. Dalgarno and W. D. Davison, Adv. At. Mol. Phys. **2**, 1 (1966).

[48] R. J. Buehler and J. O. Hirschfelder, Phys. Rev. **83**, 628 (1951).

[49] J. Y. Zhang and J. Mitroy, Phys. Rev. A **76**, 022705 (2007).

[50] M. Marinescu and A. Dalgarno, Phys. Rev. A **52**, 311 (2007).

[51] M. Marinescu, Phys. Rev. A **56**, 4764 (1997).

[52] K. Singer, J. Stanojevic, M. Weidemüller, and R. Côté, J. Phys. B **38**, S295 (2005).

[53] M. Marinescu and A. Dalgarno, Phys. Rev. A **50**, 3096 (1994).

[54] M. Aubert-Frécon, G. Hadinger, S. Magnier, and S. Rousseau, J. Mol. Spectrosc. **188**, 182 (1998).

[55] A. Derevianko, W. R. Johnson, M. S. Safronova, and J. F. Babb, Phys. Rev. Lett. **82**, 3589 (1999).

[56] Sergey G. Porsev and Andrei Derevianko, J. Chem. Phys. **119**, 844 (2003).

[57] B. Bussery and M. Aubert-Frécon, J. Chem. Phys. **82**, 3224 (1985).

[58] B. Bussery and M. Aubert-Frécon, J. Chem. Phys. **88**, 5663 (1988).

[59] H. Wang, P. L. Gould, and W. C. Stwalley, J. Chem. Phys. **106**, 7899 (1997).

[60] F. Robicheaux and J. V. Hernandez, Phys. Rev. A **72**, 063403 (2005).

[61] P. R. Bunker and V. S. D. Papoušek, J. Mol. Spectrosc. **32**, 419 (1969).

[62] W. Ubachs, *Notes on: Molecular Physics*, *Vrije* Universiteit *Amsterdam*, (2004).

[63] M. Hamermesh, *Group Theory and its Application to Physical Problems*, Dover Publications, New York (1989).

[64] L. D. Landau and E. M. Lifshitz, *Quantum Mechanics non-relativistic theory*, Butterworth-Heinemann (1981).

[65] M. Weissbluth, *Atoms and molecules*, Academic Press Inc., New York (1978).

[66] J. F. Cornwell, *Group Theory in Physics*, Academic Press Inc., San Diego (1989).

[67] J. M. Brown and A. Carrington, *Rotation Spectroscopy of Diatomic Molecules*, Cambridge University Press (Cambridge 2003).

[68] J. Stanojevic, R. Côté, D. Tong, S.M. Farooqi, E.E. Eyler and P.L. Gould, Eur. Phys. J. D **40**, 3 (2006).

[69] M. R. Doery, E. J. D. Vredenbregt, J. G. C. Tempelaars, H. C. W. Beijerinck, and B. J. Verhaar, Phys. Rev. A **57**, 3603 (1998).

[70] A. Schwettmann, J. Crawford, K. R. Overstreet, and J. P. Shaffer, Phys. Rev. A **74**, 020701(R) (2006).

[71] R. J. Le Roy, Can. J. Phys. **52**, 246 (1974)

[72] D. Tong *et al.*, to be published.

[73] L.N. Shabanova and A.N. Khlyustalov, Opt. Spectrosc. (USSR), **56**, 128 (1994).

[74] L. Wenhui, I. Mourachko, M. W. Noel, and T. F. Gallagher, Phys. Rev. A **67**, 052502 (2003).

[75] A. Reinhard, T. Cubel Liebisch, B. Knuffman, and G. Raithel, Phys. Rev. A **75**, 032712 (2007)

[76] M. Saffman and T. G. Walker, Phys. Rev. A **66**, 065403 (2002)

[77] J. V. Hernandez and F. Robicheaux, J. Phys. B: At. Mol. Opt. Phys. **39**, 4883 (2006).

[78] U. Raitzsch, V. Bendkowsky, R. Heidemann, B. Butscher, R. Löw, T. Pfau, arXiv:0706.3869 (Jun 2007).

[79] R. Heidemann, U. Raitzsch, V. Bendkowsky, B. Butscher, R. Löw,1 L. Santos, and T. Pfau, quant-ph/0701120 (Jun 2007).

[80] A. de Lange, E. Reinhold, and W. Ubachs, Int. Rev. Phys. Chem. **21**, 257 (2001).